RMIT UNIVERSITY

EFFECTS OF HYBRIDIZATION OF FIBERS ON THE PROPERTIES OF HIGH VOLUME FLY ASH CONCRETE AND ITS NUMERICAL SIMULATION

A thesis submitted in fulfilment of the requirements for the degree of Doctor of Philosophy

Mahzabin Afroz

B.Sc. in Civil Engineering, Khulna University of Engineering & Technology (KUET), Bangladesh

School of Engineering

College of Science, Engineering and Health

RMIT University

February, 2020

Declaration

I hereby declare that this submission is my own work and to the best of my knowledge it contains no material previously published or written by another person, or substantial portions of material which have been accepted for the award of any other degree or diploma at RMIT or any other educational institute, except where due acknowledgment is made in the thesis. Any contribution made to the research by others, with whom I have worked at RMIT or elsewhere, is explicitly acknowledged in the thesis. I also declare that the intellectual content of this thesis is the product of my own work, except to the extent that assistance from others in the project's design and conception or in style, presentation and linguistic expression is acknowledged.

Finally, I acknowledge the support I have received for my research through the provision of an Australian Government Research Training Program (RTP) Scholarship.

Name: Mahzabin Afroz

Dated: 06/09/2019

Dedication

I dedicate this thesis to my mother Nasima Hossain who passed away during my PhD candidature. Her endless love, sacrifices, supports were my inspiration throughout this journey.

Acknowledgement

Firstly, All Praises to The Almighty for everything.

I express my heartiest gratitude to my supervisor Dr Indubhushan Patnaikuni and Dr Srikanth Venkatesan, for giving me the opportunity to work on this project and their untiring support during my study. They trained me to be an independent researcher and taught me the very important traits a researcher should possess. Their useful suggestions, kind supports, precious discussions and constant encouragements at the various stages throughout the research work are highly appreciated. This work would not have been possible without their never-ending support and guidance starting with the scholarship application until the last bit of this thesis.

I also extend my appreciation to all the laboratory and workshop staffs at the School of Engineering at RMIT University, especially Pavel Ryjkov, Shamir bhuiyan, Eric Xiang Gao, Dr. Matthew Field, Peter Tkatchyk and Peggy Chang for their help in tackling all experimental challenges.

I would also like to thank my colleagues and officemates Shamima Moazzem, Sadia Rahman, Nusrat Rezwana Binte Razzak and Zubayeda Zahan for their support, encouragement and friendship.

Special thanks are due to my father and all of my family members for their endless patience, encouragement, continuous support and help during this study. Special thanks to my beloved husband Mohammad Jobaer Hasan to support and inspired me continuously. Thanks to my lovely son Saad Ibn Jobaer and daughter Safiyyah Bint Jobaer, who were with me in this journey.

Abstract

High volume fly ash (HVFA) is used as cement substitute in many cementitious materials. In recent years, hybrid fibers such as steel and polypropylene have been added to improve the mechanical characteristics. The usage of three fibers combinations is relatively a new concept in HVFA concrete. In this thesis, natural basalt fiber has been combined with steel and polypropylene due to its availability and low cost. Due to the concern about chemical resistance, chemical durability and performance of silane coated modified and non-modified basalt fibers are studied. The fibers were immersed into twelve solutions for 62 days considering the concrete medium. The failure pattern and damage features of the fibers were sorted with the observation of surface by scanning electron microscope (SEM) and their compositions were identified using energy dispersive X-ray spectroscopy (EDX). Long term mass retention capacity was also summarized. The result revealed that the modified fiber exhibits superior properties compared to the non-modified fibers based on morphological and chemical analysis of basalt fibers.

Post this analysis; varied hybrid fiber combinations (both two types and three types) were tested on cement mortar specimens to identify the optimal fiber percentages. Based on the experimental results, equations and artificial neural network were developed to predict the compressive and flexural strength. Two optimum hybrid fiber percentages were found out from the overall analysis of compressive and flexural properties i.e., 1.5% steel, 0.5% polypropylene (1.5S0.5P) and 1.0% steel, 0.5% polypropylene, 0.5% basalt (1.S0.5P0.5B). Optimal percentages were then used to test concrete specimens.

Pre and post cracking mechanical tests of the concrete were carried out. The result of the compressive strengths of three types of hybrid fiber concrete showed appreciable increase by 5.44% and the splitting tensile strength increase was 6.77% in comparison with two type hybrid. Detailed durability properties of optimum hybrid fiber HVFA concrete were conducted along with advanced computed tomography X-ray scans to investigate the durability characteristics of HVFA hybrid fiber concrete. These techniques together confirmed the reduction in porosity and hence the durability of concrete directly suggesting the benefit of the added silane coated basalt fiber.

Numerical models were validated using experimental results for the use of three different fibers in concrete. The model was prepared considering the separate geometry and random orientation of individual fibers. Nonlinear analysis was performed under static load to investigate their failure modes in terms of ultimate load. This model will provide a guideline for the optimum use of three different fibers.

Publications related to this thesis

Journal Articles

1. **AFROZ, M.,** VENKATESAN, S. and PATNAIKUNI, I. (2019), "Effects of Hybrid Fibers on the Development of High Volume Fly Ash Cement Composite", Construction and Building Materials, Vol. 215, pp 984-997.
2. **AFROZ, M.,** PATNAIKUNI, I. and VENKATESAN, S. (2017), "Chemical durability and performance of modified basalt fiber in concrete medium", Construction and Building Materials, Vol. 154, pp 191-203.

Conference Paper

1. **AFROZ, M.,** PATNAIKUNI, I. and VENKATESAN, S. (2018), "Performance analysis of hybrid fiber reinforced high volume fly ash cement composite", In: Mechtcherine V., Slowik V., Kabele P. (eds) Strain-Hardening Cement-Based Composites. SHCC 2017. RILEM Book series, vol 15. Springer, Dordrecht.
2. PATNAIKUNI, I., **AFROZ, M.** and VENKATESAN, S. (2020), "Influence of Silane Coated Basalt Fiber in Hybrid Fiber Reinforced HVFA Concrete", Proc. Of International Conference on Construction Materials and Smart Structures for Sustainable Development (ICCMSSSD - 2020), 29-31 January 2020, pp xi-xxvii.

Table of Contents

List of Figures

List of Tables

List of Notations

A_{lig}	Fracture area
A_i	Immersed absorption
A_b	Boiled absorption
a_c	Effective critical crack length
B	Single basalt fiber raw fly ash
BU	Single basalt fiber ultra-fine fly ash
b	Width of the beam
b_p	Dimensionless component
C	Control raw fly ash
CU	Control ultra-fine fly ash
$C1, C2, C3$	Control concrete
CS_t	Compressive strength with respect to time
D_0^{el}	Initial elastic constitutive tensor
D_v	Damage variable
D	Double fiber raw fly ash
DU	Double fiber ultra-fine fly ash
E	Young modulus of steel fiber reinforced concrete
E_{init}	Initial material Young's modulus
FS_t	Flexural strength with respect to time
$f_t(\theta)$	Strength of fiber concrete
f_{cu}	Uni axial compressive strength of steel fiber reinforced concrete
f_c	Flexural strength
G_f	Fracture energy
h	Depth of the beam
L_o	Initial length
L_t	Final length
L_g	Gauge length
l	Span length
l_f	Length of the fiber
K_p	p^{th} parameter
K_I	Critical stress intensity factor
m	Total amount of factors considered
n_θ	Fiber orientation coefficient

P	Single polypropylene fiber raw fly ash
PU	Single polypropylene fiber ultra-fine fly ash
P_{max}	Maximum load
p_s	Hydrostatic stress
p	Factors variable for strength calculation
q	Von mises equivalent effective stress
r	Position vector
S	Single steel fiber raw fly ash
SU	Single steel fiber ultra-fine fly ash
s	Deviatoric part of the effective stress tensor σ
T	Triple fiber raw fly ash
TU	Triple fiber ultra-fine fly ash
T_b	The area under the load deflection curve
t	Time
UY	Displacement along y axis
UZ	Displacement along z axis
z	Apex of the surface
θ	Orientation angle
$\mu(\theta)$	Shape parameter of stress strain curve
δ_{tb}	Mid span deflection for variables
δ_{max}	Maximum displacement
ε_{csd}	Drying shrinkage
ε	Strain tensor
ε^{pl}	Plastic strain tensor
σ_a	Average principal stress
σ_b	Flexural toughness factor
$\sigma_1, \sigma_2, \sigma_3$	Principal stress components in X, Y, Z axis.
σ	Effective stress tensor
φ_1, φ_2	Opening angles of hydrostatic cone
τ_a	Average shear stress
1.5S0.5P	Hybridization of 1.5% steel and 0.5% polypropylene fiber
1.0S0.5P0.5B	Hybridization of 1.5% steel, 0.5% polypropylene and 0.5% basalt fiber

Chapter 1 Introduction

1.1 Background

It is well-known that concrete is a widely used construction material. About 4.4 billion tons of concrete is used in construction as of today and the quantity is expected to rise over 5.5 billion tons by 2050 (Lehne and Preston, 2018). Although concrete possesses excellent properties, continuous research has seen the growth from Ordinary Portland Cement (OPC) concrete to High Strength Concrete to the use of cement replacements such as fly ash. The use of the fibers in concrete in recent years has outlined the benefits in the improvement of properties (Sevil et al., 2011, Dawood and Ramli, 2010, Kayali, 2004, Malhotra et al., 1994). Nonetheless, there appears to be significant knowledge gaps that exist in the usage of fibers and models that can be used in the design of fiber concrete. This thesis sets out to investigate the varied forms of fiber usage and proposes a model to predict the analysis of fiber mixed high volume fly ash concrete. Finite element models with a comprehensive laboratory program were undertaken in the process. Further details are mentioned below.

The use of high-volume raw fly ash (RFA) or ultra-fine fly ash (UFFA) as concrete admixture for producing high strength concrete has been documented by many researchers. These works have demonstrated strength development, resistance to alkali-silica reaction, freezing and thawing, chloride-ion penetration, sulphate attack and water permeability (Supit et al., 2014, Solis et al., 2010). The most well-known motive for the incorporation of fibers in concrete or cement mortar is to increase the flexural strength, impact strength, tensile strength, ductility and flexural toughness (Ahmed et al., 2006, Li et al., 2016). Many researchers have concentrated on the different types of fibers ranging from steel, glass, plastic and natural fibers in cement mortar subjected to various types of loading. Several studies have shown that high volume fly ash (HVFA) concrete has excellent mechanical properties due to the incorporation of fibers (Ahmed

SFU, 2003, Tabatabaeian et al., 2017). Hybridization of fibers has the potential to be used as reinforcement to overcome the deficiencies of individual fibers in cementitious materials. By combining micro and macro fibers hybridization, pre-peak mechanical performance, strength can be improved by delaying the formation of macro cracks (Ahmed et al., 2007). Although several literature works are available for two fibers hybridization in HVFA concrete, their basic properties of different fibers are not well understood, and the investigation of triple fiber usage is still limited. Therefore, in this study, three types of fibers (steel, polypropylene and basalt) with different volume fraction and aspect ratios were considered. Further research gaps identified are presented below.

1.2 Research gaps

1.2.1 Effect of basalt fibers in concrete medium

Basalt fiber is a low cost natural inorganic fiber that is found in volcanic rocks originated from frozen lava, with a melting temperature comprised between 1500^0C and 1700^0C. Concrete is mainly an alkaline medium and the natural inorganic basalt fiber cannot sustain in an alkaline medium. The current knowledge on the chemical stability of basalt fibers in alkaline, chloride and sulphate medium is insufficient for construction works involving concrete material.

1.2.2 Effect of three different fibers in HVFA mortar and concrete

HVFA is used as cement substitute in many cementitious materials. The usage of three fibers combinations is relatively a new concept in HVFA concrete. Moreover, combination of three types (steel, polypropylene and basalt) of fibers from three different sources is rare. There is a virtuous possibility to use varied hybrid fiber combinations (both two types and three types) on mortar and concrete to identify the optimal fiber percentages.

1.2.3 Usage of low cost modified basalt fiber in hybrid

Extensive works have not considered the usage of low cost basalt fiber. As a naturally occurring material, the usage of such products must be accounted towards reduced energy consumption.

1.2.4 Resistance in acute environment

Durability of concrete depends on its acquaintance to the environment. Moreover, properties of the used material and design have an impact. The durability characteristics of the hybrid fiber combinations haven't been well quantified.

1.2.5 Numerical simulation and advance technology

Finite element Method (FEM) is a well-established analysis technique for concrete structures. The use of computer software to model these concrete elements is much faster and enormously cost-effective. A unified model for high volume fly ash concrete along with the incorporation of hybrid fiber into FE software package can rarely be found in the literature. Moreover, use of recent technologies such as computed tomography x-ray scan or microstructure analysis techniques may provide firm conception about high volume fly ash hybrid fiber concrete.

1.3 Key research questions

Based on the research gaps noted above, following research questions were developed:

a. What is the effect of natural basalt fiber in alkaline concrete medium?
b. How hybrid fiber influences on mechanical properties of ultra-fine or raw high performance high strength high volume fly ash mortar and concrete?
c. What is the effect of hybrid fiber on post cracking displacement?
d. How hybrid fiber influences the durability properties of HVFA concrete in acute environment?

e. How the behavior of hybrid fiber on HVFAC can be verified and modelled by Finite Element Method?

1.4 Aim of the research

The aim of this research is to model the influence of hybrid fiber types and combinations on high volume fly ash concrete using an experimental approach and develop model using finite element method.

1.5 Research objectives

The objectives of this research consistent with the aim and research questions are listed below:

a. To determine the durability of natural basalt fiber based on physicochemical analysis.
b. To study and optimize the mix designs of the Ultrafine and raw HVFA mortar with focus on the three different types of fibers (steel, polypropylene and basalt) with or without hybridization.
c. To understand the mechanical properties of optimized hybrid fibre HVFAC.
d. To determine the effect of hybridization of optimum fiber dosage on the post cracking performance.
e. To evaluate the durability properties.
f. To validate the experimental result with developed model by Finite Element Method (FEM).

1.6 Scope of the thesis and methodology

To develop a hybrid fiber high performance high strength high volume fly ash concrete with 50% cement replacement with fly ash and its finite element model verification with experimental work, a detailed literature review has been conducted on the existing literature. This work is conducted in four steps to achieve the final outcome.

Step 1: To procure suitable natural fibers, initial step is to measure the chemical durability of basalt fibers in alkaline concrete medium. Investigation on two types of basalt fiber is to be done. For, investigating the mass retention and physicochemical characteristics including SEM, EDX analysis, appropriate basalt fiber was selected.

Step 2: Experimental study for control, with or without hybrid fibers was done to test the hypothesis on HVFA cement mortar specimens. An experimental program was designed to capture the influence of hybrid fibers in HVFA cement mortar, and optimum percentages of fibers have been selected for further analysis in HVFA concrete. The results obtained from the experimental study of mortar are also used to do regression analysis and to verify the performance of the developed prediction equations.

Step 3: Developing final mix designs and investigating the basic mechanical and durability properties of the final concrete. The tests include compressive strength, splitting tensile strength, flexural strength, modulus of elasticity, poisson's ratio. For post cracking performance, crack mouth opening has been measured. Drying shrinkage, water absorption, carbonation test was investigated. Computed tomography X-ray has been measured for porosity analysis of concrete samples. Microstructure analysis was done for investigating the short and long term durability characteristics of natural basalt fibers in alkaline HVFA concrete medium.

Step 4: Developing unique model of HVFA concrete incorporating different volume fractions of fibers. The fibers geometry was generated separately by using MATLAB programming and distributed throughout the concrete by spherical coordination system. Verification was done for several experimental results for single and hybrid combinations.

1.7 Outline of the thesis

This thesis is divided into seven chapters, as described below:

Chapter 1: Introduction

The introductory chapter provides a brief overview of high performance high strength high volume fly ash concrete and finite element analysis, covering its history and advantages. A brief description of the application of hybrid fibers in concrete is presented. In addition, the research questions, aim, objectives and the scope of the thesis are also presented.

Chapter 2: **Literature Review**

This chapter presents a literature review to understand the role of three types of fibers (steel, polypropylene and basalt) in high volume fly ash concrete in improving properties of concrete and the deterioration properties of natural basalt fibers. This chapter also presented the literature to use the finite element method as a simulation method for concrete analysis.

Chapter 3: Chemical durability and performance of basalt fiber in concrete medium

This chapter provides brief description about the durability of natural basalt fiber in concrete medium. It describes about basalt fibers properties and methods used to determine the suitability of this fiber in fly ash concrete. It provides details investigations of modified and non-modified basalt fibers by using physical and physicochemical analysis including mass retention, SEM and EDX etc.

Chapter 4: Effects of hybrid fibers on the development of high volume fly ash cement mortar

This chapter presents the preliminary analysis carried out to find the best mix proportion for the concrete. The first one being the experimental work on mortar and then Microstructure study is carried out. After that, regression analysis was done to establish prediction equations for hybrid fiber reinforced HVFA cement mortar.

Chapter 5: Mechanical and durability properties of hybrid fibers reinforced HVFA concrete

This chapter describes final mix designs and investigating the mechanical and durability properties of ultimate concrete mixes. Compressive strength, splitting tensile strength, flexural strength, modulus of elasticity, poisson's ratio, crack mouth opening displacement were measured to determine mechanical performance. Drying shrinkage results were also presented. The durability tests include water absorption and carbonation. Moreover, computed tomography X-ray scan was performed to analyse the porosity of hybrid fiber reinforced HVFA cement concrete.

Chapter 6: Validation and numerical simulation of fiber reinforced HVFA concrete by finite element analysis

Chapter 6 contains the study of static analysis of fiber reinforced concrete by finite element method. FE models were developed for HVFA concrete. Matlab coding was developed to produce the geometry of fibers and distributed randomly in concrete volume by using spherical coordination system. Detailed comparisons were presented to verify the finite element analysis with the experimental results.

Chapter 7: Conclusions and Recommendations

This chapter summarizes the work conducted in the thesis, and then recommendations of the current research are made for future work.

Chapter 2 Literature Review

2.1 Introduction

This chapter presents a comprehensive review of previous studies relevant to this thesis. Previous studies on high volume fly ash (HVFA) concrete with one or two types of fibers are reviewed in detail. It is shown that the benefits and durability of natural basalt fiber in fly ash concrete is relatively unknown. A numerical modelling procedure of concrete with fibers was thoroughly investigated. In addition, it is worth noting that specific literature will also be reviewed where appropriate in other chapters.

2.2 High volume fly ash (HVFA) concrete

Fly ash is a commonly used material in concrete from early 1940s. It is a well-known pozzolanic material that can be used in high volume as a partial replacement of cement to get beneficial effect on concrete. It contains silicon dioxide (SiO_2) (both amorphous and crystalline), aluminium oxide (Al_2O_3) and calcium oxide (CaO). Depending upon the source and composition of coal, the main mineral components of fly ash may vary. Generally, fly ash can be divided into two types by ASTM C618, i.e., Class F and Class C. The main difference between these two classes is the percentage of calcium, silica, alumina, and iron content. When fly ash is mixed with water, it reacts with calcium hydroxide during cement hydration, to form additional Calcium Silicate Hydrate (CSH) and Calcium Aluminate Hydrate (CAH) which are effective in forming concrete leading to higher strength and better durability.

Fly ash is considered as eco-friendly and cost effective because it is a recycle material when used in construction. Fly ash can improve the workability, easier flowability, pumpability, compactability, reduce heat of hydration and increase resistance to sulphate attack, alkali-silica reactivity and other types of deterioration as compared to normal concrete (Solis et al., 2010).

Ultrafine fly ash can be processed from parent raw fly ash through a classifier or micronizer. Generally, it is produced from pure class F fly ash. Ultrafine fly ash provides greater reactive surface area to develop higher early strength and lower permeability in the fly ash concrete. It is considered as one of the highly reactive pozzolans which can obtain earlier strength when compared to the ordinary fly ash.

High volume fly ash concrete hydration process:

Step 1: Cement hydration reaction

$$\text{Cement } (C_3S;C_2S) + H_2O \longrightarrow \text{C-S-H gel} + Ca(OH)_2$$

Step 2: $Ca(OH)_2$ produced in step 1 reacts with fly ash

$$\text{Fly ash } (SiO_2;\ Al_2O_3) + Ca(OH)_2 \longrightarrow \text{C-S-H gel} + \text{C-A-H gel}$$

Generally, 15 to 20% by mass of fly ash is used as a replacement for cementitious materials in concrete. High volume fly ash (HVFA) concrete was introduced by Malhotra at CANMET in the 1980s. According to Malhotra (2005), HVFA concrete is the concrete where at least 50% of ASTM class F or class C fly ash replaces Portland cement. A wide range of benefits has helped this material to gain popularity in concrete industry. To reduce the production of high carbon-di-oxide in cement manufacturing process, fly ash is a great replacement. It is environmentally friendly which is a by-product of coal and less expensive materials than cement. The use of high volume fly ash and the use of ultra-fine fly ash as concrete admixture for producing high strength concrete have been commonly used.

2.2.1 Fresh HVFA concrete property

2.2.1.1 Workability/ Water binder ratio

The HVFA concrete has excellent workability in comparison to OPC concrete. The workability and water requirement mainly depends upon particle size distribution, void and particle packing effect in matrix. HVFA concrete can reduce up to 20% of water requirement depending on the

quality of fly ash and the amount of cement replaced (Owen, 1979, Malhotra et al., 2000). Mehta (2004) described the mechanism very clearly for lower water requirement and good workability of fly ash concrete. Initially, surface charges of cement particle absorb the fine particles of fly ash and prevent from flocculation. Thus, cement particles are effectively dispersed and can trap large amounts of water to achieve a good consistency. Moreover, particle packing effect is also responsible for the reduction of water demand as both Portland cement and fly ash particles are mostly in the 1 to 45 μm size range, and therefore serve as excellent fillers.

2.2.1.2 Drying shrinkage

Drying shrinkage is directly related to the amount and quality of the cement paste present. It can be increased with the increase of aggregate to cement paste ratio. Water-reducing property of fly ash is very helpful to reduce the drying shrinkage. According to Mehta, (Mehta, 2004), the total volume of the cement paste in the HVFA concrete is only 25% as compared to 29.6% for the conventional portland-cement concrete which represents a 30% reduction in the cement paste to aggregate volume ratio.

2.2.1.3 Thermal cracking

Thermal cracking is materials expanding or shrinking when subjected to changes in temperature. Temperature fluctuates because of environmental effect or cement hydration process. Replacing partially of cement with fly ash to simply reduce the heat of hydration is a basic idea for incorporating fly ash in concrete. For 50% cement replaced HVFA concrete with a Class F fly ash the rise is expected to be 30-35^{o}C increment of adiabatic temperature. As a thumb rule, the maximum temperature difference between the interior and exterior concrete should not exceed 25^{o}C to avoid thermal cracking.

2.2.1.4 Setting time

One of the important concerns of high-volume fly ash (HVFA) concrete is to delay the setting time that is sometimes unexpected in the field concrete mixtures. In consideration to normal OPC concrete, setting time of HVFA concrete increases 2-3 hours (Malhotra, 2005). Several methods have been demonstrated to alleviate the delay of setting times of HVFA mix including lowering the water-binder ratio, using conventional accelerators, replacing a portion of the fly ash with a fine $CaCO_3$ powder, using ultra-fine fly ash particle in spite of raw fly ash and use of saturated lime water (Bentz, 2013a, De la Varga et al., 2014, Solikin, 2012, Malhotra, 2005).

2.2.2 Hardened HVFA concrete

2.2.2.1 Mechanical properties

In early 1990s, France has developed very high strength concrete to obtain compressive strength up to 800 MPa and tensile strength of up to 100 MPa. The maximum particle size was very low, only 0.3mm and there was no coarse aggregate. The steel fibres were used of about 5 vol.%, including microfibres < 3 mm long to improve the ductility. Other components used in the experiment were silica fume, ground quartz, superplasticizer, and high amount of Portland cement (up to 1000 kg/m^3) (Brandt, 2008). High strength concrete produced by high volume ultra-fine fly ash (UFFA) or raw fly ash (RFA) has been documented by many researchers. High volume fly ash has established good strength development, water permeability, alkali-silica reaction resistance, sulphate attack and chloride-ion penetration. Literatures of the hardened HVFA concrete mechanical properties are summarized in a Table 2.2.

2.2.2.2 HVFA fiber reinforced concrete

Fiber Reinforced Concrete (FRC) by adding discrete short fibres randomly in cementitious composites exhibits substantially improved engineering properties in tensile strength, flexure strength, fracture toughness, and resistance to fatigue and impact. Fibres have been used since

Biblical times to strengthen brittle matrices; for example straw and horse-hair was mixed with clay to form bricks and floors. In contemporary technology, steel fibers were first proposed as reinforcement for concrete by Romualdi and Batson (1963). Since that time, the concept of dispersed fibres in cement-based materials has developed considerably: hundreds of books and papers, many dissertations, and also applications in building and civil engineering structures all over the world.

Fiber commonly used in concrete can be classified according to their source and production (Figure 2-1).

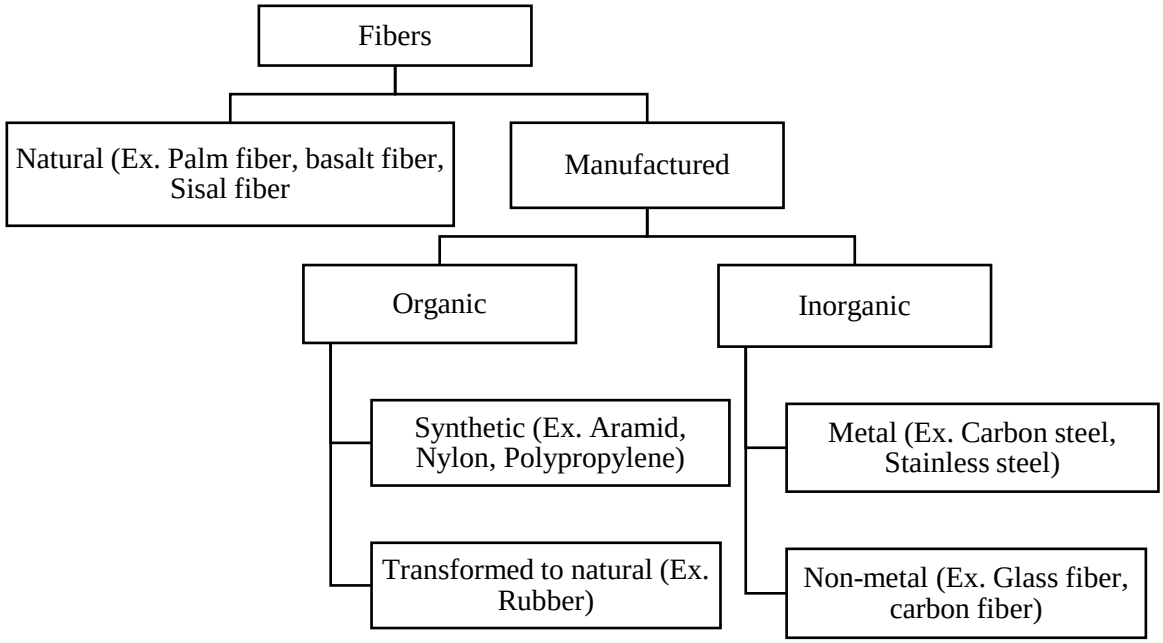

Figure 2-1: Classification of fibers

Many researchers have concentrated on the different types of fibers ranging from steel, glass, plastic and natural fibers in concrete subjected to various types of loading. Several studies have shown that HVFA concrete has excellent mechanical properties and durability due to the incorporation of fibers. Hybrid fiber-reinforced concrete is the combination of a conventional concrete matrix with a mixture of more than one type of discontinuous fibers. Moreover, HVFA concrete shows superior durability properties and high packing density than ordinary concrete incorporating with fiber (Ahmed et al., 2006). It is observed that the use of a combination of

macro and microfibers help in improving the concrete properties extensively. Moreover, the use of both metallic and non-metallic type of fibers attribute maximum improved properties. Flexible fibers with metallic fibres results in good fresh mortar properties and a reduction in early age cracking. Because of the concerns about environment protection and overall cost reduction, usage of natural fibers in concrete is getting attention. In hybrid fiber reinforcement concrete, proper volume ratio can be expected to show simultaneous improvement in structural strength and strain capacity. Table 2.1 classifies the properties and benefits of macro and micro fibers. Figure 2-2 illustrates the mechanical properties of different known materials. Previous literature of fiber reinforced HVFA concrete is summarized in Table 2.3.

Table 2.1: Properties and benefits of macro and micro fibers

Properties & benefits	**Fibers**	
	Macro	**Micro**
Length (mm)	19~80	10~50
Volume used in concrete	High	Low
Modulus	High	Low
Benefits	Enhance strength and toughness properties	Reduce the plastic shrinkage potential

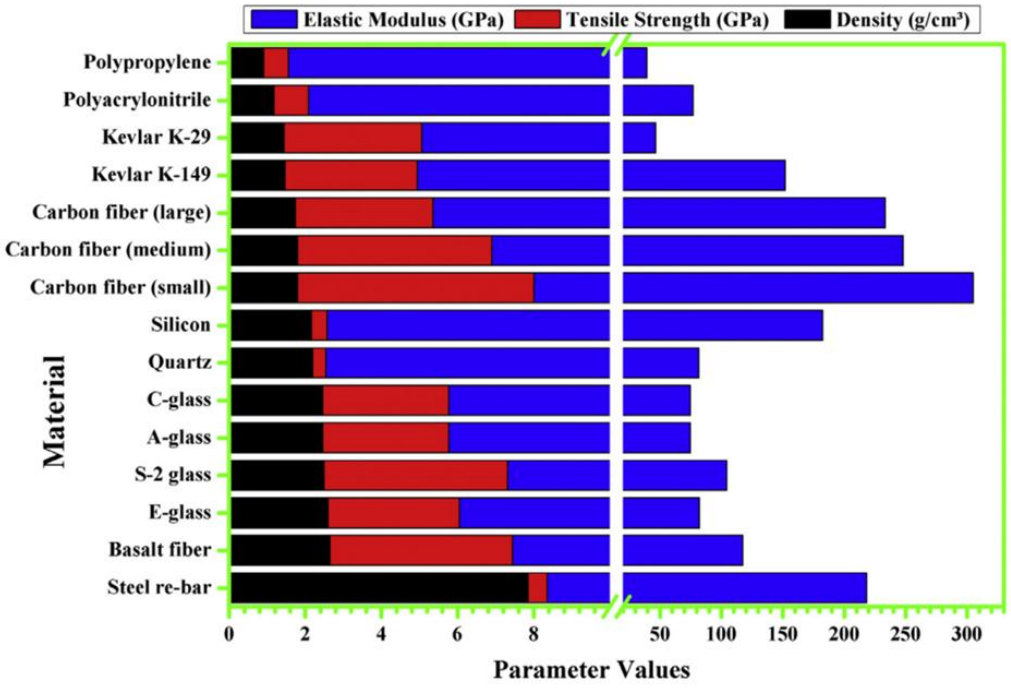

Figure 2-2: Comparative Mechanical Properties of different known materials (Dhand et al., 2014).

Table 2.2: Previous literature of hardened HVFA concrete

Literature	**HVFA**	**Compressive (MPa)**		**Indirect Tensile (MPa) 28d**	**Flexure (MPa)**		**MOE**			**Poisson's ratio**			**Drying Shrinkage strain x 10^{-6}**			**Residual crack width (µm)**		**Comments**
		28d	**90d**		**28d**	**91d**	**28d**	**56d**	**91d**	**28d**	**56d**	**91d**	**7d**	**28d**	**112d**	**28d**	**90d**	
Sivasundaram et al. (1989)	58		52.8						42.8									Drilled core
Bouzoubaâ et al. (2001)	55	30.5	41.6	2.2	4.0		22.4		30.6				142	272	414			Higher chloride ion penetration
Xie et al. (2002)	50	58.2 77.9 (56d)																ultrapulverized fly ash
Atiş (2003)	70	33.25	40.7	2.53	3.81								144	231				With SP
		30.55	41.1	2.51	4.60								100	163				Without SP
	50	57	60.2	4.06	5.63								153	256				With SP
		66.55	79.9	4.20	6.11								113	169				Without SP
Li (2004)	50	54.4 71.6 (56d)																4% nano silica

	50	75.8 85 (56d)																
Mehta (2004)	50	25																
Yang et al. (2007)	54.5	52.6	54.0													31±6	17±5	PVA fibers High range water reducer
	61.5	47.5	49.0													36±12	26±10	
	66.7	34.2	35.5													15±3	16±6	
	70.6	38.4	43.4													22±6	16±8	
	73.7	35.2	38.9													15±8	11±3	
	75.6	26.7	28.2													8±2	8±2	
	78.3	23.9	25.9													8±1	7±1	
	84.8	21.4	22.2													15±2	9±1	
Crouch et al. (2007)	Class C 50.1	50																Air entrainer, ASTM Type A and E admixure
	Class F 50.1	33																
Kayali (2008)	50	44.6			3.70		16.7						550	840				pelletized fly ash lightweight aggregate
	50	56.3			3.55		32.5						590	810				Granite natural aggregate

	50		62.9			3.75		23.7						400	560				Fly ash aggregate
Durán-Herrera et al. (2011)	60	w/c 0.5	16.8																
	75		7.0																
	60	0.55	13.1																
	75		6																
	60	0.60	9.8																
	75		5																
Solikin (2012)	50		70.9	91.9		6.50			43.9										UFFA, tap water
			66.7	81.9		5.23			36.9										RFA, Lime water
			73.78	89.4		7.01			44										UFFA, basalt fiber, lime water
Huang et al. (2013)	60	Low LOI	34.5	47.8		5.0	6.3	26.2	31.8	32.8	0.169	0.163	0.177						
	80		30.0	40.4		3.7	5.8	18.7	23.5	23.9	0.167	0.181	0.168						
	60	High LOI	30.5	39.0		4.5	5.3	23.3	29.3	30.9	0.149	0.175	0.171						
	80		25.2	34.1		3.2	4.2	15.9	21.1	23.2	0.122	0.147	0.124						

Table 2.3: Previous literature of fiber reinforced HVFA concrete

Literature	**HVFA**	**Single fiber**				**Double fiber**	**Triple fiber**	**Major Findings**
		Steel	PP	PVA	NF			
Ramanalingam et al. (2001)	50					1.5st and 0.5PVA		Cement mortar reinforced with 1.5% steel (6mm in length) and 0.5% PV A fibers (12mm in length) showed a flexural strain-hardening behaviour accompanied by multiple cracking when a large amount of cement in the composite (about 50 percent) was replaced by fly ash.
Wang et al. (2001)		Five types of fiber.				Two types		Depending on the fibers and their characteristics, the total plastic shrinkage crack area can be reduced by 30 to 40% when 0.1% (by volume) of fiber is used.
Chen and Liu (2003)	50					1% st and 1% glass fiber		The efficiency of hybrid fibers on expansion resistance is greater than that of monofibers because of its restraint roles at different scales.
Ahmed SFU (2003)	50					Steel-PVA		1% steel and 1.5% PVA was found to show highest flexural strength and deflection capacity. Ultimate flexural strength values as high as 11.2MPa and toughness indices 135 as high as achieved.
Kayali (2004)	50	0.75	0.75					Steel fibers at the rate of 1% by volume of concrete resulted in the highest gains in the strength of high volume fly ash concrete
		1.0	1.0					
Siddique (2004)	35				0.25, 0.5 and 0.75			Fly ash increased the workability, decreased compressive strength, splitting tensile strength and flexural strength.
	45							

					San			Addition of san fibers reduced the workability, did not significantly affect the compressive strength, increased the splitting tensile strength and flexural strength and enhanced the impact strength of fly ash concrete.
	55							
Sahmaran and Yaman (2005)	50					Two types of steel fiber		In self-compacting concrete, increased the workability and reduce strength properties.
Ahmed et al. (2006)	50					Steel-PVA and Steel-PF		Hybrid combination of 1.5% steel and 1.0% PVA exhibited best performance in terms of highest flexural strength, 0.5% steel and 2.0% PE exhibited highest deflection and energy absorption capacities. The 50% replacement of cement by fly ash is found to be an optimum fly ash content in hybrid fiber composites.
	60							
	70							
Wang and Li (2007)	50			0.02				HVFA tends to reduce the PVA fiber/matrix interface bond and matrix toughness in favor of attaining high tensile strain capacity. The limit of cement substitution with ash is constrained by compressive strength development.
	55			0.02				
	60			0.02				
Topcu and Canbaz (2007)	20		0.08					Addition of fibers provide better performance for the concrete, while fly ash in the mixture may adjust the workability and strength losses caused by fibers, and improve strength gain.
			0.05					
		0.65						
Atiş and Karahan (2009)		0.25						Fly ash replacement reduce strength properties, improves workability, reduces drying shrinkage and increases freeze–thaw resistance of steel fiber reinforced concrete.
		0.5						
		1.0						
		1.5						

Şahmaran and Li (2009)	55			26kg/m3				ECC mixtures with high volumes of FA remain durable in terms of mechanical performances after accelerated aging period.
	70			26kg/m3				
Rong et al. (2010)	25	3						Results show that impact resistance of UHPCC is improved with an increase of fiber volume fraction. The numerical values (used finite element method (LS-DYNA)) are in good agreement with experimental results.
	25	4						
Karahan and Atis (2011)	30		0.05					Inclusion of fly ash improves; however, polypropylene fiber decreases the workability of concrete. And did not improve the compressive strength and elastic modulus, reduce drying shrinkage of fibrous concrete with fly ash.
			0.1					
			0.2					
Şahmaran et al. (2011)	55			26kg/m3 (2%)				Adding micro PVA fiber to the ECC matrix substantially improves the fire resistance and eliminates the explosive spalling behaviors of the ECC matrix.
	70							
Khaliq and Kodur (2011)	25					Steel-PP		The test results indicate that the presence of steel and hybrid fibers slows the loss of tensile strength of concrete with temperature
Rao.P and A (2012)	50					Steel-palm		Hybrid fibers were most effective in improving the mechanical strength characteristics.
Tosun-Felekoglu and Felekoglu (2013)	50					PP-PVA		Hybrid usage of PP and PVA fibres caused no significant improvement on flexural strength, relative toughness values and multiple cracking performances of composites.
Zhang and Li (2013)	15% FA					PP		However, the addition of polypropylene fiber has greatly improved the durability of the concrete composite containing fly ash and silica fume.

Aldahdooh et al. (2014)	50					Two different steel fiber		The highest flexural and uniaxial tensile strength values indicating the potential of utilizing ultrafine palm oil fuel ash (UPOFA) as an efficient pozzolanic mineral admixture.
Li et al. (2016)						Steel-PVA		The composites reinforced with 1.4% steel fiber and 2.5% polyvinyl alcohol (PVA) fiber exhibit the best flexural properties in the test.
Banyhussan et al. (2016)	45 70						Steel-PVA-Nylon	Production of hybrid fiber composite mixtures with high concentrations of coarse aggregates and industrial by-products can contribute to superior mechanical and durability performance
Pakravan et al. (2016)	55					PVA-PP		The hybridization with non-round PP fiber and low modulus PVA fiber have remarkable effect on the improving strain-capacity of resultant composite.
Novák and Kohoutková (2017)	30					Steel-PP		Both the tensile and compressive strength of hybrid fibre reinforced concrete decrease with increasing temperature.

2.2.3 Durability properties of HVFA concrete

2.2.3.1 Permeability

Permeability of concrete can be defined as the property that allows the rate of flow of a fluid into the porous solid of concrete. There are several factors affecting the permeability of concrete, like water-cement ratio, compaction and curing, age and pore structure of concrete. Maximum permeability of concrete should not be above 1.5×10^{-11} m/s. According to Malhotra (2005), the permeability value of HVFA concrete is 10 times lower than OPC concrete. This mainly happens due to the reduced water requirement in fly ash concrete than OPC. The high-volume fly ash concrete having 50% cement replacement showed the lowest water and chloride ion permeability compared to OPC (Naik et al., 1994).

2.2.3.2 Resistance to sulphate attack

This is a very common durability property of concrete where water containing sulphate penetrates into it. Sulphate attack mainly happens if the concrete is in contact with sea water. Moreover, oxidation of sulphide minerals in clay adjacent with concrete can produce sulphuric acid. Again, in sewers, anaerobic bacteria produce sulphur dioxide which dissolves in water and then oxidizes to form sulphuric acid. The addition of fly ash can improve the resistance to sulfate attack effectively (Liu et al., 2013).

2.2.3.3 Carbonation

HVFA concrete is capable to maintain low carbonation. In fly ash concrete, lower amount of $Ca(OH)_2$ remains available to react with CO_2, which helps to slow down carbonation process. Moreover, low penetration facility of fly ash concrete benefits in reduced carbonation not allowing CO_2 inside the matrix. Khunthongkeaw et al. (2006) stated that in comparison the cement-only mixtures and low volume fly ash mixtures (less than 30%), carbonation coefficients of mortars are approximately equal to those of the concrete that have the same

mixture condition. However, for mixtures with 50% fly ash, carbonation coefficients of mortars are much higher than those of the concrete that had the same mixture condition.

2.2.3.4 Resistance to corrosion of steel

Due to the low permeability and $Ca(OH)_2$, fly ash concrete shows better resistance to corrosion of steel than normal concrete (Gu et al., 1999, Choi et al., 2006). In HVFA concrete, fly ash minimizes the continuous pozzolanic reaction by reducing the chloride induced and carbonation induced corrosion (Malhotra, 2005).

2.2.3.5 Resistance to ASR

The alkali–silica reaction (ASR) is a swelling reaction which happens in concrete over time. It is a common phenomenon due to the presence of highly alkaline cement paste and the reactive non-crystalline (amorphous) silica in given moisture. Fly ash can reduce the alkalinity of cement with lower alkali content. Moreover, reduction of concrete permeability and diffusivity due to the pozzolanicity of the fly ash experiences resistance to ASR. Fly ash reduces alkalinity of the pore solution expressed from paste samples for controlling ASR expansion (Shehata and Thomas, 2000).

2.2.3.6 Freezing and thawing

Concrete deterioration from freeze thaw occurs when the concrete pore is approximately 91% filled with water. When water freezes to ice it expands 9% more volume than that of water. If there is no space for this volume expansion, freezing may cause distress in the concrete. It can be found that the durability of HVFA concrete in freezing and thrawing is superior in comparison to normal concrete.

2.3 Durability analysis of natural basalt fibers

There is prevalent literature on the manufacture and uses of basalt fibers, but little attempts have been made to use basalt fibers in concrete environment for long term specific applications. At

early age, however it appeared that basalt has an excellent imperviousness to alkaline attack both at room and at elevated temperatures (Ramachandran et al., 1981). However it was stated by Wang et al. (2008) that basalt has better acid resistance than alkaline solutions. Moreover, basalt fiber has strong resistance to corrosion in ocean water and especially in tap water solutions (Wu et al., 2015). In alkaline solutions, the hydroxyl ions react with Si–O–Si group which leads to the breakdown of silicon linkage. The rate of this corrosion depends on the chemical composition of the fiber and the alkalinity of the solution as well as on time and temperature (Scheffler et al., 2009).

$$[Si–O–Si–] + OH^- \qquad [Si–OH] + [SiO]^-$$

In saturated $Ca(OH)_2$ solution, while basalt fiber shows very low weight loss and high stability however may reduce 60% strength after 3 months of immersion of fibers (Rabinovich et al., 2001, Lee et al., 2014). Studies also indicated basalt fibers instability following 28 days in concrete medium (Huang and Deng, 2009, Patnaikuni et al., 2015). The basalt fibers lost 80% strength at 28 days if it was immersed in a 1 M NaOH solution (Sim et al., 2005). SEM images of microstructure have shown a good bond between basalt fiber surface and hydrated cement matrix which is obtained in the early age, whereas a debonding phenomenon between cement matrix and basalt fiber is observed at 28 days (Jiang et al., 2014).However, studies are also available by using different surface coating agents in basalt fibers (Rybin et al., 2013, Wei et al., 2011, Kim et al., 2012), it is required to verify the durability properties of natural basalt fiber before using as hybrid with other fibers.

2.4 Finite element method

Finite element analysis is a well-established method for the study of the behaviour of concrete considering the economic reason. A group of papers regarding finite element analysis of reinforced concrete structures was provided by Willam and Tanabe (2001). This group covers the study area of seismic behavior of structures, cyclic loading of reinforced concrete columns, shear failure of reinforced concrete beams, and concrete steel bond models. Under seismic

loads, a collection of papers about inelastic behaviour of reinforced concrete structure was put together by Shing and Tanabe (2001). Kachlakev et al. (2001) validated carbon fiber reinforced concrete beam, which is externally strengthened and no stirrups being used in the experiment. Kachlakev et al. (2001) set up a calibration model from experimental data by using commercial finite element package ANSYS, SAS 2003 and a mild-steel reinforced concrete beam with flexural and shear reinforcement was analysed. A huge number of literatures have been found about the different structural analysis of reinforced concrete by using commercially available finite element software. Generally, the flexural behaviors of beams including maximum load, deflection capacity are fairly well predicted through the finite element analysis.

2.4.1 Material modelling for fiber reinforced concrete

Continuous efforts on the development of the numerical analysis model for fiber reinforced concrete have been made. However, the fiber geometry and orientation is not designed separately for analysis. Most of the literature was found to consider the same concrete element as fiber reinforced concrete element by using different constitutive laws. Xu et al. (2008) showed comparatively accurate results on the shear behavior of steel fiber reinforced concrete deep beams using the finite element analysis program. In their analysis, four basic assumptions were considered to constitute the model such as, taking account of concrete crushed into pieces, the Young's modulus of SFRC is calculated by the empirical Eq.(2.1) and the elastic-perfectly plastic material model was adopted to simulate the steel bar (Xu et al., 2008).

$$E = \frac{10^5}{2.2+\frac{34.74}{f_{cu}}} \tag{2.1}$$

Ozcan et al. (2009) proposed nonlinear analysis model of SFRC till the ultimate failure cracks by ANSYS. Triaxial failure surface model was used in this study which was developed by Willam and Warnke (1974). The failure surface in principal stress-space is shown in Figure 2.3. The mathematical model considers a sextant of the principal stress-space because the stress components are ordered according to $\sigma_1 \geq \sigma_2 \geq \sigma_3$. These stress components are the major

principal stresses. The failure surface is separated into hydrostatic (change in volume) and deviatoric (change in shape) sections. The hydrostatic section forms a meridianal plane which contains the equisectrix $\sigma_1 \geq \sigma_2 \geq \sigma_3$ as an axis of revolution (Figure 2-3). The deviatoric section in Figure 2.4 lies in a plane normal to the equisectrix (dashed line in Figure 2-4). The deviatoric trace is described by the polar coordinates r and h, where r is the position vector locating the failure surface with angle. The failure surface is defined as Eq. (2.2)

$$\frac{1}{z}\frac{\sigma_a}{f_{cu}} + \frac{1}{r(\theta)}\frac{\tau_a}{f_{cu}} = 1 \qquad 2.2$$

Where σ_a and τ_a are the average stress components, z is the apex of the surface, and f_{cu} is the uni-axial compressive strength. The opening angles of the hydrostatic cone are defined by φ_1 and φ_2. The free parameters of the failure surfaces z and r are identified from the uni-axial compressive strength (f_{cu}), biaxial compressive strength (f_{cb}), and uni-axial tension strength (f_t).

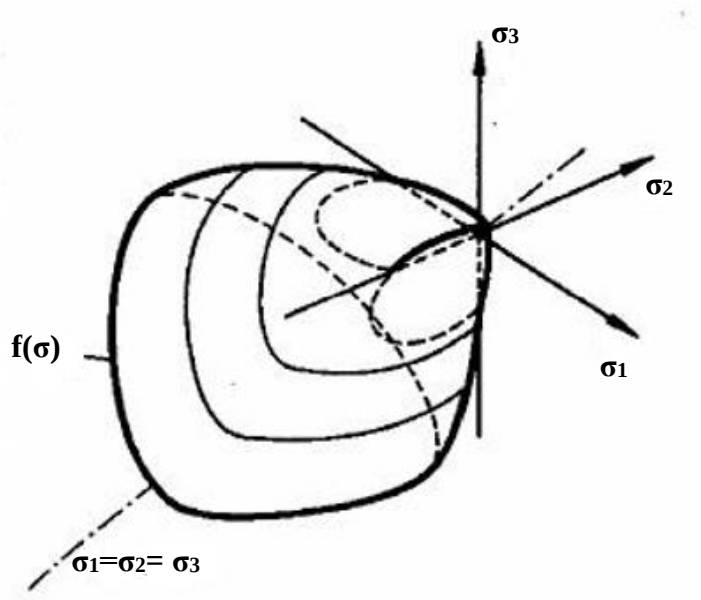

Figure 2-3: Failure surface of plain concrete under triaxial conditions (Willam and Warnke, 1974)

This mathematical model has the following advantages:

1. Close fit of experimental data in the operating range;

2. Simple identification of model parameters from standard test data;

3. Smoothness (e.g. continuous surface with continuously varying tangent planes);

4. Convexity (e.g. monotonically curved surface without inflection points).

Based on the above criteria, a constitutive model for the concrete suitable for FEA implementation was formulated. This model can assume an appropriate description of the material failure (Ozcan et al., 2009).

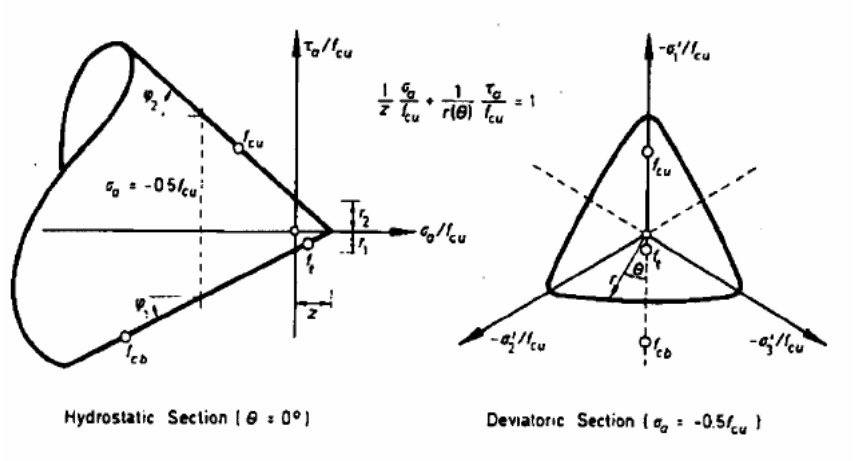

Figure 2-4: Three parameter model

Similar analysis technique was considered by Bouziadi et al. (2018) for creep behaviour and thermal loading of steel fibre reinforced high strength concrete beams. The modulus of elasticity of fiber reinforced concrete is calculated from the following expression Eq. (2.3):

$$f_c' = \left(\frac{E_c}{5000}\right)^2 \tag{2.3}$$

Where, E_c = Modulus of elasticity of fiber concrete (MPa)

f'_c= Uniaxial compressive strength (MPa)

Lee et al. (2012) proposed direct tension force transfer model (NLFEA with DTFTM) to predict the shear behavior of SFRC members. Here, steel fibers were considered as a direct tension force transfer elements. This method can consider the directionality of fibers, difference of bond characteristics according to the types of fibers, and pull-out failure mechanism of fibers with a relatively simple approach. Finite element analysis of natural fibers in concrete also was studied (Mastali et al., 2018). Padmarajaiah and Ramaswamy (2002) simulated the multiaxial stress state in concrete due to the presence of fibers by modifying the parameters used to describe the concrete failure surface and stress–strain properties. Moreover, the fibers along the beam length have also been modeled as truss elements explicitly in order to capture the crack propagation resistance through bridging action.

Limited literature evidence has been found considering the numerical analysis of hybrid fiber reinforced concrete. Chi et al. (2014) proposed a constitutive model for steel-polypropylene hybrid fiber reinforced concrete using a non-associated plasticity. The numerical implementation of this constitutive model is specifically carried out by using a User-defined Material (UMAT) subroutine through ABAQUS. Comparison in between plain and steel fiber concrete was done by Nyström and Gylltoft (2011), carried out using ANSYS AUTODYN 2D simulation program. Moreover, hybrid steel simulation works subjected to blast loading were also found (Yusof et al., 2013). A study was proposed based on the cohesive fracture approach for macro-polymer fibre reinforced concrete (PFRC). This model has been successfully used when applied by the authors to plain concrete and even non-isotropic cohesive materials (Alberti et al., 2017).

Shear load of hybid fiber (steel and polypropylene) reinforced concrete deep beam was analysed by considering a constitutive law of concrete damage plasticity (Liu and Xu, 2013). Abrishambaf et al. (2015) illustrated the stress-crack width (σ–w) relationship of the steel fiber self-compacting concrete obtained from the numerical simulations of the splitting tensile results with a nonlinear 3D finite element model. Concrete damage plasticity (CDP) model was used to simulate the mechanical behaviour of concrete in ABAQUS. Literature showed that concrete

damaged plasticity (CDP) constitutive model which is available in finite element (FE) software can be used in ultra-high performance fibre reinforced concrete (Yoo et al., 2017, Mahmud et al., 2013, Tysmans et al., 2015, Singh et al., 2017, Yoo and Banthia, 2015).

In general, the flow potential surface and the yield surface make use of the principal stresses or the stress invariants. The yield function defines a surface in the effective stress space in order to represent the states of failure or damage (Figure 2-5).

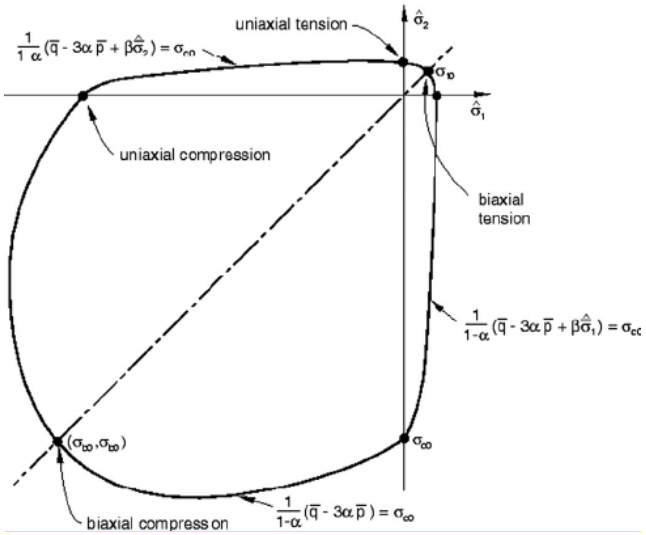

Figure 2-5: Yield surface under biaxial stress used in the concrete damage plasticity model.

The effective stress tensor is determined by Eq. (2.4)

$$\sigma = D_0^{el} : (\varepsilon - \varepsilon^{pl}) \tag{2.4}$$

Where, D_0^{el} is the initial (undamaged) elastic constitutive tensor of the material, ε is the strain tensor and ε^{pl} is the plastic strain tensor. On the other hand, the yield function and the flow potential surface use two stress invariants of the effective stress tensor, namely the hydrostatic stress (p_s) and the Von Mises equivalent effective stress (q) that can be determined from Eq. (2.5) and (2.6), respectively

$$p_s = -\frac{I_1}{3} = -\frac{1}{3trace(\sigma)} \quad (2.5)$$

$$q = \sqrt{3J_2} = \sqrt{\frac{3}{2(s:s)}} \quad (2.6)$$

Where s is the deviatoric part of the effective stress tensor σ.

Yoo et al. (2017) performed nonlinear finite element analysis to simulate the flexural behaviors of ultra-high-performance steel fiber-reinforced concrete beams. Failure occurs when either of the materials (matrix or fiber) reaches its failure strain. Tensile strength of the composites was calculated by using the following Eq. (2.7):

$$\sigma_c(\varepsilon_c) = \sigma_m(\varepsilon_c)V_m + n_l n_\theta \sigma_f(\varepsilon_c)V_f \quad (2.7)$$

Where, $n_l = 1 - \frac{\tanh(\frac{\beta_1 l_f}{2})}{\beta_1 l_f/2}$ (2.8)

$$n_\theta = \int_{\theta_{min}}^{\theta_{max}} p(\theta)cos^2\theta d\theta \quad (2.9)$$

n_θ = fiber orientation coefficient. Moreover, to verify the micromechanics-based fiber-bridging curve, a finite element analysis was carried out by Yoo et al. (2017) with the commercial program DIANA (2007). A few studies were found to develop methods for steel fiber reinforced geopolymer concrete to randomly distribute fibres in a volume with given geometries which give a good agreement with the experimental works (Sanjayan et al., 2015, Sliseris, 2018b). Sliseris (2018a) assume the nature of fiber concrete by using discrete lattice model. Each lattice member is obtained from edge geometry of the standard tetrahedron mesh. Lattice members are discretised by 3D non-linear truss finite elements. Small strain theory is used. For each tetrahedron, all six edges are assumed to have the same stiffness that is defined by cross-sectional area and Young's modulus. Young's modulus was assumed to be the same as for fiber concrete. A single damage variable was used in Eq. (2.10)

$E = E_{init}. (1-D_v)$ (2.10)

Where,

E_{init} = The initial material Young's modulus

D_v = A damage variable (0-undamaged, 1-damaged material).

The evolution of the damage variable is computed in a following Eq. (2.11)

$$D_v = 1 - \frac{f_t\theta * \mu(\theta) * \frac{1}{\varepsilon_t(\theta)}}{E_{init} * \text{Error! Bookmark not defined.}} \quad (2.11)$$

Where, θ – the orientation angle between the lattice member and the average fiber orientation, $f_t(\theta)$ – the strength of fiber concrete, $\mu(\theta)$– a shape parameter of stress-strain curve, $\varepsilon_t(\theta) = \frac{f_t}{E_{init}} * k_\varepsilon(\theta)$strains at peak stress, $k_\varepsilon(\theta)$– a strain multiplier.

The material parameters are non-linearly interpolated depending on the orientation angle between the lattice member and the average fiber orientation Eq. (2.12):

$$f_t(\theta) = f_{t,90} + cos(\theta)^n(f_{t,0} - f_{t,90}) \quad (2.12)$$

Where,

$f_{t,90}$ = material strength in 90 degrees to fiber orientation

$f_{t,0}$ = material strength in 0 degrees to fiber orientation

n = a parameter that characterize accuracy of fiber alignment (here, n = 2).

2.4.2 Element selection

Among commercially available software, ANSYS, ABACUS and DIANA are commonly used programs for finite element analysis of concrete. SOLID65 is generally used as a concrete element in ANSYS analysis software. This element is capable of cracking in tension and crushing in compression. This element is defined by eight nodes having three degrees of freedom at each node. In concrete applications, the solid capability of the element may be used

to model the concrete while the rebar capability is available for modeling reinforcement behavior. In the simulation process of SFRC, SOLID65 element is used to simulate the SFRC element (Xu et al., 2008, Ozcan et al., 2009). LINK8 is a spar which is uniaxial tension-compression element with three degrees of freedom at each node element. Depending upon the application, the element may be thought of as a truss element, a cable element, a link element, a spring element, etc.

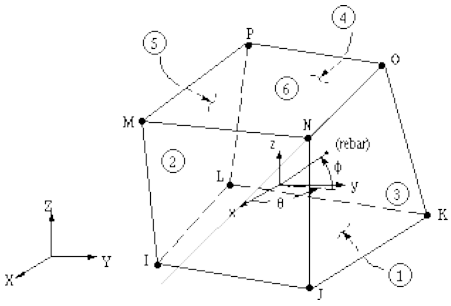

Figure 2-6: Solid 65 3-D Reinforced Concrete Solid

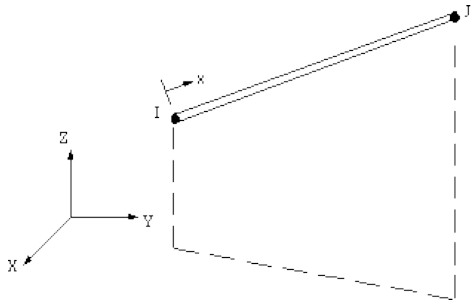

Figure 2-7: LINK 8 3-D Spar

3-D nonlinear elastic spring element COMBIN39 (Figure 2-8) was chosen to simulate the interaction between steel bar and concrete (Xu et al., 2008). This is a unidirectional element with nonlinear generalized force-deflection capability. The element has large displacement capability for which there can be two or three degrees of freedom at each node. Again COMBIN14 was also considered to create interfacial bond in between steel and concrete with appropriate properties to capture the effects of bond, bond-slip and peel off (Padmarajaiah and Ramaswamy, 2002).

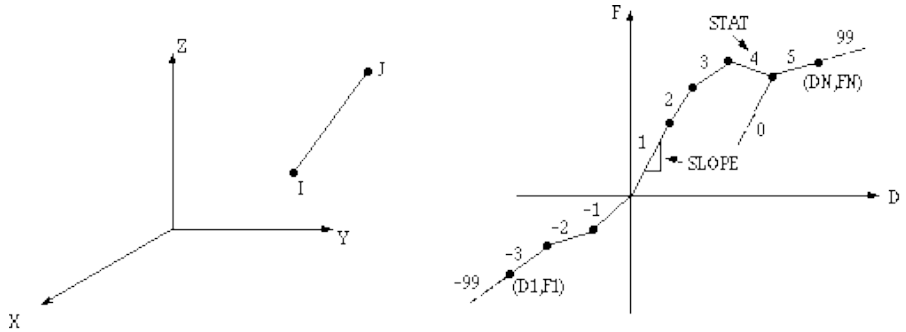

(a) Element (b) F-D relationship

Figure 2-8: Combine 39 element

In ABAQUS, concrete or reinforced concrete beams were modelled by reduced integrated 4-noded plain stress elements CPS4R which is very similar to the eight-node shell element. The CPS4 and CPS4R elements are expanded into C3D8 and C3D8R elements, respectively. The steel reinforcements are modelled as 3D truss elements (T3D2) considering their axial deformations only. It is considered that the steel reinforcements are embedded in the solid concrete elements with a full bond.

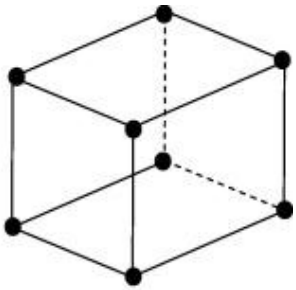

Figure 2-9: Eight node brick element (C3D8R)

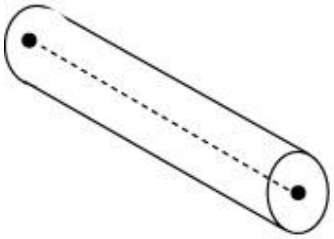

Figure 2-10: T3D2 3-D truss element

In order to 2D model the concrete in DIANA, four-node quadrilateral isoparametric plane stress element (Q8MEM) is used, which is based on linear interpolation and Gauss integration. The L8IF element is an interface element between two lines in a two-dimensional configuration.

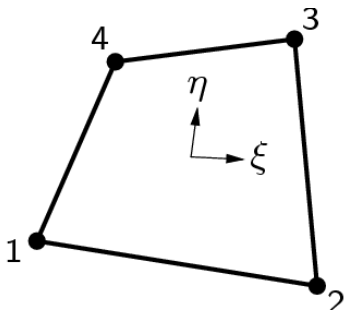

Figure 2-11: Q8MEM element

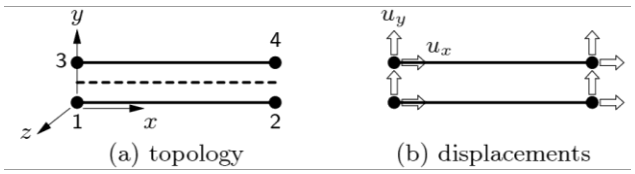

Figure 2-12: L8IF element

2.4.3 Meshing

To obtain the satisfactory result, generally square or rectangular mesh was recommended for concrete volume. For some notch beam, 3D representation of the tetrahedron mesh was found (Sliseris, 2018a). Meshing can be also obtained by using a tri-linear softening function (Alberti et al., 2017).

2.4.4 Boundary condition and applied load

For flexural investigation, basically three point and four point static loading beam was considered for analysis. Common boundary conditions were chosen: constraints in x, y, and z directions. In nonlinear analysis, the total load applied to a finite element model is divided into a series of load increments called load steps. In general, Newton–Raphson equilibrium iterations for updating the model stiffness were used in the nonlinear solutions (Xu et al., 2008, Ozcan et al., 2009, Sliseris, 2018a). Loading in abacus can be simulated by using available Abaqus modules – Standard and Explicit. The modules of the model were integrated with the backward Euler method (Tysmans et al., 2015).

2.5 Conclusions

In HVFAC, 50% fly ash replacement of cement can be used for hybrid fiber analysis considering the detailed properties of previous literature. In hybridization, steel, polypropylene and basalt fibers may provide reasonable improvements of overall performance of HVFA cement composite and negate some of the disadvantages for the use of single or two fibers. Moreover, as basalt is a natural fiber, its durability properties needs to be confirmed first. Literature on the numerical analysis of hybrid fiber for HVFA concrete is clearly lacking and needs great attention to get rid of the trial and error from the use of different fraction and types of fibers in concrete.

Chapter 3 Chemical durability and performance of basalt fiber in concrete medium

3.1 Introduction

Basalt fibers show several advantages including modulus of elasticity, specific strength and nontoxic (Quagliarini et al., 2012), low cost (Fiore et al., 2015), non-combustible (Wei et al., 2010) and high thermal insulating properties (Novitskii, 2004). It has the feature of wider application temperature range of -270° C to +750° C (Morozov et al., 2001, Militký et al., 2002). The chemical and mechanical properties depend on the composition of the raw material. Different fiber composition and concentration provide different thermal and chemical stability and also show variance in mechanical and physical properties (Novitskii, 2004).

Chemical structure of basalt fiber is nearly related to glass. The most important components of basalt fibers are SiO_2, Al_2O_3, CaO, MgO, Fe_2O_3 and FeO. The different oxides compose a large cross linked molecule with primary bonds (Deak and Czigany, 2009 , Anade et al., 2016). Basalt fibers are chemically composed of pyroxene, clinopyroxene, olivine and plagioclase minerals (Dhand et al., 2014). Basalt materials are classified according to their SiO_2 content. If the basalt has scarcity in silica, it is categorized as alkaline basalt. Further, if the basalt is rich in silica, it is known as acidic basalt (Deak and Czigany, 2009 , Dhand et al., 2014). Compared to the other natural fibers (Table 3.1), it has excellent mechanical properties; lightweight, easily affordable and ecofriendly which makes it an ideal material for civil engineering application. The addition of basalt fibers can improve the deformation and energy absorption capacity, toughness index, flexural strength, abrasion resistance and reduce dry shrinkage of fiber reinforced concrete (FRC) significantly (Li and Xu, 2009, Dias and Thaumaturgo, 2005, Kabay, 2014, Jiang et al., 2010). SEM images of microstructure have shown a good bond between basalt fiber surface and hydrated cement matrix which is obtained in the early age, whereas a

debonding phenomenon between cement matrix and basalt fiber is observed at 28 days (Jiang et al., 2014).

Table 3.1: Mechanical properties of some natural fibers (Fiore et al., 2015, Mahjoub et al., 2014)

Fiber	Density (gm/cm^3)	Tensile Strength (GPa)	Elastic Modulus (GPa)	Elongation at break (%)
E-glass	2.56	1.4-2.5	76	1.8-3.2
Carbon	1.4	4.0	230-240	1.4-1.8
Basalt	2.8	2.8	89	3.15
Jute	1.3	0.3-0.7	26.5	1.5-1.8
Flax	1.5	0.5-1.5	27.6	2.7-3.2

There is a prevalent literature on the manufacture and uses of basalt fibers, but little attempts have been made to use basalt fibers in concrete environment for long term specific applications. At early age, however it appeared that basalt has an excellent imperviousness to alkaline attack both at room and at elevated temperatures (Ramachandran et al., 1981). However it was stated by Wang et al. that basalt has better acid resistance than alkaline solutions (Wang et al., 2008). Moreover, basalt fiber has strong resistance to corrosion in ocean water and especially in tap water solutions (Wu et al., 2015). In alkaline solutions, the hydroxyl ions react with Si–O–Si group which leads to the breakdown of silicon linkage. The rate of this corrosion depends on the chemical composition of the fiber and the alkalinity of the solution as well as on time and temperature (Scheffler et al., 2009). In saturated $Ca(OH)_2$ solution, while basalt fiber shows very low weight loss and high stability however may reduce 60% strength after 3 months of immersion of fibers (Rabinovich et al., 2001, Lee et al., 2014). It also shows instability following 28 days in concrete medium (Huang and Deng, 2009, Patnaikuni et al., 2015). The

basalt fibers lost 80% strength at 28 days if it was immersed in a 1 M NaOH solution (Sim et al., 2005). However, studies are also available by using different surface coating agents in basalt fibers (Rybin et al., 2013, Wei et al., 2011, Kim et al., 2012) but particularly in concrete, it is not adequate.

From the available literature, it appears that the investigation on chemical stability of basalt fibers in alkaline as well as in chloride and sulphate medium is not sufficient, which generally happens in building and construction involving concrete material. In most cases, the approaches were on short term basis and are inadequate to explain the long term variance of modified and non-modified fibers. This chapter investigates the capacity of two types of commercially available basalt fibers to retain in alkaline medium and the effect of pH and long term (62 days) mass retention at room temperature. Moreover, physicochemical characterization of basalt fibers is investigated before and after the immersion in alkaline using SEM and EDX analysis. The contents of this chapter are published in the Journal of Construction and Building Materials, volume 154, pp 191-203.

3.2 Materials

Two different types of basalt fibers were used in this experiment. One was supplied by Kamenny Vek Ltd, Dubna, Moscow, Russia (Group A) and the other one was imported from Jiuxin basalt fiber industry Co. Ltd, Jilin Province, China (Group B). Group A fiber was modified by silane (SiH_4) surface coating agent. The organofunctional group of silane is epoxy functional. The nominal length and thickness of Russian fibers were 25mm and about 15µm respectively. Chinese fibers have 3mm nominal length and similar thickness as Russian fibers. Chemical compositions of both fibers are shown in Table 3.2.

Table 3.2: Chemical components of two different basalt fibers (supplied)

Component	Content (% wt)	
	Group A	Group B
SiO_2	54.5-55.5	48-60
MgO	4.0-4.6	3-6
CaO	7.5-8.5	5-9
Fe_2O_3+ FeO	10.0-11.5	9-14
Al_2O_3	16.5-18	14-19
TiO_2	0.9-1.25	0.5-2.5
R_2O	4-5	--
Li_2O	0.1-0.3	--
Na_2O+ K_2O	--	3-6
Others	--	0.09-0.13

Fibers were investigated under various chemical solutions considering concrete medium. Twelve solutions were prepared using NaOH, NaCl, Na_2SO_4, $Ca(OH)_2$, $CaCl_2$ and $CaSO_4$. Chemical solutions were prepared in view of three different conditions of alkaline, chloride and sulphate medium. Mixtures of these ions were also considered to explore the combined effects.

3.3 Methodology

Concrete is alkaline because of the portland cement hydration product calcium hydroxide. Besides, the common deterioration of concrete emerges due to the attack of chloride and sulphate ions from ocean, de-icing salts, soil and groundwater. In this project, strong base 1M NaOH and 1M $Ca(OH)_2$ solutions were applied to represent the contamination of alkaline ion. Therefore, 3% NaCl and $CaCl_2$ and 10% Na_2SO_4 and $CaSO_4$ solutions were prepared to determine the effect of chloride and sulphate ions.

3.3.1 Mass retention test

Chemicals were measured based on designed concentration; for example, to make a 1M NaOH solution, 20g NaOH needed to be dissolved in 500g distilled water. Again, 15g NaCl is required for preparing 500ml 3% NaCl solution. Fibers were washed and oven dried before taking the initial mass. For every group, basalt fibers (45g) were immersed into twelve solutions in twelve glass containers (Figure 3-1). Each series were labelled with the immersing solutions. After the designated time of immersion phases, basalt fibers were washed with distilled water and dried in oven at 105^0C for 24 h. Temperature and pH of solutions were measured and weight of basalt fiber was taken after it has dried. The procedure was repeated for 3, 7, 14, 21, 28, 42 and 62 days.

Figure 3-1: Immersion of Basalt Fibers in twelve chemical solutions

The mass retention was calculated by using following Eq. (3.1),

$$\text{Mass retention (\%)} = \left(1 - \frac{m_0 - m}{m_0}\right) \times 100 \quad (3.1)$$

Where,

m_0= Dry mass before immersion (g)

m= Dry mass after immersion (g)

3.3.2 Physicochemical Analysis

Photomicrography of the exterior surface of basalt fiber was obtained by using FEI Quanta 200 ESEM. SEM test was performed in the RMIT Microscopy and Microanalysis Facility. Samples were coated with a thin gold film in order to avoid the influence of charging effect during the SEM operation. SEM was also used to determine the diameter and shape of basalt fiber. The physical properties were also observed and recorded for further analysis by using computerized data acquisition system.

SEM analysis of dried basalt fibers was carried out equipped with an EDX analysis system. Data were processed with AZtec Energy software. EDX was used to determine spectrum of basalt fiber before and after immersion in 1M NaOH and 1M $Ca(OH)_2$ solutions. Quantitative analysis was also carried out to identify the changes of chemical components.

3.4 Results and discussions

3.4.1 Density

The density of basalt fibers were measured through water pycnometer technique following 62 days submerging in twelve solutions with balance equipment with 0.005g sensitivity. The averages of twelve samples from each group were determined that are shown in Table 3.3. The result shows substantial variation in Group B. This was due to the increased density in alkaline solutions.

Table 3.3: Statistical parameter of density.

Fiber Group	Density Control Specimen (g/cm^3)	Density after Chemical Treatment (mean) (g/cm^3)	Standard Deviation (SD)	Coefficient of variation (COV, %)
Group A	2.498	2.37467	0.14778	6.21
Group B	1.622	2.16508	0.47862	22.1

3.4.2 pH measurement

All pH values were measured at room temperature. After immersing fibers, initial pH value was taken and final value was determined after 62 days. Results are presented in Table 3.4.

Table 3.4: pH of Group A and B in different solutions

Solution Nos.	Chemical Solutions	Group A		Group B	
		Initial pH	Final pH	Initial pH	Final pH
I	NaOH	12.95	13.41	13.56	13.46
II	NaCl	7.02	8.08	7.02	7.89
III	Na_2SO_4	7.02	7.49	7.02	8.14
IV	NaOH +NaCl	12.84	13.28	13.35	13.28
V	NaOH +Na_2SO_4	12.92	13.56	13.44	13.34
VI	NaOH + NaCl+ Na_2SO_4	12.76	13.36	13.27	13.17
VII	$Ca(OH)_2$	12.22	12.62	12.76	12.51
VIII	$CaCl_2$	7.02	8.38	7.02	7.27
IX	$CaSO_4$	7.01	8.43	7.02	7.92
X	$Ca(OH)_2$ +$CaCl_2$	11.83	13.00	12.30	11.98
XI	$Ca(OH)_2$ +$CaSO_4$	12.09	12.57	12.71	12.59
XII	$Ca(OH)_2$ +$CaCl_2$ +$CaSO_4$	11.93	12.12	12.39	11.50

Group B fibers show decreased final pH for all alkaline solutions than initial pH value. However, pH value increases for salt and Group A solutions conversely. Usually, when alkaline solution is mixed with basalt fiber, a corrosion layer is formed on the surface of the fiber. Hydroxyl ion attacks the silica network directly and the hydroxide ions of the alkali break the Si-O-Si linkage (Elshafie and Whittleston, 2016):

$$[Si–O–Si–] + OH^- \longrightarrow [Si–OH] + [SiO]^-$$

Thus reduces the concentration of hydroxyl ion in solutions and decreases final pH value. Group B fibers illustrate the general pattern of deterioration in alkaline medium. For Group A, silane coating confines the swelling of the fiber by creating a crosslinked network (Lipatov et al., 2015). For Group A solutions, OH^- ion slowly diffuses with the existing silane coating and decreases the amount of breakdown. Alkali solution also leads to a decrease of sodium, potassium, aluminium and silicon (Na^+, K^+, Al^{3+}, Si^+) on the surface of all basalt fibers (Agrawal et al., 2000). Furthermore, –Si–O– structure is inert to salt but in contact with water, some alkaline ions enter into the internal structure of fiber (Ying and Zhou, 2013). Due to these phenomena, hydroxyl ion of solution was increased for basalt fiber in Group A and salt solutions.

3.4.3 Surface Appearance

3.4.3.1 Physical Appearance Analysis

The following observations are prepared based on the visual analysis. A great difference was found in between two groups feature. Physical appearances of Group A are shown in Figure 3-2. From the observation, physical properties of basalt fibers were unaffected after 62 days for NaOH, NaCl, Na_2SO_4 and their combined solutions. The $CaCl_2$ and $CaSO_4$ solution also showed similar effects for the basalt fibers. On the other hand, comparatively higher damage was observed in the fiber treated with $Ca(OH)_2$ and the combination of $Ca(OH)_2$ with $CaCl_2$ and $CaSO_4$. The fibers lost their original texture and some of them split into many strands. It could be seen that concentrated NaOH cannot damage the fiber structure but concentrated $Ca(OH)_2$ shows a rough and damaged surface.

Figure 3-2: Group A basalt fiber after 62 days treatment (Table 3.4 is referred for solution Nos.)

The effects of different solution treatment for Group B fibers are shown in Figure 3-3. Salt solutions show undamaged texture after full treatment of fibers. Surface damage was mainly detected in the fibers treated with NaOH and $Ca(OH)_2$ and their combination with chloride and sulphate ions. Initially, fibers lost their original texture and created fiber ball by sticking together after soaking in hydroxyl ions. After 62 days treatment in high alkali medium, if the

fibers separated from the sticky ball, they split into many strands and some of them became powder (Figure 3-4).

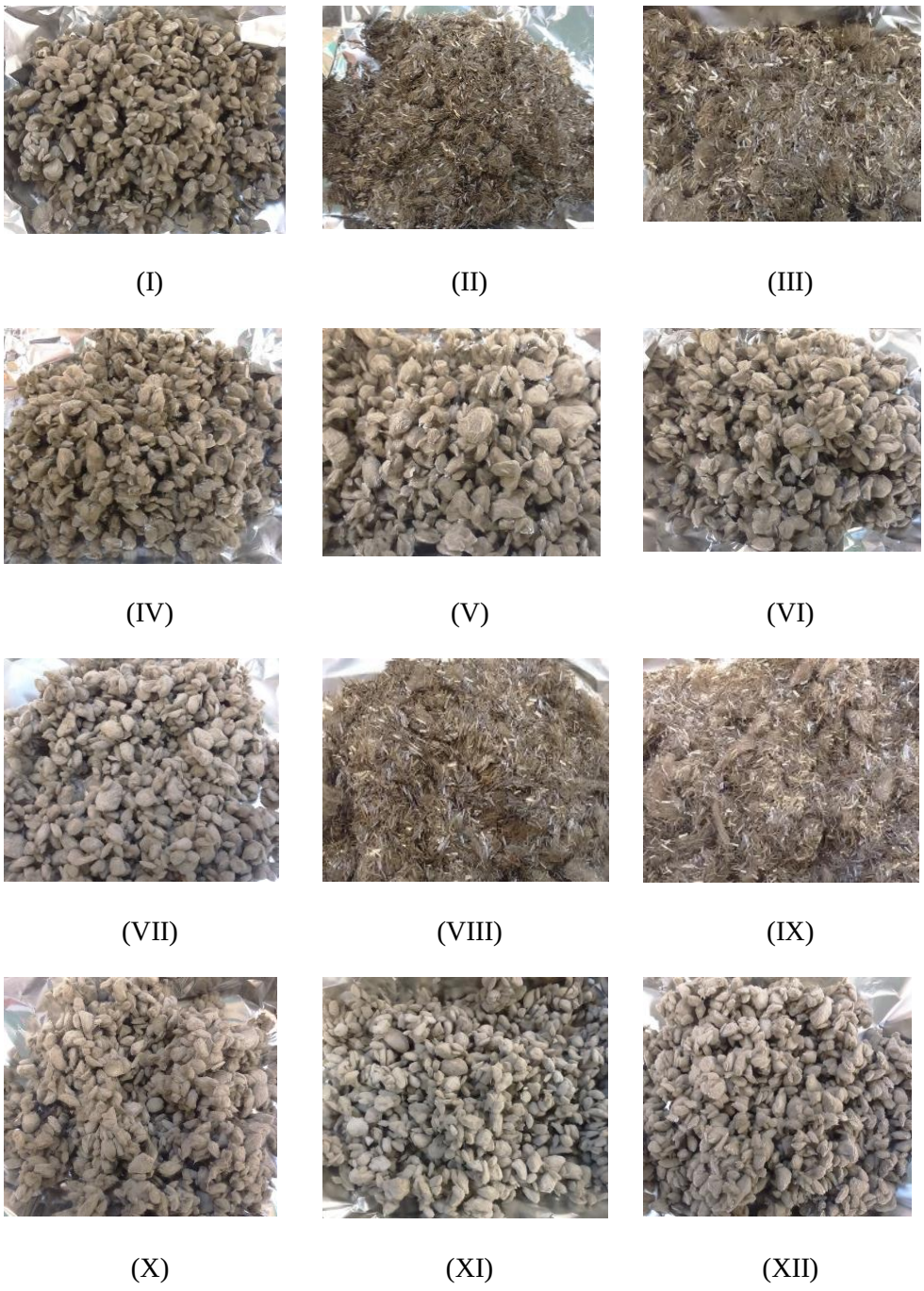

Figure 3-3: Group B basalt fiber after 62 days treatment (Table 3.4 is referred for solution Nos.)

Figure 3-4: After 62 days treatment with $Ca(OH)_2$ solution (Group B)

3.4.3.2 Morphology analysis

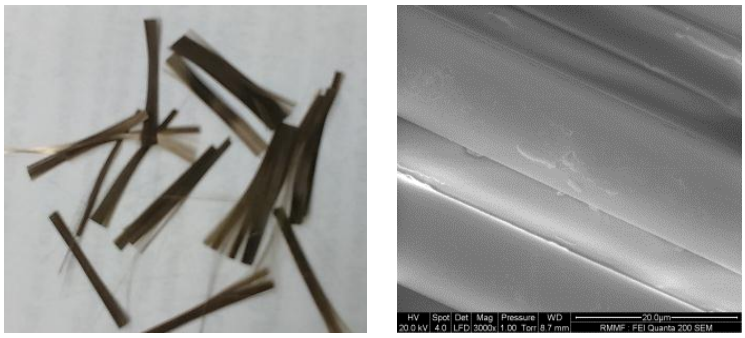

(a) Group A Fibers

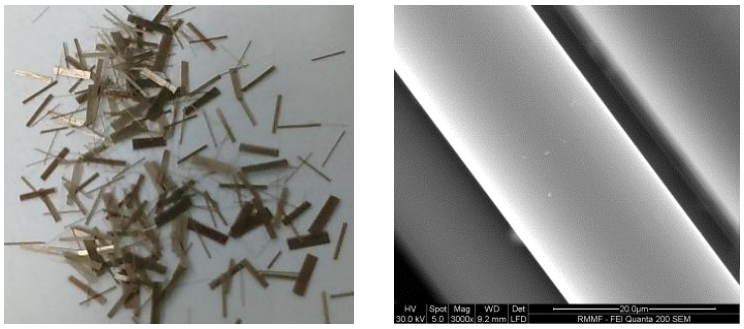

(b) Group B Fibers

Figure 3-5: Basalt fibers.

In order to get an idea of the microscopic structure and to estimate the deterioration mechanisms, the surface of basalt fiber was analysed by SEM. The physical and SEM images of reference samples are shown in Figure 3-5. The effect of chemical solution on Group A and Group B are shown in Figure 3-6 and Figure 3-7 respectively.

Hydrolysable alkoxy group of silane with moisture leads to the formation of silanols and the silanol then reacts with the hydroxyl group of the fiber to form constant covalent bonds that are chemisorbed onto the fiber surface (Lipatov et al., 2015). Hence, the hydrocarbon chains

generated by the application of silane confine the swelling of the fiber by creating a crosslinked network. The reaction is as follows (Lipatov et al., 2015).

$$CH_2CHSi(OC_2H_5)_3 \longrightarrow CH_2CHSi(OH)_3 + 3C_2H_5OH$$

$$CH_2CHSi(OH)_3 + H_2O + \text{fiber-OH} \longrightarrow CH_2CHSi(OH)_2O\text{-}$$

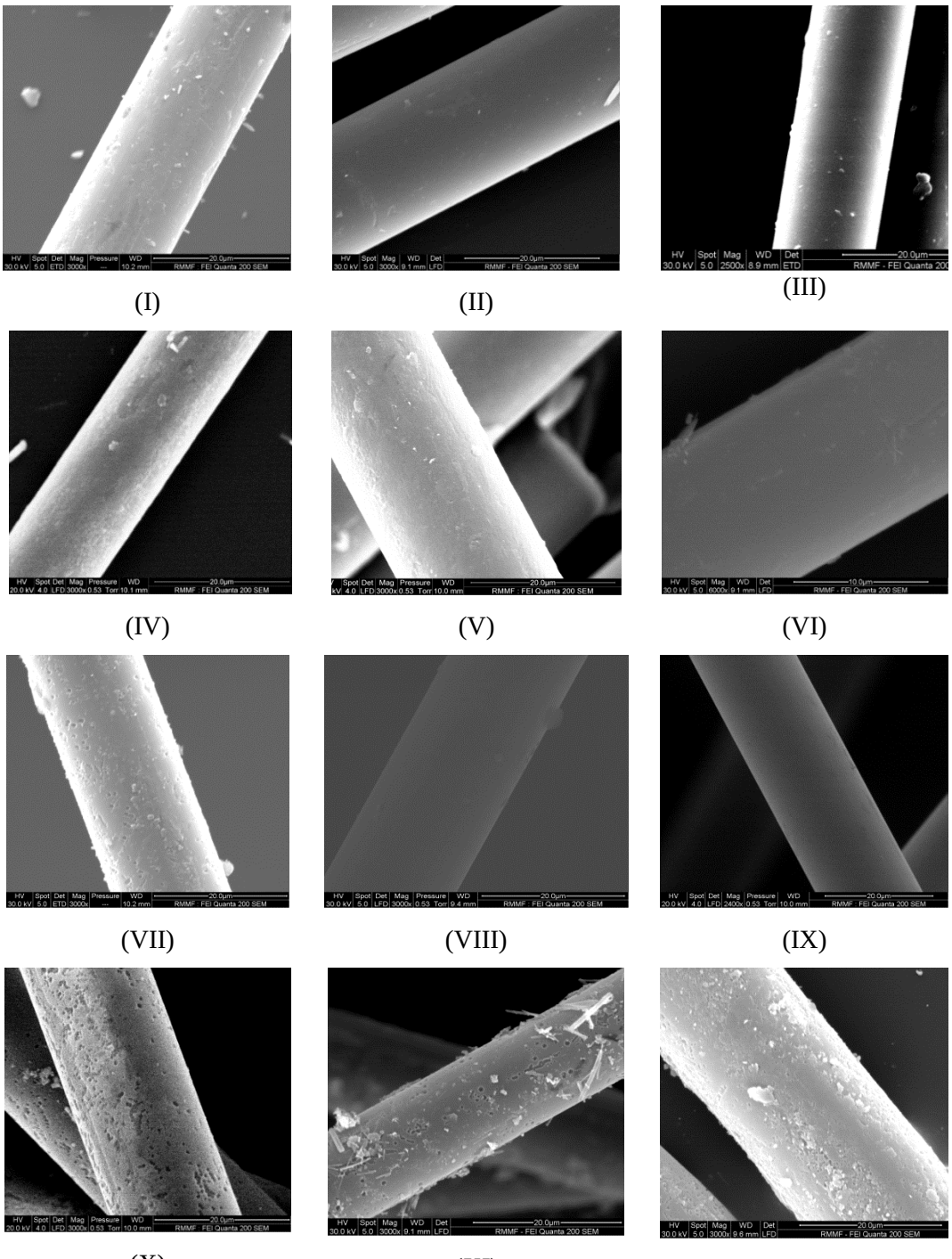

(I) (II) (III)

(IV) (V) (VI)

(VII) (VIII) (IX)

(X) (XI) (XII)

Figure 3-6: SEM images of the effect of immersions in different chemicals on Group A basalt fibers (Table 3.4 is referred for solution number)

Hydrocarbon network linkage with fiber exhibit increased interfacial bond even in strong alkaline solution. At room temperature, base is not strong enough to deprotonate the molecules as it decreases the reaction rate with hydroxyl ion. This is the reason in the solid state where NaOH and cross linked network of silane and fiber cannot be fused together at room temperature. From figure 3-6 (I), (IV), (V) and (VI), it can be seen that surface of basalt fiber is slightly rough. The surface of Group A fiber may slow down the diffusion of OH^- ions.

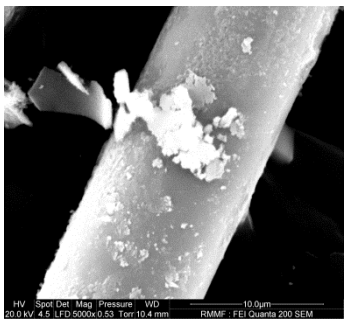

(I)

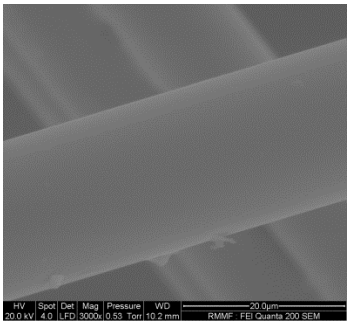

(II)

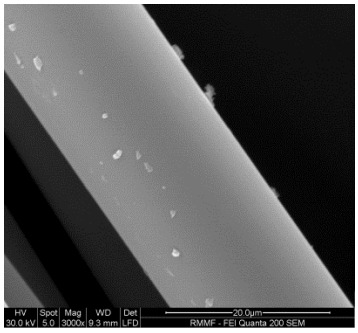

(III)

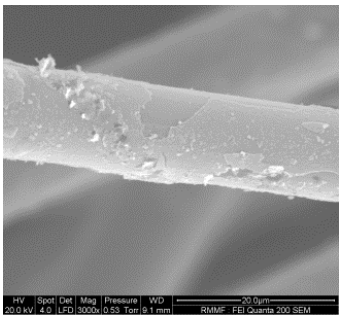

(IV)

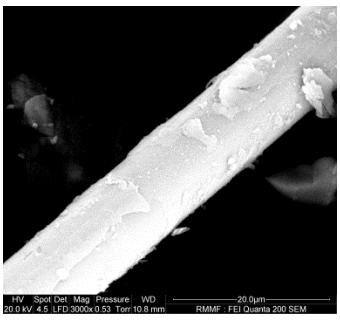

(V)

(VI)

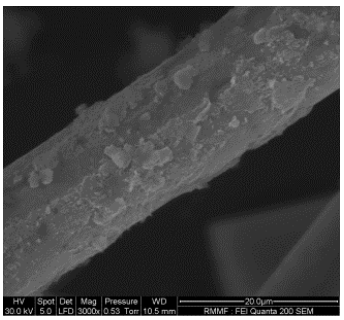

(VII)

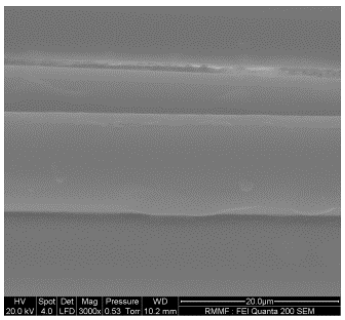

(VIII)

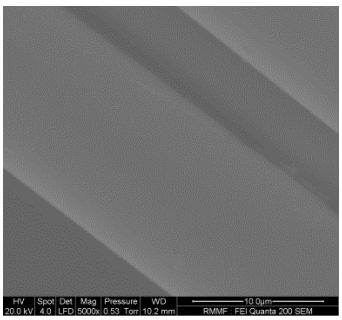

(IX)

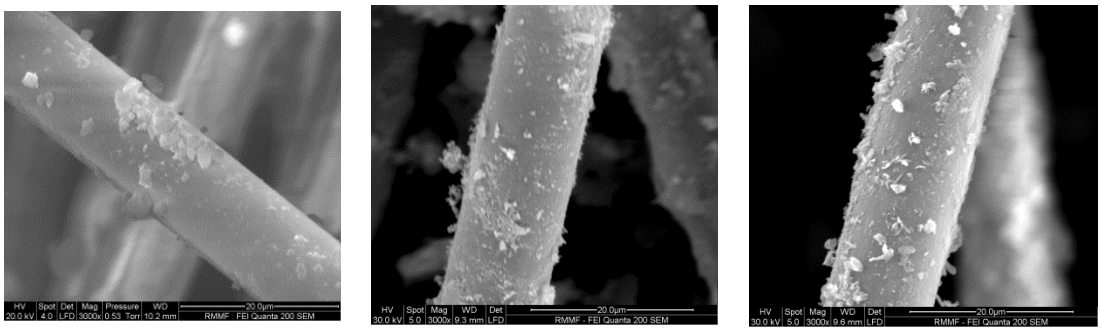

(X) (XI) (XII)

Figure 3-7: SEM images of the effect of immersions in different chemicals on Group B basalt fiber (Table 3.4 is referred for solution number)

On the other hand, figure 3-6 (VII), (X), (XI) and (XII), it appears that surface roughness increase with the presence of cavities which very likely play a major role in the intra particle diffusion and degradation. In a typical OH^- adsorption experiment, it can be seen that the affinity of silica results from the ability of the large cations to lose their water of hydration and form polar bonds with the structural oxygen of silica (Papirer, 2000). Among Na^+ and Ca^{2+} cations, deterioration is greater for the larger, less hydrated cations Ca^{2+} than for the smaller ions Na^+. However, in case of dense and homogeneous coating, pores can only be present at outer part (Zomorodian et al., 2012).

From the figure 3-7 (I), (IV), (V) and (VI), it can be seen that surface of basalt fiber not only have cavity but also crack. Figure 3-7 (VII), (X), (XI) and (XII) also show the irregular damaged surface. This mainly weakens the original lattice bonds by forming weak hydroxyl ion bonds with silicon atoms on the surface.

3.4.3.3 Energy dispersive analysis of X-ray (EDX)

To highlight the mechanism of ion exchange, EDX analyses were carried out before and after effect in NaOH and $Ca(OH)_2$ solutions following 62 days by comparing the peaks intensity of exchangeable ions. The respective EDX micrographs are presented in Figure 3-8 and 3-9.

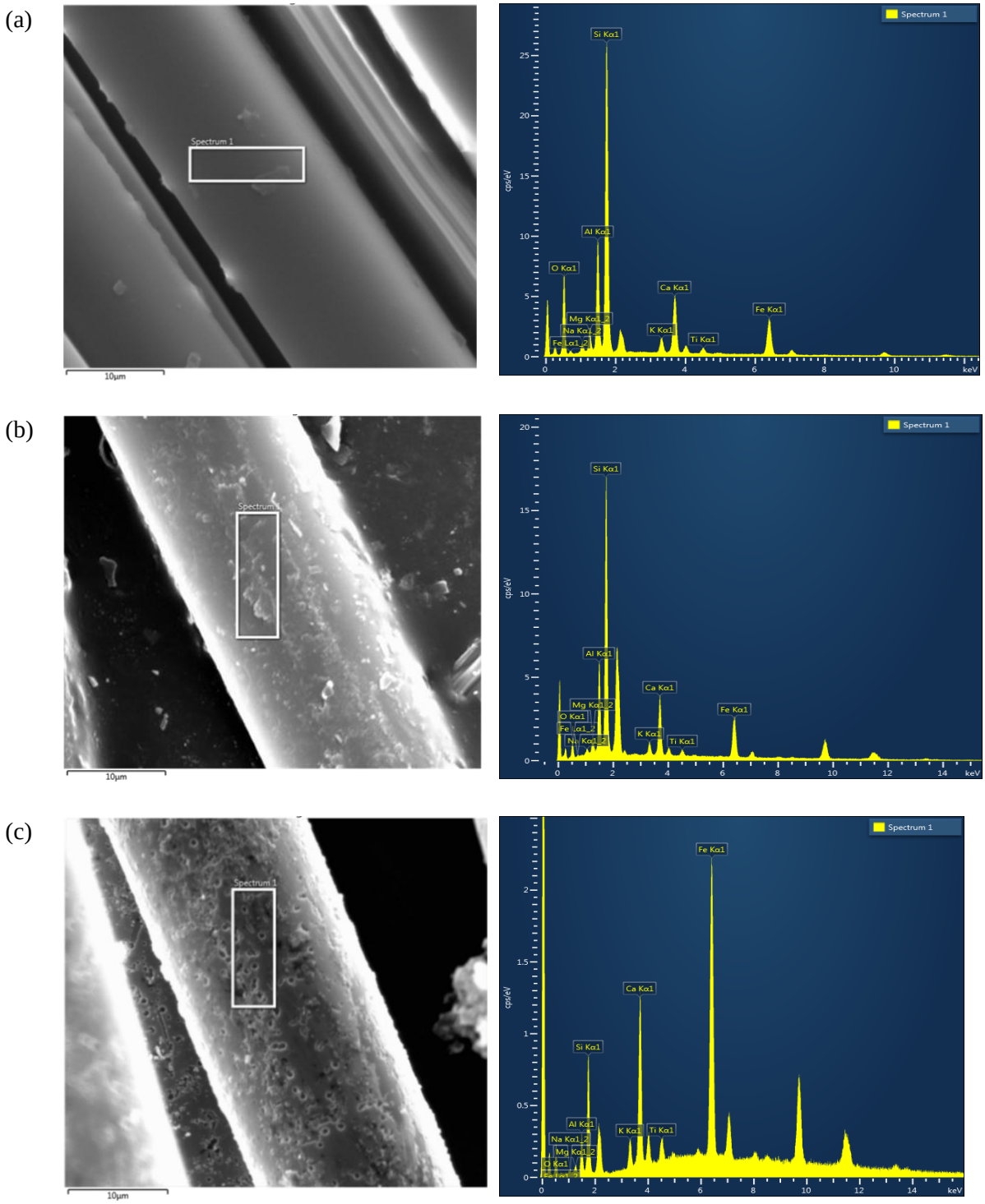

Figure 3-8: Energy dispersive X-ray (EDX) analyses of Group A fiber (a-Before treatment; b-After 62 days 1M NaOH treatment; c-After 62 Days 1M $Ca(OH)_2$ treatment)

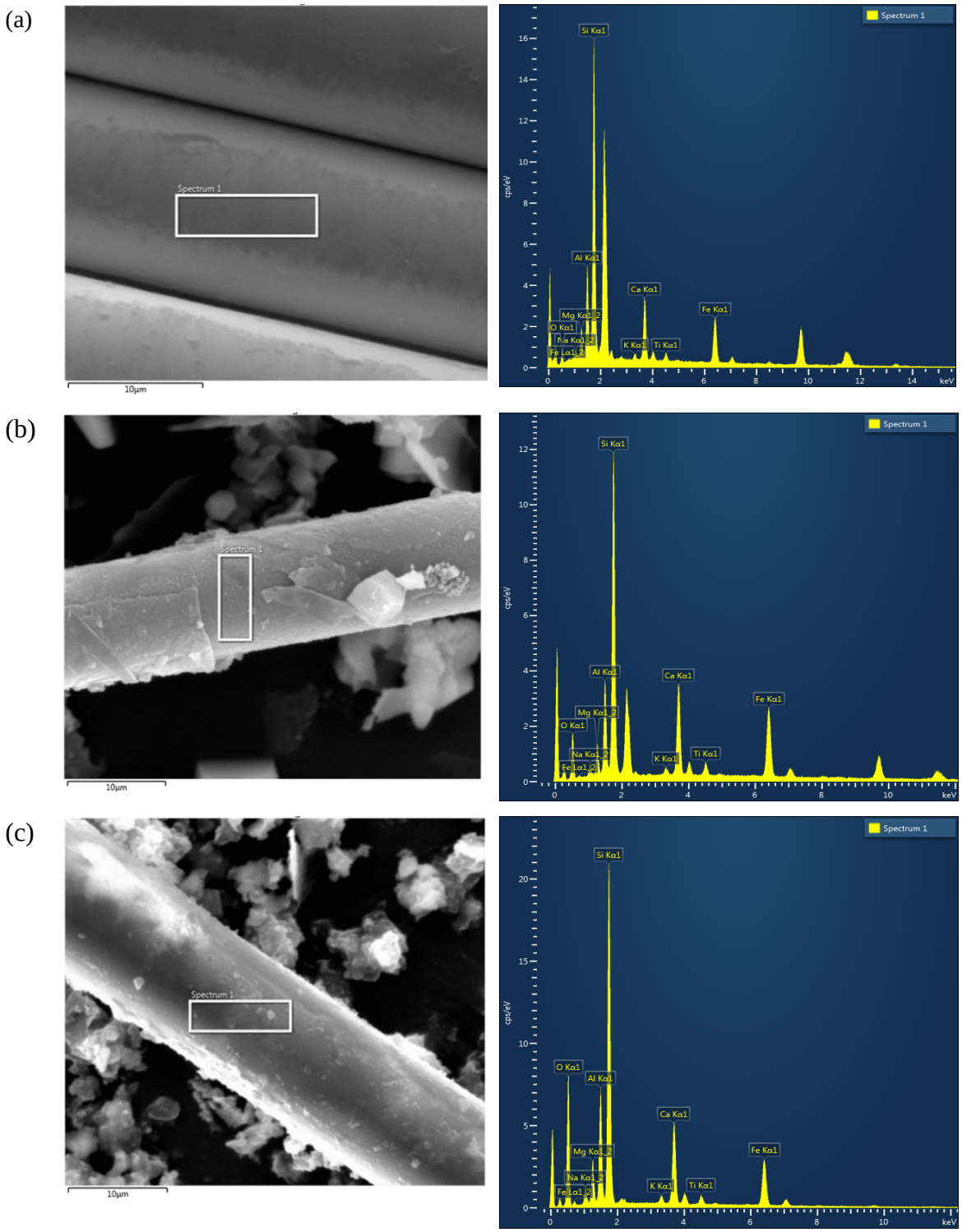

Figure 3-9: Energy dispersive X-ray (EDX) analyses of Group B fiber (a-Before treatment; b-After 62 days 1M NaOH treatment; c-After 62 Days 1M $Ca(OH)_2$ treatment)

According to the analysis, the basic exchangeable cations of fibers are Si, Ca, Fe, Al, Mg, Ti ions. While it can be inferred the importance of cations, expecially the peaks of Si, Al, Fe and Ca ions. More details of the chemical composition of the fibers are presented in Table 3.5. The concentration of the basic elements like silicon and aluminium is decreased. In contrast, the intensities of iron and calcium increase for these fibers. It becomes apparent by SEM analysis that fiber in alkaline is composed of two layers, i.e., corrosion layer and core material.

Modified basalt fiber in $Ca(OH)_2$ solution, presents small pores where corrosion product iron accumulates (Figure 3-8 (c)). The results indicate high-level concentration of calcium and iron and reduced concentration of silicon and aluminum in comparison with those for as supplied basalt fiber. The high iron concentration on the surface can be in favor of the fact that the internal corrosion layer is composed of iron oxy-hydroxides, and/or iron hydroxocarbonates. Crystallization of iron oxy-hydroxides takes place in strong alkali media (Rybin et al., 2013, Mohapatra and Anand, 2010).

Table 3.5: EDX analysis of fiber surface composition (wt%)

Component	Group A			Group B		
	Control	NaOH	$Ca(OH)_2$	Control	NaOH	$Ca(OH)_2$
Si	26.51	26.18	8.71	26.36	23.73	24.88
O	45.74	45.20	31.59	45.28	43.58	44.95
Al	9.65	9.16	3.92	8.04	7.66	7.78
Fe	6.47	8.44	39.67	8.32	10.79	9.07
Ca	5.32	6.02	10.63	5.79	7.15	6.27
Mg	2.47	1.90	0.96	3.29	3.23	4.11
K	1.33	1.23	1.76	0.57	0.51	0.56
Na	1.86	1.06	0.81	1.41	2.15	2.57
Ti	0.64	0.81	1.94	0.95	1.21	0.85

3.4.4 Mass retention

In order to evaluate the chemical durability, basalt fibers were immersed in different chemicals for a period of 62 days. There were two sorts of fiber groups. Twelve different treatments were applied for every one considering concrete medium. From the graph (Figure 3-10), calcium hydroxide and compound of calcium salt indicates lower mass retention than sodium hydroxide and its compounds. Maximum weight loss was detected around 30% for $Ca(OH)_2$ solutions. This may be due to the presence of pores, which may allow aqueous solution to permeate into and breakdown the silicon linkage.

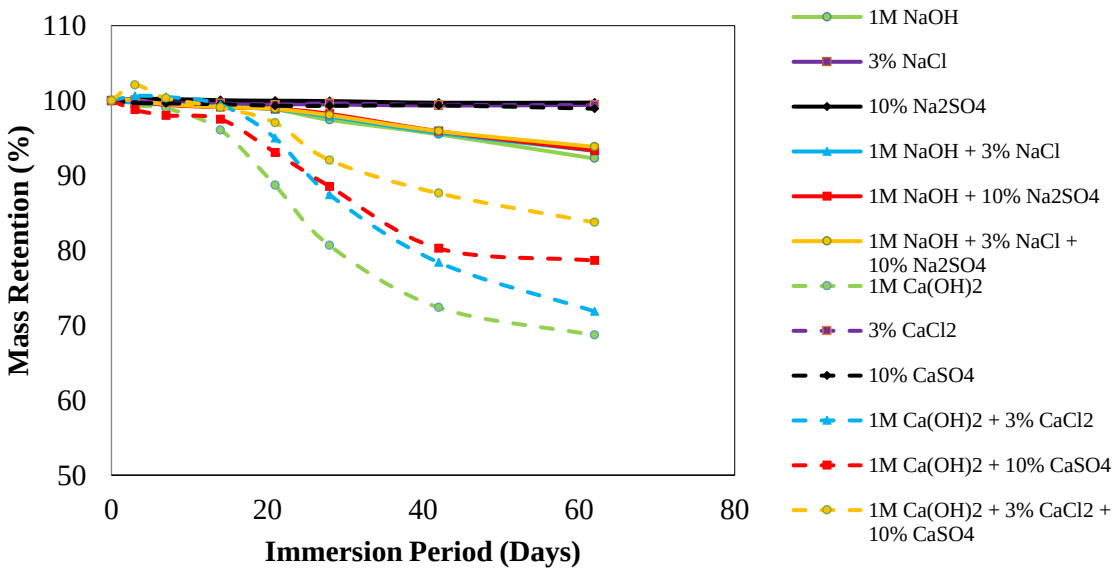

Figure 3-10: Mass retention of different treatment conditions of Group A.

On the other side, initial mass was increased for Group B fiber when treated with $Ca(OH)_2$ and its combinations with salts (Figure 3-11). Two factors mainly influence in this circumstances i.e., solution saturation condition and fiber balling effect. The weight loss was around 10.5% at the end of 62 days for NaOH with NaCl. There is no substantial difference between Group A and Group B fibers in salt solutions.

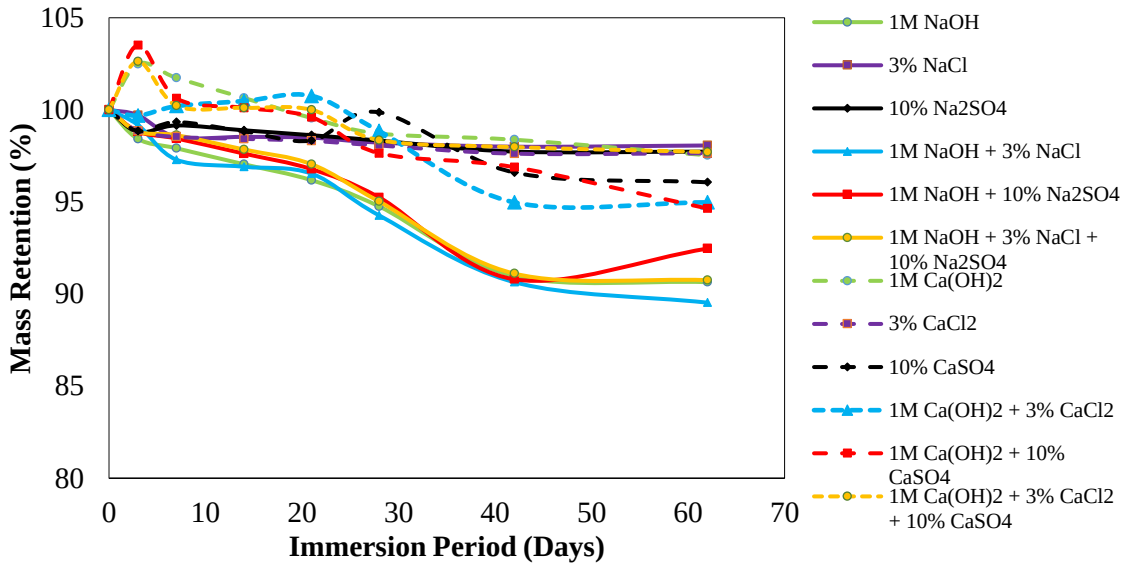

Figure 3-11: Mass retention of different treatment conditions of Group B

3.5 Conclusions

As a result of this study, it is identified that silane modified basalt fibers have long term suitable properties to be used in concrete as fiber reinforcement even in severe environment. Further findings of this study are summarized below:

(1) Basalt fibers are long term compatible reinforcement fibers for chloride and sulphate solutions.

(2) At room temperature, pH measurement after 62 days also confirms the stability of modified basalt fibers than non-modified basalt fiber in alkaline medium.

(3) $Ca(OH)_2$ solution damaged the texture of fiber which is more brittle and have cavity than with NaOH solutions for Group A fibers at room temperature. As a result, the mass of basalt fiber diminished around 30% in solution by immersion time of 62 days. However, $Ca(OH)_2$ makes a non-smooth surface on the fibers which can give better interlocking amongst concrete matrix.

(4) Group B fibers show weakened surface in all alkaline solutions by debonding original lattice bond of silicon atoms and created fiber ball. The deterioration rate is more in NaOH solutions than $Ca(OH)_2$.

(5) From the mass retention test, it appears that in absence of coating (Group B fiber) may give better results in terms of mass loss because of the creation of fiber ball in alkaline solution. However, physiochemical analysis showed that the coating is a good protective in considerable alkaline ion. The results obtained in the present work reveal that surface conditioning process is a key step to achieve the required anti-degradation properties of fibers for concrete medium. Only based on mass retention test, it may be inappropriate to determine the long term durability. Consequently, due to balling effect, this sort of fiber has probability to show reduced mechanical properties of concrete.

(6) The deterioration also depends upon the pH value, contact period, concentration, and surface of area exposed and presence of coating materials etc. The long term (62 days) mass deterioration rate for coated basalt fiber in extreme alkaline solution is comparatively low.

Chapter 4 Effect of hybrid fibers on the development of HVFA cement mortar

4.1 Introduction

The use of high strength concrete production by high volume ultra-fine fly ash (UFFA) or raw fly ash (RFA) has been documented by many researchers. These works have demonstrated strength development, water permeability, alkali-silica reaction resistance, sulphate attack and chloride-ion penetration (Solis et al., 2010, Langley et al., 1989). The incorporation of fibers mainly increases the flexural, tensile and impact strength, ductility and flexural toughness in mortar or concrete (Solikin et al., 2011, Gutierrez et al., 2005, Ghazy et al., 2016). Many researchers have focused on the uses of several fibers (glass, steel, synthetic, natural fibers etc.) in mortar and/or concrete by applying different types of load. Several studies have shown that HVFA cement concrete has good mechanical and durability characteristics owing to the incorporation of fibers (Sevil et al., 2011, Dawood and Ramli, 2010, Wang, 1990, Malhotra et al., 1994). Hybrid fiber reinforcement in cementitious materials have been used to eliminate the deficits of single fibers. Micro fibers can be added to enhance pre peak mechanical characteristics by delaying the formation of micro cracks. Moreover, it is advantageous in arresting macro cracks and conveying ductility to the specimen (Peled et al., 2000, Topcu and Canbaz, 2007, Wu et al., 2013). Although literature references are available for two fibers hybridization in HVFA concrete, their basic properties of different fibers are not well understood and the investigation of triple fiber usage is still limited.

Therefore, three different fibers (steel, polypropylene and basalt) are considered in this study. Steel fiber (ST) has a higher modulus of elasticity and flexural rigidity. It also has excellent potential for crack control while polypropylene fiber (PP) has the capacity to strengthen brittle

cementitious materials and to retain heat for a prolonged time which leads to improved toughness and delays early cracks (Sahmaran and Yaman, 2005, Banthia and Nandakumar, 2003, Lawler et al., 2003). Natural inorganic basalt fiber (BF) is an eco-friendly, nontoxic, lightweight and low cost material. It shows improved strength, modulus and strain, high stability and resistance of high temperature. It shows better performance in the hybrid form than individual usage (Huang and Deng, 2009). However, basalt fiber is not sufficiently durable in alkaline medium, which happens in construction involving concrete material (Lee et al., 2014, Jiang et al., 2014, Dhand et al., 2014). Furthermore, basalt fibers modified with silane coating have long term durability capacity in concrete medium (Afroz et al., 2017). Hence, this low cost silane coated natural fiber can be used in hybrid combination without compromising the mechanical and durability properties of high strength high volume fly ash concrete.

Thus the combination of these three fibers may provide reasonable improvements on the overall performance of HVFA cement composite and negate some of the disadvantages of single or two fibers. Therefore, these three fibers were chosen for further analysis. It is noted that artificial neural network (ANN) has been used to solve several civil engineering problems for years because of its ability to mimic natural behaviour. Moreover, it can produce a correct or nearly correct response to incomplete data and produce generalized results for new cases. These abilities allow ANN to be an extremely useful method for solving problems that are complex and have no direct correlation or insufficient information (Açikgenç et al., 2015). Studies in the literature have proven that the ANN is also successful in learning and predicting concrete properties (Nazari and Riahi, 2011, Hossain et al., 2016, Uysal and Tanyildizi, 2012, Prasad et al., 2009). Many researchers have worked on developing accurate cement composite properties & prediction models. It is noted that regression analysis has been used to solve strength analysis of concrete and produce generalized results for new concrete mixes (Atici, 2011, Sarıdemir, 2009, Tabatabaeian et al., 2017, Song and Hwang, 2004). Artificial neural network and regression analysis technique has been used to predict the strength properties of HVFA cement mortar for different fiber mix proportions.

Since mortar is a main component within concrete formation and exhibits typical homogenous properties, the mechanical characteristics of mortar are investigated first instead of concrete.

This chapter investigates the compressive strength and flexural strength properties of single and hybrid fiber HVFA mortar and the validation of neural network and prediction equations by using experimental data. Furthermore, to investigate the durability of basalt fiber, SEM analysis has been used in HVFA cement mortar. Following sections of this chapter are partially published in Journal of Building and Construction Materials, Vol. 215 (2019), pages 984–997.

4.2 Materials and mix proportions

4.2.1 Materials

As per AS 3972 type GP (AS, 2010) & AS 3582.1-1998 (AS, 1998), Ordinary Portland Cement (OPC) and Gladstone fly ash (FA) class F were used in this study. The RFA and UFFA with a specific gravity of 2.35 and 2.20 were obtained from Cement Australia Pty Ltd and Flyash Australia respectively. The RFA had 80% fineness passing 45μm sieve and UFFA has 99% fineness. Both the fly ashes maintain specified requirements of AS3582.1-1998(AS, 1998). UFFA has a nominal median particle size of 3.5 μm where a typical median particle diameter of raw fly ash varies 10 to 50 μm. Specific gravity of OPC was 3.16. The chemical analysis of OPC and fly ashes are shown in Table 4.1.

Table 4.1: Chemical compositions (%wt) of cementitious materials

Materials	Chemical compositions (%wt)											
	SiO_2	Al_2O_3	Fe_2O_3	CaO	MgO	K_2O	Na_2O	TiO_2	P_2O_5	Mn_2O_3	SO_3	LOI
OPC	19.90	4.62	3.97	64.27	1.73	0.57	0.15	0.23	--	0.06	2.56	--
RFA	51.10	25.70	12.50	4.30	1.50	0.70	0.80	1.30	0.90	--	0.20	0.60
UFFA	70.70	20.70	3.90	1.13	0.77	1.09	0.26	0.92	0.15	0.05	--	0.70

Fine aggregates used in experiment were in saturated surface dry (SSD) condition. The specific gravity of river sand was 2.65. All the samples were prepared by using 50% fly ash as cement replacement. Mortar mixes were prepared by polycarboxylic ether based water reducer (WR) which is commercially known as Master Glenium SKY 8379 by BASF, Australia. To achieve early strength, saturated lime water was mixed in HVFA composites (Figure 4-1) (Solikin et al., 2013).

Figure 4-1: Lime water

Basalt fibers were supplied by Kamenny Vek Ltd, Dubna, Moscow, Russia. Polypropylene and steel fibers were obtained from Fibercon and One Steel Reinforcing, Australia respectively (Figure 4-2).

(a) Steel (b) Polypropylene (c) Basalt

Figure 4-2: Fibers used in this experiment

Silane coated modified basalt fiber was used in this work to inhibit the deterioration in concrete medium (Afroz et al., 2017). Three types of fibers were used in 0.5, 1.0, 1.5, 2.0 and 2.5 percent of volume fractions (Vf) with single and hybrid fibers in HVFA cement mortar. Fiber properties are presented in Table 4.2. Due to the long fiber length (47 mm) for mortar sample, each polypropylene fiber was cut into two pieces (23.5 mm).

Table 4.2: Fibers properties

Properties	ST	PP	BF
Avg. Dia (mm)	0.16	0.80	0.02
Avg. Length (mm)	18.5	23.5	25
Specific gravity (g/cm^3)	7.80	0.97	2.61
Tensile Strength (MPa)	2500	500	4100
Melting Point (^{o}C)	1510	160-170	1500

4.2.2 Mix proportions

The mortar mix proportions are shown in Table 4.3. Total of sixty (60) mixes were cast by water-binder ratio of 0.3. Two sets of mix design were carried out for RFA and UFFA cement composites. Cement, fly ash and water amount were 275, 275 and 165 kg/m^3 respectively for all mix proportions. For proper flowability of mortar mixes, super plasticizer was altered from 1.0% to 1.5% by weight. All mixtures corresponded to the method proposed for high performance concrete by Aïtcin (1998).

Table 4.3: Fiber percentage used in mix proportions of cement mortar

Mix No.	Fiber (%)	Index	ST (%)	PP (%)	BF (%)	Sand (kg/m^3)	WR (%)
1.	0.0	C	0.00	0.00	0.00	1632	1.2
2.		CU				1610	1.0
3.	0.5	S1	0.50	--	--	1618	1.2
4.		SU1				1597	1.0
5.		P1	--	0.50	--	1618	1.2
6.		PU1				1597	1.0
7.		B1	--	--	0.50	1618	1.5
8.		BU1				1597	1.3
9.	1.0	S2	1.00	--	--	1605	1.2
10.		SU2				1584	1.0
11.		P2	--	1.00	--	1605	1.2
12.		PU2				1584	1.0
13.		B2	--	--	1.00	1605	1.5
14.		BU2				1584	1.3
15.	1.5	S3	1.50	--	--	1592	1.2
16.		SU3				1571	1.0
17.		P3	--	1.50	--	1592	1.2
18.		PU3				1571	1.0
19.	1.5	D1	1.00	0.50	--	1592	1.2
20.		DU1				1571	1.0
21.		D2	1.00	--	0.50	1592	1.5
22.		DU2				1571	1.3
23.		D3	--	1.00	0.50	1592	1.5
24.		DU3				1571	1.3
25.	2.0	D4	1.50	--	0.50	1579	1.5
26.		DU4				1557	1.3
27.		D5	1.50	0.50	--	1579	1.2
28.		DU5				1557	1.0
29.		D6	--	1.50	0.50	1579	1.5
30.		DU6				1557	1.3
31.	2.5	D7	1.50	--	1.00	1565	1.5
32.		DU7				1544	1.3
33.		D8	1.50	1.00	--	1565	1.2
34.		DU8				1544	1.0
35.		D9	--	1.50	1.00	1565	1.5
36.		DU9				1544	1.3

37.	1.0	T1	0.50	0.25	0.25	1605	1.2
38.		TU1				1584	1.0
39.		T2	0.75	0.13	0.13	1605	1.2
40.		TU2				1584	1.0
41.	1.5	T3	0.50	0.50	0.50	1592	1.5
42.		TU3				1571	1.3
43.		T4	1.00	0.25	0.25	1592	1.5
44.		TU4				1571	1.3
45.		T5	0.75	0.50	0.25	1592	1.5
46.		TU5				1571	1.3
47.		T6	0.75	0.25	0.50	1592	1.5
48.		TU6				1571	1.3
49.	2.0	T7	1.00	0.50	0.50	1579	1.5
50.		TU7				1557	1.3
51.		T8	0.75	0.75	0.50	1579	1.5
52.		TU8				1557	1.3
53.		T9	0.75	0.50	0.75	1579	1.5
54.		TU9				1557	1.3
55.	2.5	T10	1.00	0.75	0.75	1565	1.5
56.		TU10				1544	1.3
57.		T11	1.50	0.50	0.50	1565	1.5
58.		TU11				1544	1.3
59.		T12	1.00	1.00	0.50	1565	1.5
60.		TU12				1544	1.3

Note: i) The letter 'U' in the index refers tp ultra-fine fly ash mortar; ii) Index without 'U' refers to raw fly ash mortar. C= Control RFA; CU= Control UFFA; S= Single steel RFA; SU= Single steel UFFA; P= Single polypropylene RFA; PU= Single polypropylene UFFA; B= Single basalt RFA; BU= Single basalt UFFA D= Double fiber RFA; DU= Double fiber UFFA; T= Triple fiber RFA; TU= Triple fiber UFFA.

Generally, optimum fiber percentage for hybrid fiber reinforced HVFA concrete lies in between 1.5 and 2.5% (Ahmed et al., 2006, Chen and Liu, 2003). In combination of two types of fibers, the maximum chance for any fibers use will be in the range of 0.5 to 1.5%. This is the reason to select the different fiber percentage in this manner.

4.3 Methodology

4.3.1 Experimental method

Fly ash, cement and sand were first mixed for 2–3 min. Then, all the fibers were added gradually. The super plasticizer was mixed with the lime water before adding into the mixture. Flow tests were executed consistent with ASTM C230 [36], where the target flow of mixes was 160 mm ± 10 mm (Figure 4-3).

Figure 4-3: Flow test

The mortar specimens were left at room temperature for around 48hr before demoulding and water curing. At least three specimens were cast for all mixes. The compressive strength tests were carried out at different ages (14, 28 and 56 days) as per ASTM C109 (ASTM, 2002a). Flexural tests were completed on 160 x 40 x 40 mm prisms at ages 14, 28 and 56 days by using ASTM C348 (ASTM, 2002b) (Figure 4-4).

Figure 4-4: HVFA Cement mortar specimens

Figure 4-5: Compressive Strength test

Figure 4-6: Flexural Strength test

Hydraulic compression testing machine (300 kN capacity) was used to measure compressive strength of 50 mm mortar cube (Figure 4-5). For flexural test, Universal Electromechanical

Testing machine (50 kN capacity) was used for mortar samples. Axial displacement was measured using testing machine and two lasers linear variable displacement transducer (LVDT) for three point loading (Figure 4-6).

The outcomes from the tests were further analyzed to obtain a measure of the flexural toughness of the hybrid composition by using Japanese standard recommendations (JSCE). Indeed, in the ASTM C1018 procedure, it is difficult to objectively identify the exact location of the first crack on the curve, which affects the calculation of the toughness indices. As compared to the ASTM procedure, JSCE has much greater confidence in cement mortar and concrete to measure flexural toughness (AS, 2014b, AS, 1985c). The flexural toughness factor as determined by the JSCE recommendations is then calculated using Eq. (4.1):

$$\sigma_b = \frac{T_b}{\delta_{tb}} \times \frac{l}{bh^2} \quad (4.1)$$

Where,

$\sigma_b =$ Flexural toughness factor (N/mm^2)

$\delta_{tb} =$ Mid span deflection of the beam (mm), it is variable and consider here δ_{tb} = l/150, l/100, l/50.

$T_b =$ The area under the load–deflection curves up to a limited deflection of δ_{tb} (N.mm)

$l =$ Span length (mm)

$b =$ Width of the beam (mm)

$h =$ Depth of the beam (mm)

4.3.2 Analytical prediction

4.3.2.1 Artificial Neural Network (ANN)

Although each component of fiber reinforced cement composites can influence strength properties, main concern was to keep the strength variation due to different fiber volume fractions in RFA and UFFA cement mortar. Therefore, in this approach, the flexural strength is a function of the following six (6) input features, such as, compressive strength, RFA, UFFA, ST, PP and BF volume fractions. The presence or absence of two types of fly ash was indicated by using number one (1) or zero (0) respectively. In this study, the ANN toolbox (nntool) in the

program MATLAB was used to perform the necessary computations. The back-propagation algorithm, which is one of the most widely used algorithms for a multilayer perceptron, is a gradient descent technique that minimizes the error for a particular training pattern in which it adjusts the weighting by a small amount each time. In this study, the momentum rate and learning rate were determined and the model was trained through multiple iterations.

A data base of 60 average mortar mixes was considered, each containing the six components for the input vector and one output value was flexural strength. To test the reliability of the methodology, all of the records were combined and simply shuffled using random sampling, dividing them into training and testing groups. Four different models with varying mix proportions were considered for predicting the flexural strength of HVFA cement mortar using the ANN approach (Table 4.4). The training, validation, and testing phases employed 70%, 15%, and 15% of the total training data set (selected randomly), respectively. The numbers of training and testing examples for these experiments are listed in Table 4.4.

Table 4.4: Training and testing data set

ANN Analysis	Training Set	Test Set	Number of training examples	Number of testing examples
A1	Random 4/5	Rest 1/5	48	12
A2	Random 4/5	Rest 1/5	48	12
A3	Random 4/5	Rest 1/5	48	12
A4	Random 4/5	Rest 1/5	48	12

Number of hidden layer neurons and output layer neurons used in this research was 10 and 1 respectively. Gradient descent with momentum and adaptive learning rate technique has been considered with adaptive learning rate of 0.1 and momentum rate of 0.8. The number of epochs was 1000. The neural network considered is shown in Figure 4-7.

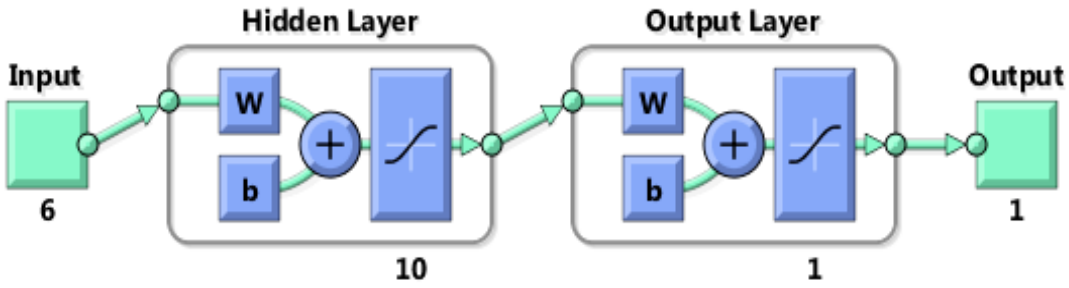

Figure 4-7: Neural network applied in this study

4.3.2.2 Regression analysis

Compressive strength (CS) and flexural strength (FS) were derived in terms of raw or ultrafine fly ash and fiber volume fractions. The key parameters such as volume fraction of ST, PP and BF in RFA or UFFA mixture are initially expressed regarding the parameters taken as shown in Eq. (4.2) and a total of 180 strength data for 60 mixes was considered. To observe the effects of individual factors on strength, time and different fiber volume fractions, simple equation formations were chosen.

$$CS_t = (ln(t) - 1) \times \prod_{j=1}^{m} {b_p}^{K_p} \quad (4.2)$$

Where K_p is the p^{th} parameter, t is number of days (14, 28 or 56 days), b_p is dimensionless exponents where b_p indicate the influence of p^{th} factor and m is the total amount of factors considered.

Eq. (4.3) is expressed by taking logarithms on both sides of Eq. (4.2).

$$\log(CS_t) = \log\big((ln(t) - 1)\big) + P_1 logb_1 + P_2 logb_2 + \cdots + P_m logb_m \quad (4.3)$$

Flexural strength follows increased pattern up to the optimum volume fraction of fibers and then decreases. Hence, the Eq. (4.4) was defined considering different fiber volume ranges to obtain a better agreement with the laboratory data.

$$FS_t = (CS_t)^{c_k} \times (d_k \ln(t) + e_k) \quad (4.4)$$

Where, *c, d and e* are dimensionless exponents and *k* is total fiber volume fractions (V_f) range.

To get appropriate coefficient values, multiple linear regression analyses were done. Objective functions were produced in the same spread sheet. To diminish the deviation of experimental and statistically predicted data, a generalized reduce gradient nonlinear data solver was used.

The square of the deviations are summarized and afterwards used to complete an ultimate solution. A comprehensive statistical data analysis was executed to propose Eq. 4.5, 4.6(a) and 4.6(b) for the key parameters of CS and FS. Once the fiber volume fraction and fly ash mix proportions are known, the strength could be determined easily by using the following equations.

$$CS_t = 4.463 \times (\ln(t) - 1) \times 0.985^{ST} \times 0.947^{PP} \times 0.732^{BF} \times 2.858^{RFA} \times 3.144^{UFFA} \quad (4.5)$$

$$FS_t = (CS_t)^{0.173} \times (0.542 \ln(t) + 2.095) \quad \text{if} \quad 0 \leq V_f \leq 1.5 \quad (4.6a)$$

$$FS_t = (CS_t)^{0.207} \times (0.744 \ln(t) + 1.501) \quad \text{if} \quad 1.5 < V_f \leq 2.5 \quad (4.6b)$$

4.3.3 SEM analysis

The diameter of a single basalt fiber is very small. It is difficult to perceive the natural basalt fiber strand in cracked surface by only naked eyes. Thus SEM analysis is required to determine the features of basalt fiber under different time periods in RFA and UFFA cement composites. The specimens extracted from the mortar cube were irregular in shape but maximum 25mm length and had an approximate thickness of 5mm. FEI Quanta 200 ESEM under RMIT Microscopy and Microanalysis Facility was used to conduct the photomicrography of HVFA cement mortar.

4.4 Results and discussions

4.4.1 Mechanical properties of mortar

4.4.1.1 Compressive strength

The compressive strength is higher for UFFA mortar in comparison with RFA cement matrix. The reactivity rate of the elements of fly ash in UFFA is higher than RFA. Because UFFA contain more particles smaller than 10 μm which are more reasonably classified as pozzolanic reactive particles [41]. Average compressive strengths for different ages are shown in Figure 4-8.

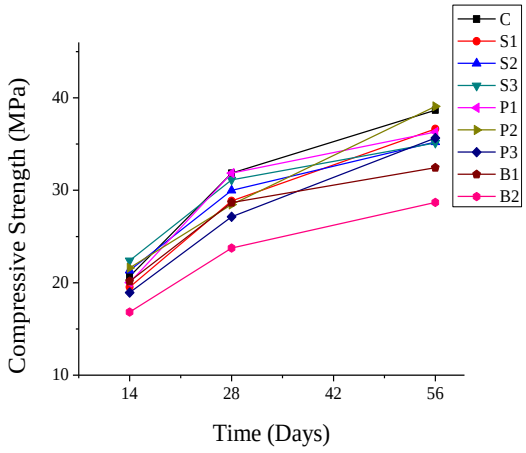

(a) Single fiber RFA mortar

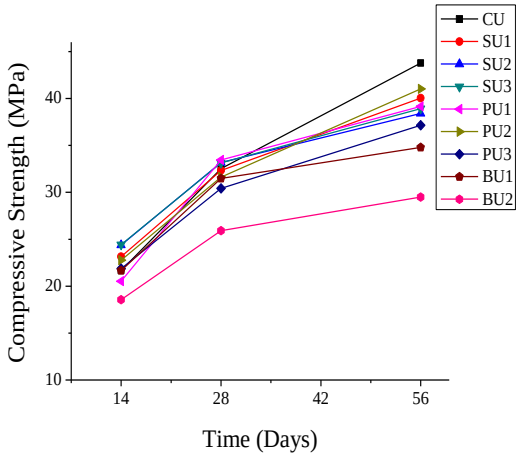

(b) Single fiber UFFA mortar

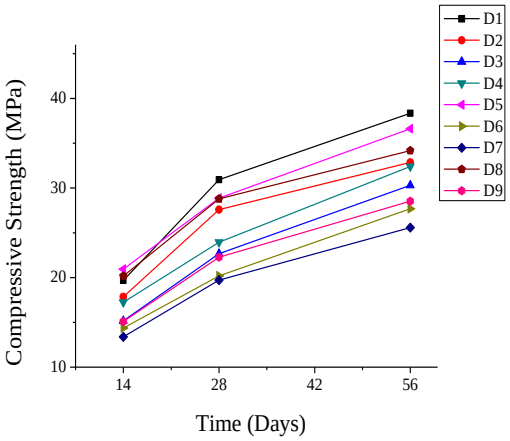

(c)Two types of fiber RFA mortar

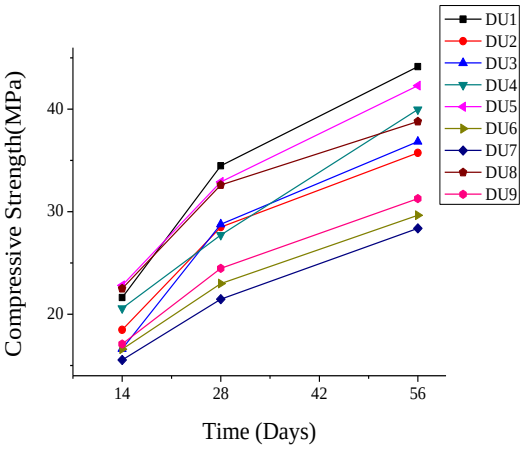

(d)Two types of fiber UFFA mortar

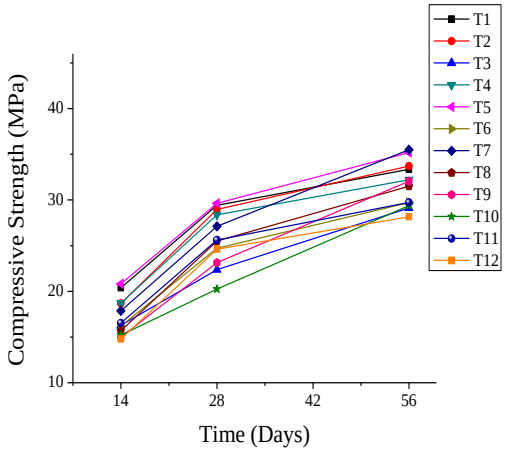

(e)Three types of fiber RFA mortar

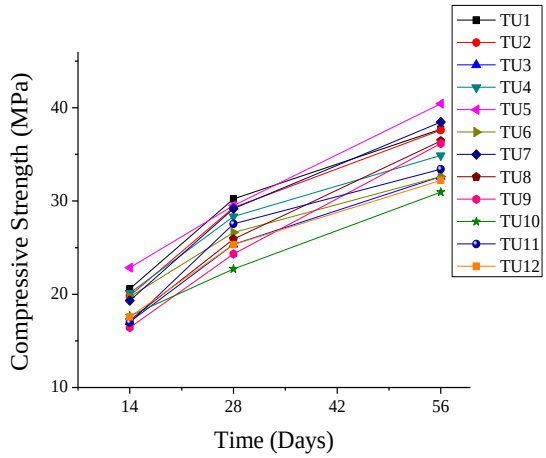

(f)Three types of fiber UFFA mortar

Figure 4-8: Average compressive strength of different volume fraction of fibers in HVFA cement mortar

In between single type fiber, for RFA and UFFA, steel and polypropylene fiber concrete had higher compressive strength than basalt fibers after 56 days of strength development.

Compressive strength increments occurred due to the better restraining of fibers and basalt fiber works good in hybrid.

In hybridization, it is confirmed that compressive strength can increase by using appropriate volume fraction of fibers combination. For two type fibers hybridization, a combination of steel and polypropylene (D1, DU1, D5, and DU5) shows increased strength than control mix (C and CU) even after 56 days. Three types of fiber mix proportions (T5, TU5 and T7, TU7) can also be found to maintain a good compressive strength in comparison to control specimens even after 56 days. Effects of basalt fibers are more prominent in a hybrid than single fiber. Because of pozzolanic fiber, basalt fiber contained SiO_2 and Al_2O_3. It also reacts with alkaline substances of cement to produce a hydrated C-S-H gel and other substances which can help the pores and cracks of the cement matrix to be effectively repaired (Punurai et al., 2018). Moreover, appropriate hybrid fiber can improve interfacial bond characteristics in between the matrix and fibers. It enhances fibers capacity to delay the initial crack development and also prevents the propagation of cracks after ultimate failure (Sahmaran and Yaman, 2005, Neves and Almeida, 2005).

4.4.1.2 Flexural properties of mortar

The flexural strengths of fiber reinforced mortar are illustrated in Figure 4-9. In one type fiber consideration, maximum increment is observed for UFFA 1.5% ST (SU3) and 1.5% PP (PU3), which is 7.05% and 4.45% more than control mix respectively.

For two-fiber hybridization cement matrices (Figure 4-9 (c and d)), overall flexural strength is increased. Maximum flexural strength increases for DU5 (1.5% steel and 0.5% PP) in comparison with the control mix and is observed to be 31.94%.

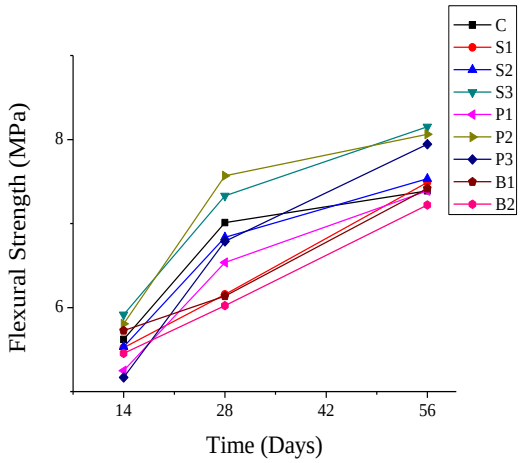

(a) Single fiber RFA mortar

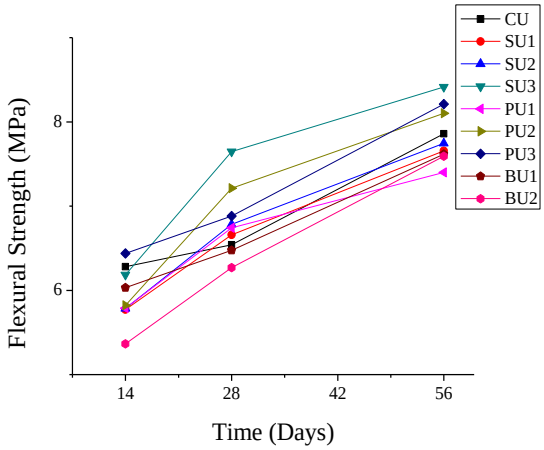

(b) Single fiber UFFA mortar

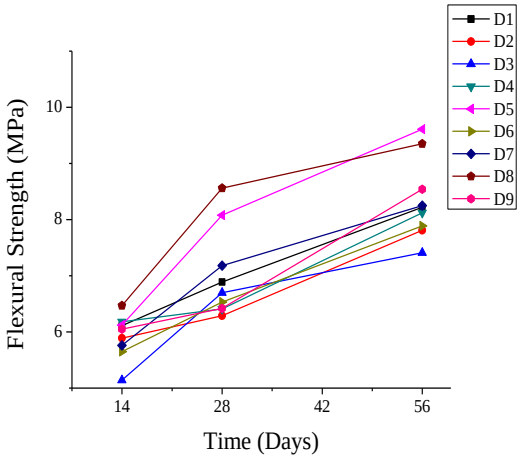

(c)Two types of fiber RFA mortar

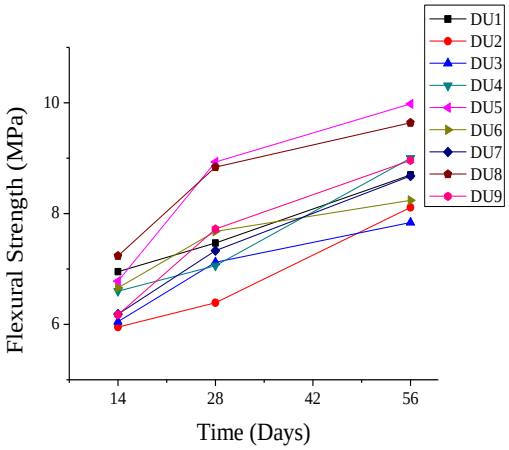

(d)Two types of fiber UFFA mortar

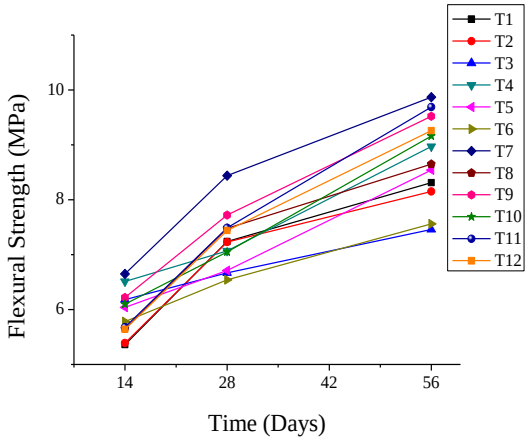

(e)Three types of fiber RFA mortar

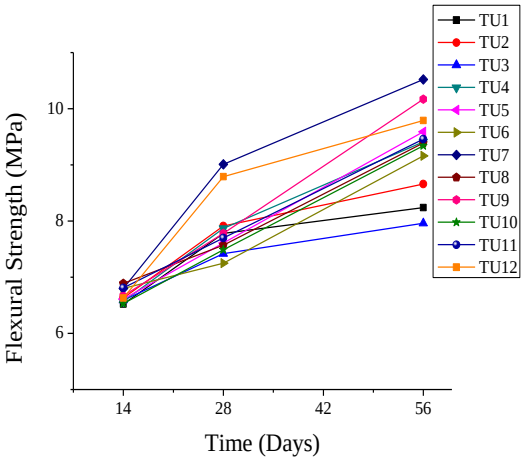

(f)Three types of fiber UFFA mortar

Figure 4-9: Average flexural strength of different volume fraction of fibers in HVFA cement mortar

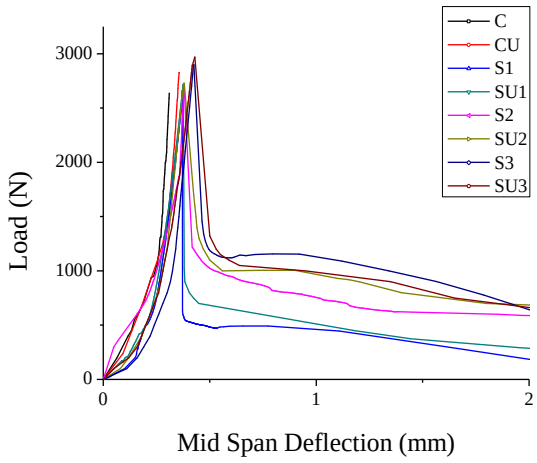

(a) Steel fiber

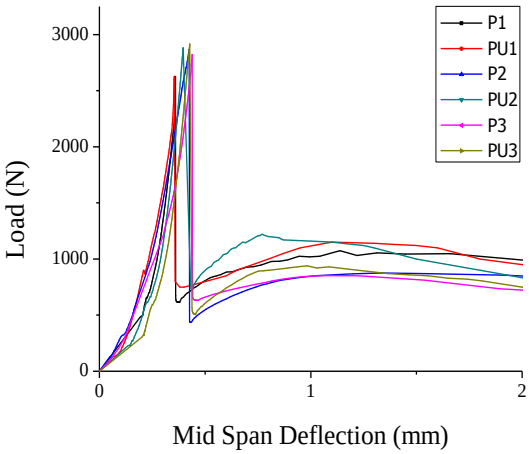

(b) Polypropylene fiber

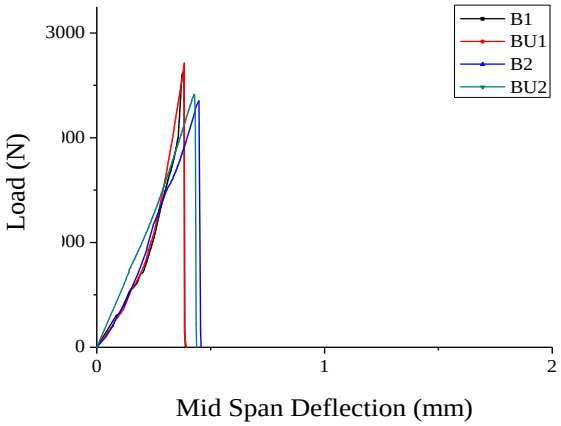

(c) Basalt fiber

Figure 4-10: Average load-deflection curves for single fiber

For three fiber hybridization (Figure 4-9 (e, f)), it is clear that appropriate fiber volume fraction of three types of fibers is a prodigious way to increase the flexural strength of HVFA cement composites. Among all three-fiber combination, maximum flexural strength can be obtained for TU7 (1.0% steel, 0.5% PP and 0.5% BF) and TU11 (1.5% steel, 0.5% PP and 0.5% BF), which was 33.84% and 33.07% higher than the control specimen respectively. The increases of flexural strength mainly depend on the higher volume fraction of steel fiber because of its better modulus of elasticity in comparison to other fibers. Moreover, an appropriate proportion of ST, PP and BF can improve flexural rigidity by enhancing the mechanical bond strength. The bridging action of more than one type of fiber across cracks is more effective to restrain the propagation of initial micro cracks. This significant improvement can also be acquired because

of the enhancement of density and toughness in hybrid fiber reinforced mortar (Sahmaran and Yaman, 2005). It also demonstrates that the early strength can be improved by using UFFA. Average load deflections for RFA and UFFA fiber reinforced HVFA cement mortar show identical curve pattern (Figure 4-10 to 4-12).

Generally the deformation capacity increase with the higher volume fraction of fibers until the fiber reached up to the optimum amount. Hybrid fibers significantly improve the deflection in comparison to the single fiber matrix because of its capability to arrest cracks at initial level and after ultimate load. In single fiber reinforced composites, the descending gradient of load deflection curve suddenly falls for a while and after that cracks propagate slowly (Figure 4-10 (a, b)). In the case of basalt fiber (Figure 4-10 (c)), it is not able to arrest the cracks after peak load and rapid breakdown takes place due to insufficient volume fraction and lower aspect ratio.

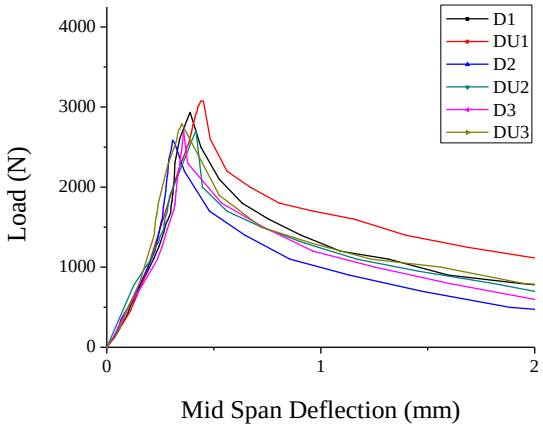

(a) 1.5% fiber volume fraction

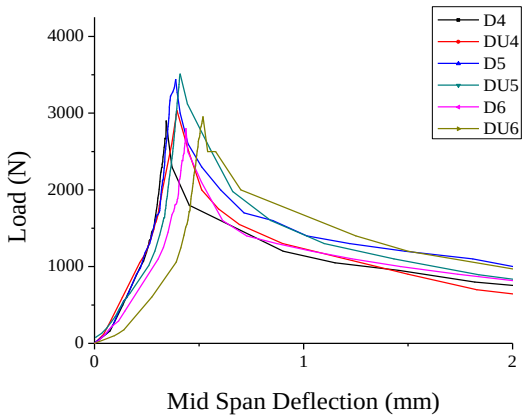

(b) 2.0% fiber volume fraction

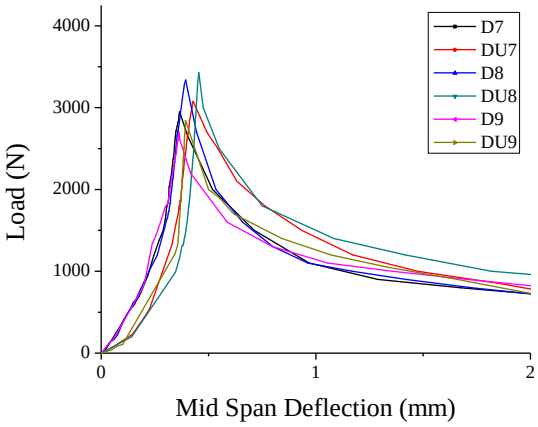

(c) 2.5% fiber volume fraction

Figure 4-11: Average load-deflection for two fiber reinforced mortar

The hybridized fibers exhibit a gradually decreasing deflection trend after the peak value (Figure 4-11 and 4-12). This is due to the fibers inhibiting the commencement of cracks and after that fiber provides bridging to increase toughness and ductility (Dawood and Ramli, 2011). Notice in Figures. 4-10 to 4-12 and Table 4.5 that maximum deflection did not increase due to hybridization of fibers.

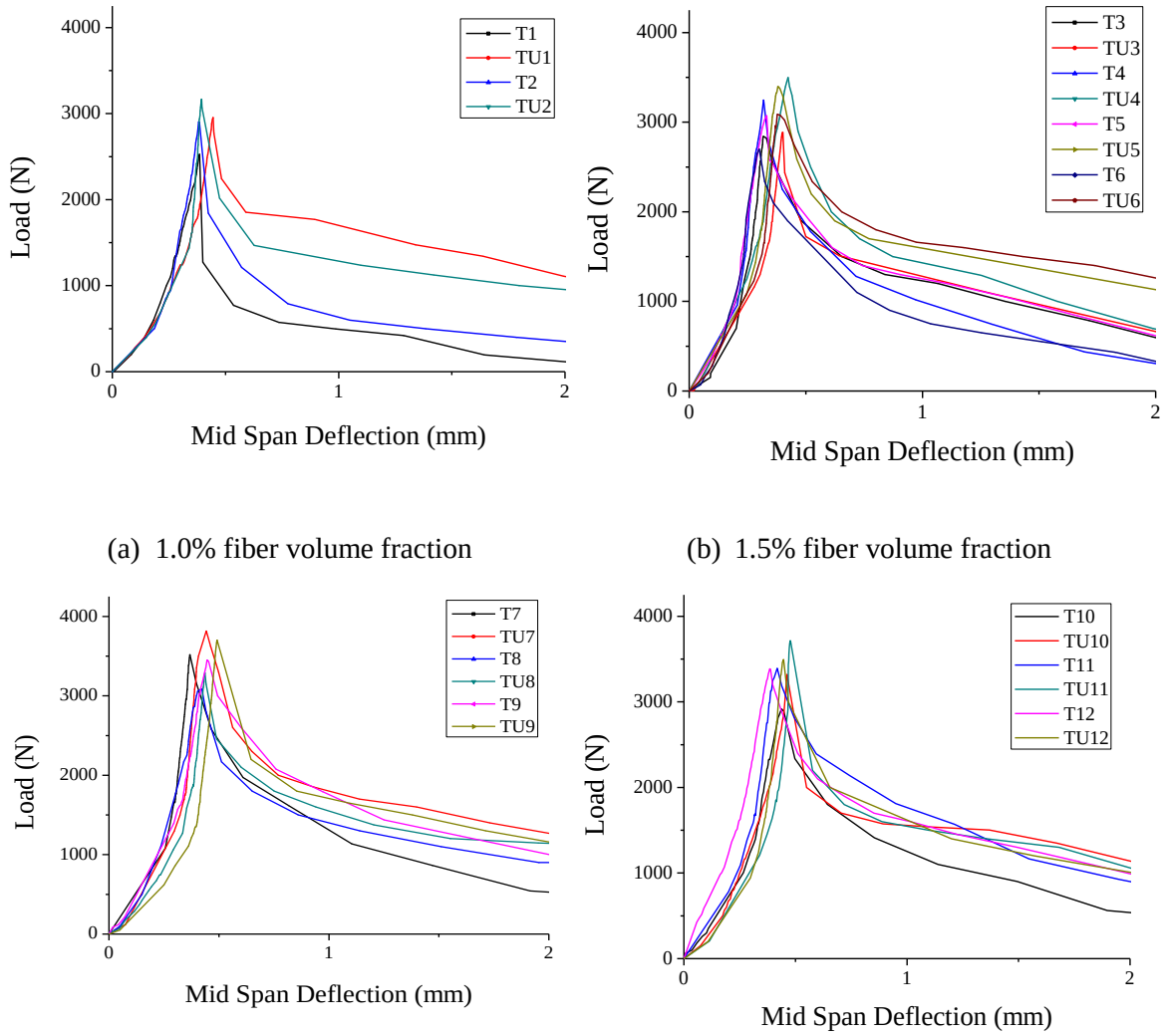

(a) 1.0% fiber volume fraction

(b) 1.5% fiber volume fraction

(c) 2.0% fiber volume fraction

(d) 2.5% fiber volume fraction

Figure 4-12: Average load-deflection for three fiber reinforced mortar

It can be seen that the toughness of the HFRM with higher steel fiber content is relatively higher than those containing less steel fibers. However, the toughness factors cannot be measured for basalt fiber reinforced mortars since they failed in a fragile way as soon as the first crack appeared. From Table 4.5, it is observed that in composites having more steel fibers with proper PP and/or BF, the amount of energy absorption increases compared to single fibers due to the

combined action of high tensile strength, length and elastic modulus of macro and micro fibers. Similarly, PP with BF hybridization can also increase the flexural toughness due to its combined effects on load deflection. Taking into account the results of flexural toughness factors shown in Table 4.5, it is concluded that the critical fibre volume is approximately 2.0% (1.0%ST+ 0.5% PP+ 0.5%BF) HU7 at the ages 56 days in comparison with other hybrid fiber reinforced cement matrices.

Table 4.5: Maximum load deflection and flexural toughness factors after 56days

Total Fiber (%)	Index	Peak Load (kN)	Max^{m} deflection (mm)	Flexural toughness factors (MPa)		
				σ_{t150}	σ_{t100}	σ_{t50}
0.5	S1	2.66	0.37	1.29	1.14	0.80
	SU1	2.72	0.38	1.39	1.26	0.94
	P1	2.62	0.36	1.29	1.48	1.63
	PU1	2.63	0.35	1.69	1.80	1.84
1.0	S2	2.68	0.37	1.98	1.77	1.44
	SU2	2.73	0.38	2.09	1.99	1.72
	P2	2.87	0.42	1.62	1.59	1.57
	PU2	2.88	0.39	1.78	1.92	1.82
	H1	2.59	0.39	1.79	1.50	0.98
	HU1	2.96	0.45	2.84	2.95	2.64
	H2	2.90	0.38	2.23	1.91	1.33
	HU2	3.17	0.39	2.59	2.52	2.20
1.5	S3	2.89	0.42	1.97	2.00	1.68
	SU3	2.97	0.43	2.25	2.11	1.76
	P3	2.82	0.44	1.69	1.64	1.54
	PU3	2.91	0.43	1.48	1.54	1.52
	D1	2.93	0.39	3.22	4.13	2.93
	DU1	3.13	0.43	3.72	3.53	2.13
	D2	2.58	0.31	2.83	2.51	1.84
	DU2	2.90	0.41	2.30	2.77	2.14
	D3	2.65	0.36	2.97	2.75	2.10
	DU3	2.79	0.34	3.03	2.80	2.24
	H3	2.84	0.32	2.84	2.65	2.02

	HU3	2.89	0.41	2.62	2.54	2.04
	H4	3.25	0.31	2.92	2.56	1.75
	HU4	3.50	0.42	3.37	3.15	2.39
	H5	3.07	0.33	3.09	2.87	2.12
	HU5	3.40	0.38	3.23	3.16	2.71
	H6	2.34	0.32	2.51	2.18	1.49
	HU6	3.08	0.38	3.19	3.19	2.85
2.0	D4	2.90	0.34	3.07	2.78	2.18
	DU4	3.03	0.39	2.96	2.75	2.15
	D5	3.43	0.38	3.36	3.15	2.58
	DU5	3.51	0.41	3.29	3.09	2.45
	D6	2.80	0.43	2.58	2.49	2.09
	DU6	2.94	0.42	2.68	2.81	2.46
	H7	3.52	0.37	3.24	3.00	2.21
	HU7	3.81	0.44	3.75	3.64	3.13
	H8	3.08	0.42	3.00	2.88	2.45
	HU8	3.29	0.43	2.92	2.96	2.70
	H9	3.44	0.44	3.49	3.42	2.79
	HU9	3.70	0.49	3.02	3.09	2.76
2.5	D7	2.97	0.36	2.95	2.67	2.08
	DU7	3.09	0.42	3.03	2.92	2.30
	D8	3.33	0.39	3.04	2.75	2.12
	DU8	3.43	0.45	2.88	2.86	2.44
	D9	2.70	0.36	2.69	2.53	2.09
	DU9	2.85	0.39	2.55	2.49	2.04
	H10	3.25	0.43	2.94	2.76	2.08
	HU10	3.32	0.46	3.72	3.45	2.85
	H11	3.39	0.42	3.49	3.47	2.81
	HU11	3.71	0.47	2.96	2.96	2.53
	H12	3.38	0.38	3.58	3.42	2.76
	HU12	3.49	0.44	3.24	3.16	2.66

4.4.1.3 Artificial neural network analysis

Table 4.6 lists regression values for the training, validation, testing, and network phases for each ANN. For models 1–4, high regression R-values of 0.97, 0.91, 0.93, and 0.92 were obtained, respectively (Table 4.6).

Table 4.6 Statistical analysis of the performance of the proposed neural network models.

Model	Regression R-value			
	Training	Validation	Testing	NN Model
A1	0.97	0.98	0.98	0.98
A2	0.91	0.92	0.96	0.92
A3	0.93	0.96	0.97	0.93
A4	0.92	0.93	0.96	0.93

The prediction of flexural strength using ANN is compared with the experimental flexural strength (Figure 4-13). The data base was divided into four data sets based on the source of the vectors, the coefficients of determination R^2 were 0.86, 0.86, 0.83, and 0.85, respectively. These coefficients and Root Mean Square Error (RMSE) indicate a significant correlation. The data reveals that the proposed ANN models are suitable, with predicted flexural strength values being similar to experimentally derived values. Moreover, the application of ANN to the prediction of flexural strength in concrete at different curing times is suitable in case of calculating nonlinear functional relationships, for which classical methods cannot be employed (Atici, 2011).

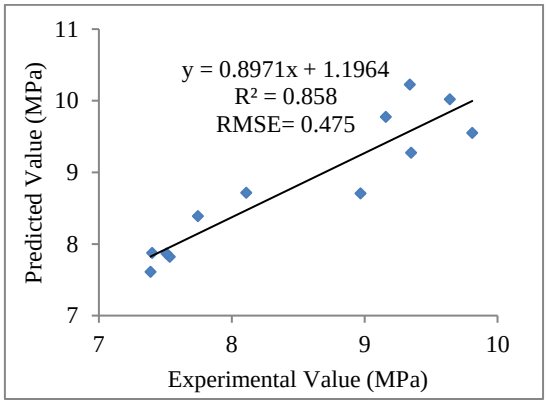

(a) A1 model

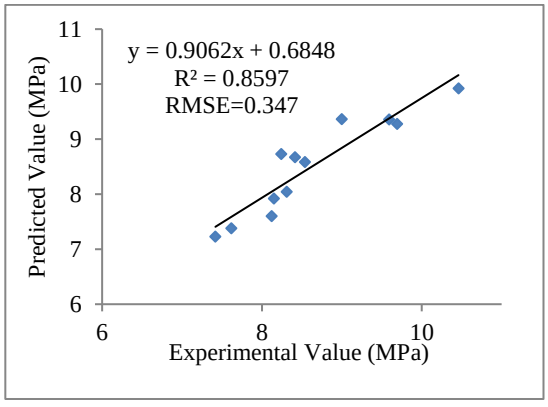

(b) A2 model

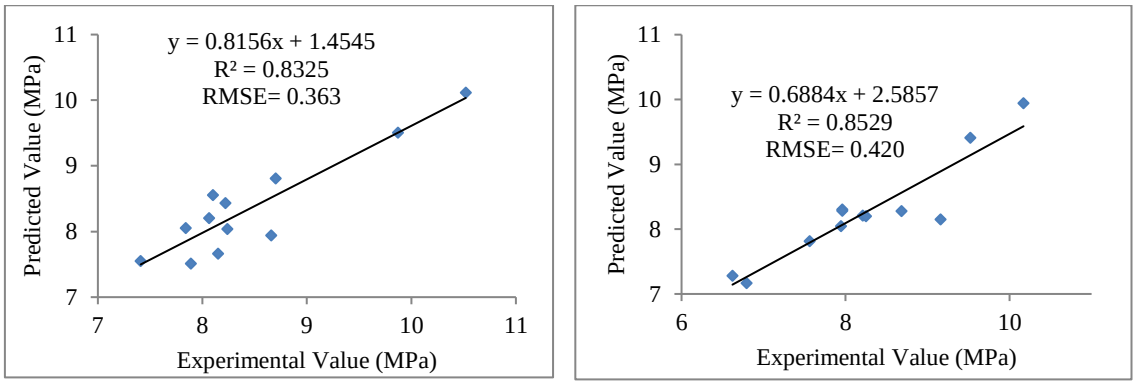

(3) A3 model (4) A4 model

Figure 4-13: Comparison between flexural strength estimated by four models and values measured

4.4.1.4 Performance of the equations to predict strength parameters

Ultrafine fly ash plays an important role than raw fly ash in early development of strength. Higher compressive strength was also observed for mortar without fibers. Flexural strength (FS) was controlled by the volume fraction range of different fibers, where the FS increases up to maximum value due to the appropriate combination of three types of fibers.

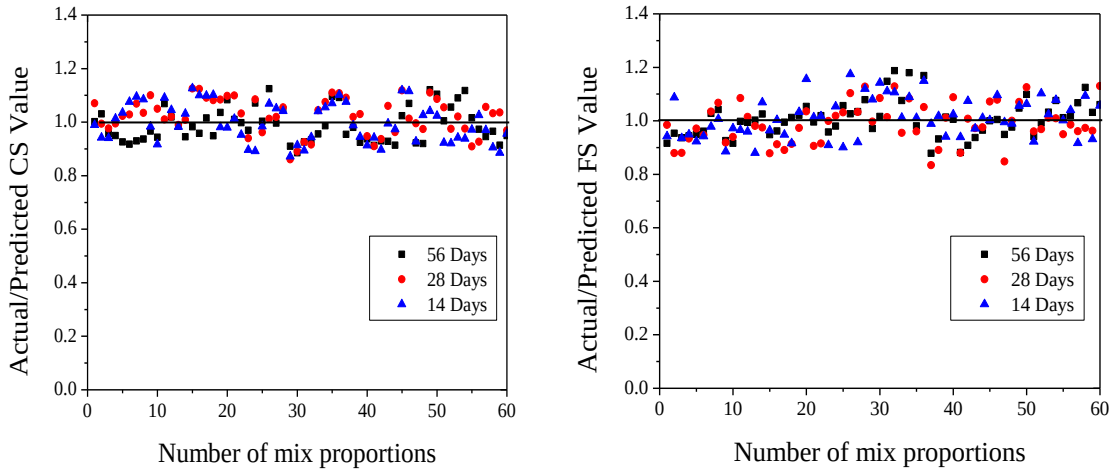

(a) Compressive strength (CS) (b) Flexural strength (FS)

Figure 4-14: Comparison of strength parameters prediction

The prediction of CS and FS by using the proposed empirical equations as given in Eq. (5) and 6(a) and 6(b) clearly describes the contribution of each fiber volume fraction and mix proportions in composites behaviour. The key factors acquired from the experiment and

prediction equations are compared in Figure 4-14. The statistical parameters are summarised in Table 4.7.

Table 4.7: Performance of the predicted equations

	Statistical parameters		
	Mean	Standard Deviation (SD)	Coefficient of Variance (COV)
CS (56d)	35.061	4.018	0.115
CS (28d)	27.028	3.097	0.115
CS (14d)	18.995	2.177	0.115
FS (56d)	8.474	0.675	0.079
FS (28d)	7.307	0.412	0.056
FS (14d)	6.056	0.217	0.036

It can be seen that the estimation for FS are comparatively more accurate than for CS as the equation was predicted with separate fiber ranges.

4.4.1.5 SEM analysis

Figs. 4-15 and 4-16 show the silane coated basalt fibers in mortar after 28 days. It can be seen that basalt fiber strands were discretely distributed throughout the paste. BF in HVFA cement mortar shows good dispersion and adhesion.

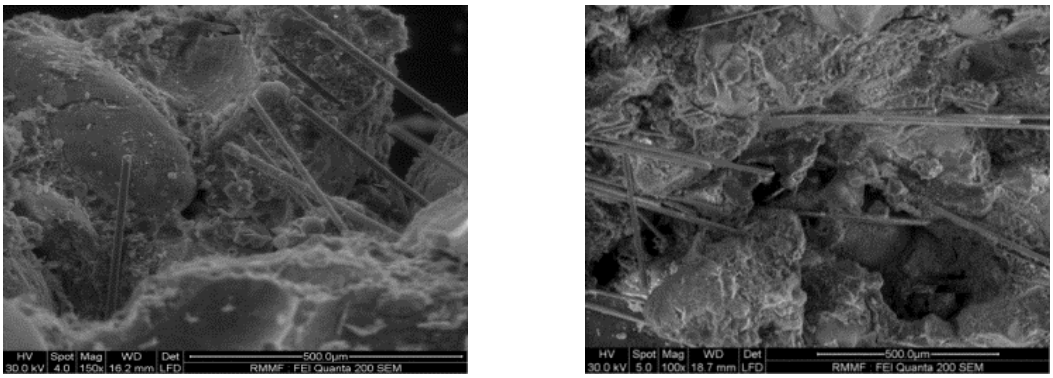

(a) RFA (b) UFFA

Figure 4-15: Distribition of silane coated basalt fiber strands in matrix.

However, unhydrated fly ash particle can be seen in both RFA and UFFA cement matrixes after 28 days (Figure 4-17). The hydration rate is higher for UFFA than RFA with cement. A good

interfacial bonding in between basalt fiber and mortar matrix can be seen by SEM microstructure images even after 56 days. The microstructures of the BF-matrix interfacial bond for RFA and UFFA are shown in Figure 4-17.

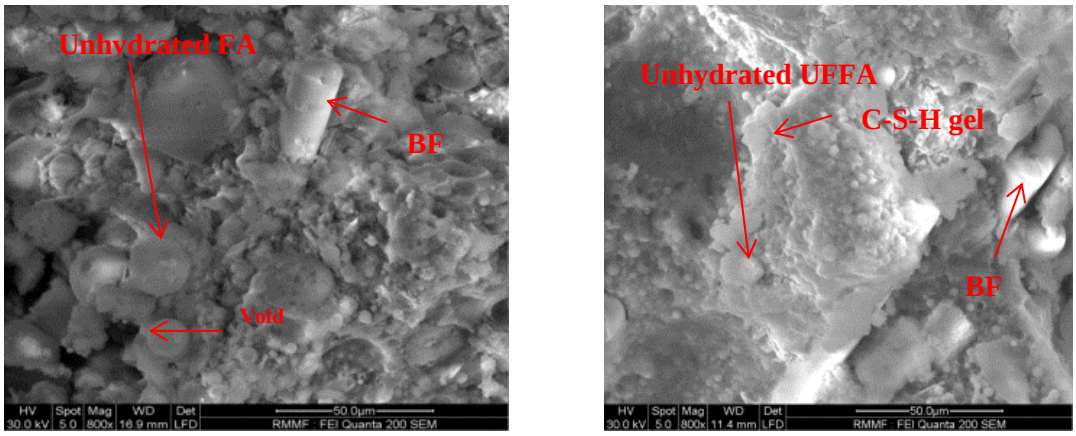

(a) RFA (b) UFFA

Figure 4-16: HVFA cement matrix bonded with fiber after 28 Days

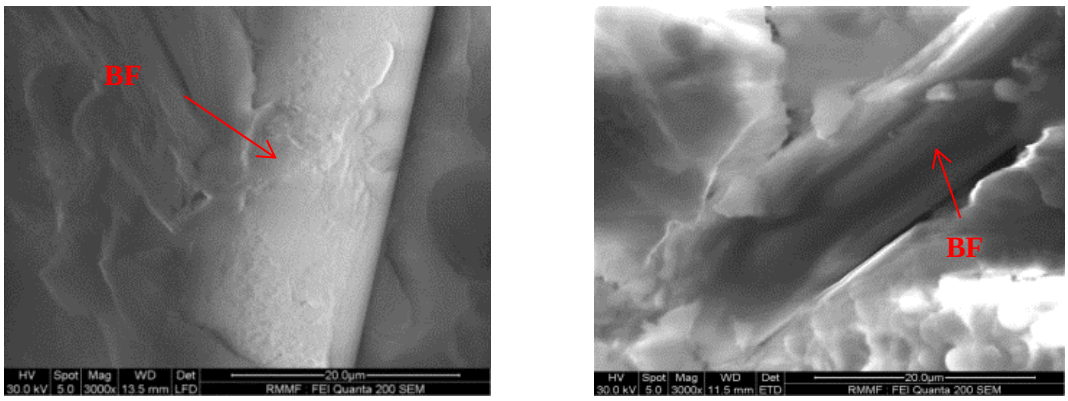

(a) RFA (b) UFFA

Figure 4-17: Interface transition zone between basalt fiber and matrix after 56 days

It does not show any noticeable voids and/or micro cracking at the interfacial bond. Moreover, the bonding zone looks denser in the microstructure analysis. Additionally, surface texture, size and shape after 56 days in fly ash cement matrix confirms the long term durability of basalt fiber in concrete medium.

4.5 Conclusions

This study has established the benefits of low cost saline coated basalt fiber as a viable addition in high volume fly ash mortar. A suite of equations for the evaluation of compressive strength

and flexural strength based on fiber percentage are provided for the benefit of practitioners. It is noted that these equations and artificial neural network compare well with the experimental data. Best results obtained for hybrid fiber reinforced HVFA mortar are given by ultra-fine fly ash cement mortar with 1.5% steel + 0.5% polypropylene fibers and 1.0% steel + 0.5% polypropylene+ 0.5% basalt fibers. Research confirms that Scanning Electron Microscope can be used to analyse the long-term durability issues in concrete.

Chapter 5 Mechanical and durability properties of hybrid fibers reinforced HVFA concrete

5.1 Introduction

Based on the characteristics of hybrid fiber HVFA cement mortar in Chapter 4, it can be concluded that hybrid fiber content DU5 (1.5% steel and 0.5% PP) and TU7 (1.0% steel, 0.5% PP and 0.5%BF) show maximum strength properties in comparison with other hybrid fiber reinforced cement matrices. Now, it is obvious to measure and compare the mechanical and durability properties of these optimum hybrid fiber ultrafine HVFA concrete. Furthermore, experimental data of single fiber reinforced HVFA concrete is required to validate the numerical simulation model and procedure as detailed in Chapter 6.

In this chapter, mechanical properties of single and optimum fiber HVFA concrete are determined. Compressive, splitting tensile, modulus of elasticity and flexural (notch and un-notch beam) test was carried out to analyse the mechanical characteristics. Moreover, detailed durability properties of optimum hybrid fiber HVFA concrete are discussed. Drying shrinkage, water absorption, carbonation and computed tomography X-ray tests were done to investigate the durability characteristics of HVFA hybrid fiber concrete.

5.2 Materials and mix proportions

5.2.1 Materials

Material properties of (Ordinary Portland Cement) OPC and fly ash were used in the concrete same as section 4.2.1. Ultra-fine fly ash was prepared by using micronizer supplied from Sturtevant Inc. Using compressed air or gas in grinding chamber, high speed rotation of the

particles are produced in micronizer which further leads the material to particle-on-particle impact (Sturtevant, 2000).

The micronizer works as per the following mechanism (Figure 5-1):

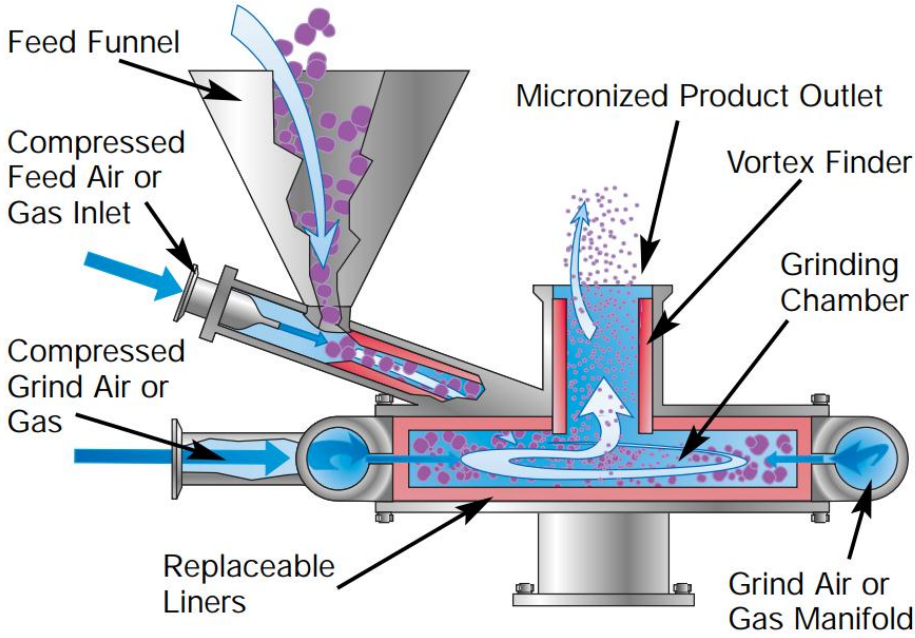

Figure 5-1: Mechanism of micronizer

a) Feed material is inserted into the inlet panel.
b) Feed material is drawn into the grinding chamber through a vacuum created by the venturi.
c) Compressed air, gas or superheated steam is forced through the grinding nozzles at high velocities.
d) The high velocity air, gas or steam accelerates the feed materials generating particle-on-particle impact.
e) Centrifugal force holds the coarser particles in the outer area of the grinding chamber until milled finer.
f) The impact generates finer particles that are carried toward the centre of the grinding chamber.

g) The micronized product exits the grinding chamber in the draft generated by the vortex finder.

In this work, feeding rate was 5 lbs/hrs. Constant feeding was maintained by feeder from Schenck AccuRate® (Figure 5-2).

Figure 5-2: Grinding raw fly ash using micronizer

The average particle size of raw fly ash (RFA) was around 20 to 30 microns and the largest at 100 microns, whereas an ultrafine fly ash (UFFA) has a maximum size of 10 microns and an average particle size of 2 to 4 microns (Figure 5-3).

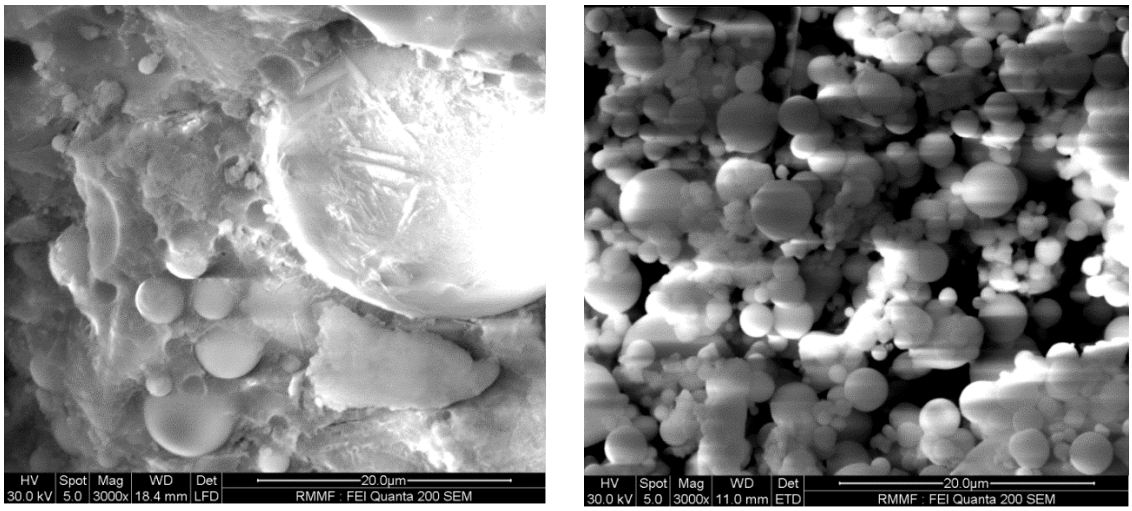

(a) RFA (b) UFFA

Figure 5-3: Comparison of particle size by SEM analysis

Both coarse and fine aggregates used in experiment were saturated surface dry (SSD) condition and maximum size of the coarse aggregate (CA) was 10 mm. The specific gravity of river sand and stone chips was 2.65 and 2.99 respectively. All the samples were prepared by using 50% fly ash as cement replacement. To control the workability of concrete mixture, polynaphthalene based water reducer was used. This superplasticizer is commercially known as Sikament NN supplied from SIKA, Australia.

Properties of the steel, polypropylene and basalt fibers are mentioned in chapter 4 Table 4.2. However, for concrete, the polypropylene fiber length was kept 47mm.

5.2.2 Mix proportions

Fly ash, cement, sand and stone were first mixed for 2–3 min. Then all the fibers were added progressively (Figure 5-4). The super plasticizer was mixed with the lime water before adding into the mixture.

Figure 5-4: Mixing of dry materials

Figure 5-5: Slump test

All the mix proportions are shown in Table 5.1 and Table 5.2. Optimum fiber percentages, obtained from the mortar mix proportions are cast and tested for concrete. Moreover, for numerical model verifications, single steel, polypropylene and basalt fibers are cast and tested. At least three samples were cast for all the mix proportions. The water-binder ratio was 0.3. For proper slump of concrete mixes, super plasticizer was altered by weight. The slump test was conducted according to AS 1012.3.1, 1998 (Figure 5-5). All mixtures corresponded to the method proposed for high performance concrete by Aïtcin (1998). The specimens were left at

room temperature for around 24hrs before demoulding (Figure 5-6) and water curing (Figure 5-7)

Figure 5-6: Specimens after casting

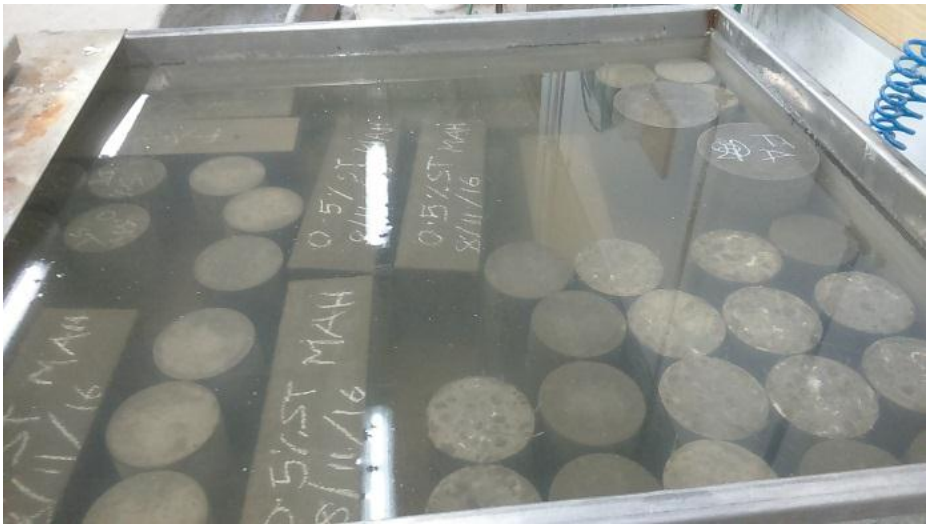

Figure 5-7: Water curing

Table 5.1: Mix proportions of optimum HVFA cement concrete.

Index	ST (%)	PP (%)	BF (%)	Cement (kg/m^3)	UFFA (kg/m^3)	Sand (kg/m^3)	CA (kg/m^3)	Water (kg/m^3)	WR (%)
Control	0.0	0.0	0.0	235	235	744	1075	152	0.4
1.5S0.5P	1.5	0.5	0.0	235	235	691	1075	152	0.4
1.0S0.5P0.5B	1.0	0.5	0.5	235	235	690	1075	151	0.5

Table 5.2: Mix proportions of single fiber HVFA cement concrete

Index	ST (%)	PP (%)	BF (%)	Cement (kg/m^3)	RFA (kg/m^3)	Sand (kg/m^3)	CA (kg/m3)	Water (kg/m^3)	WR (%)
Control	--	--	--	235	235	763	1075	151	0.6
0.5S	0.5	--	--	235	235	750	1075	151	0.6
1.0S	1.0	--	--	235	235	736	1075	151	0.6
1.5S	1.5	--	--	235	235	723	1075	151	0.6
0.5P	--	0.5	--	235	235	750	1075	151	0.6
1.0P	--	1.0	--	235	235	736	1075	151	0.6
1.5P	--	1.5	--	235	235	723	1075	151	0.6
0.5B	--	--	0.5	235	235	750	1075	150	0.7

5.3 Methodology

5.3.1 Mechanical properties testing method

At least three specimens were cast for all mixes. The experimental investigations of concrete were performed on specimens of 100 x 200 mm and 150 x 300 mm cylinders for compressive and indirect tensile strength as per AS 1012.8.1(AS, 2014a), AS 1012.9 (AS, 1985a) and AS 1012.10 (AS, 1985b).

Simultaneously 100 x 100 x 350 mm concrete beams were cast as per AS 1012.8.2 (AS, 2014b) and tested according to AS 1012.11 (AS, 1985c). Cylinders were also tested for modulus of elasticity and poisson's ratio as per AS 1012.17 (AS, 1997).

Moreover, pre-notched prismatic beams were tested as per RILEM (fracture mechanics of concrete-test methods) recommendation TC89-FMT (1989). Depth of the notch (a_0) was 25 mm.

The span length (l) was set 500mm and the depth (h) and width (b) of the three point bending beam was 150mm. More details are shown in Figure 5-8.

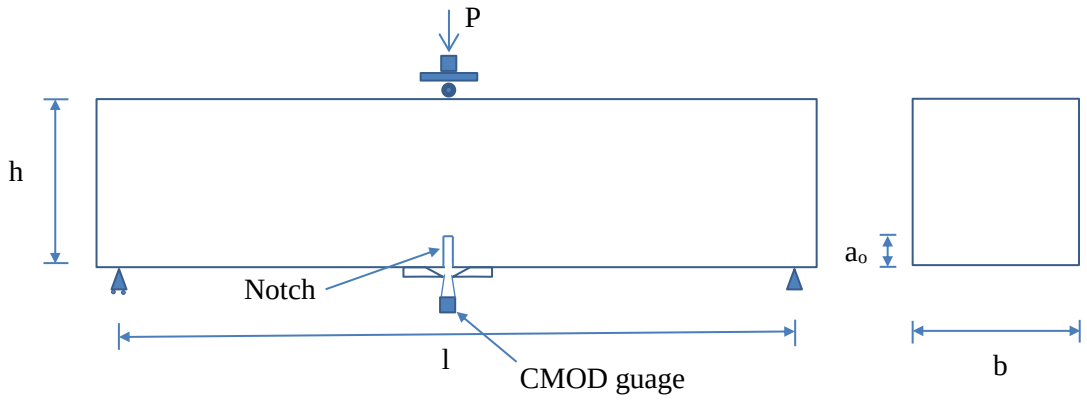

Figure 5-8: Test set up for notch beam

The flexural strength of concrete beam can be determined using the following equation:

Un-notched beam, $$f_c = \frac{P_{max} l}{bh^2}$$

Notched beam, $$f_c = \frac{3P_{max} l}{2bh^2}$$

Where,

f_c = Flexural strength (MPa)

P_{max} = Load (N)

l = Span length (mm)

b = Average width of the specimen at the failure section (mm)

h = Average depth of the specimen at the failure section (mm)

For concrete compressive and tensile strength test, MTS machine (100 tonnes capacity) was used (Figures 5-9 and 5-10). For flexural test Universal Electromechanical Testing machine (50 kN capacity) was used for concrete samples. Axial displacement was measured using testing machine and two lasers linear variable displacement transducers (LVDT) for four point loading (Figure 5-11). For modulus of elasticity, load was applied up to 40% of average compressive

strength and the loading rate was 15 ± 2 MPa. To record the deformation of specimens in two axes, two LVDTs were installed (Figure 5-12). The outcomes from the un-notched beam tests were analyzed to get a measure of the flexural toughness of the hybrid composition by using Japanese standard recommendations (JSCE) which is already discussed in Chapter 4 section 4.3.1.

Figure 5-9: Compressive strength test

Figure 5-10: Splitting tensile strength test

Figure 5-11: Flexural strength test

Figure 5-12: Modulus of elasticity & Poisson's ratio

For more detailed investigation of toughness of triple hybrid fiber reinforced HVFA concrete, notch beam crack mouth opening displacement (CMOD) was measured (Figure 5-14). Two edges were glued at the bottom of the specimen on both sides of the crack mouth and a CMOD gauge was fitted (Figure 5-13). The loading rate was controlled as 0.5mm/min, and the load-CMOD curves were recorded by computer system.

Figure 5-13: Notch beam

Figure 5-14: Notch beam test set up

This method is used to propose two fracture model parameters; critical stress intensity factor (K_I) and critical crack tip opening displacement (CTOD). The critical crack tip displacement is evaluated from the maximum load and the effective crack length (initial notch depth plus the stable crack growth at peak load). The critical stress intensity factor (K_I) and CTOD is calculated by using the calculation method described by Shah and Carpinteri (1991).

To determine the critical stress intensity factor (K_I), the following equation is used:

$$K_I = 3P_{max}\frac{S(\pi a_c)^{1/2}\,F(\alpha)}{2h^2 b} \quad (5.1)$$

In which,

$$F(\alpha) = \frac{1.99-\alpha(1-\alpha)(2.15-3.93\alpha+2.7\alpha^2)}{\sqrt{\pi}\ (1+2\alpha)(1-\alpha)^{3/2}},\ \alpha = a_c/h$$

P_{max} = Maximum load (N).

a_c = Effective critical crack length (a = a_0+ stable crack growth at peak load).

The value of CTOD is then calculated using Eq. 5.2

$$CTOD = \frac{6P_{max}Sa_c}{d^2bE}V_1(\alpha)\{(1-\beta)^2 + (-1.149\alpha + 1.081)(\beta-\beta^2)\}^{1/2} \quad (5.2)$$

In which, $\beta=a_0/a_c$ and $V_1(\alpha) = 0.76 - 2.28\alpha + 3.87\alpha^2 - 2.04\alpha^3 + 0.66/(1-\alpha)^2$

Furthermore, fracture energy (G_f) is measured as another fracture parameter. This can be calculated by the Eq. 5.3.

$$G_f = \frac{T_b + mg\delta_{max}}{A_{lig}} \quad (5.3)$$

Where, T_b is the area under the load–deflection curve (N-m), mg is the self-weight of the specimen between supports (kg), δ_{max} is the maximum displacement (m), and A_{lig} is the fracture area [h (b − a)] (m^2).

5.3.2 Drying shrinkage test

The drying shrinkage test for both with or without hybrid fiber reinforced HVFA concrete was performed according to AS 1012.13 (AS, 2015b). Concrete specimen was prepared as per standard AS 1012.8.4 (AS, 2015a). The test specimens were 75 x 75 x 300mm prisms with gauge studs at both ends (Figure 5.15(b)). Three specimens were cast for each mix. The

specimens were demoulded after 24 hours and cured in water. After 7days curing, the specimens were removed from the curing chamber and the surface was wiped dry with a damp cloth. Immediately after wiping the surface dry, the initial measurement was taken (L_0) and put in the drying chamber. The measurements were taken continuously for 7, 14, 21, 28 and 56 days. At least five consecutive data of within 0.001 mm of average measurement were made for every measurement. The mean of these five readings was used to calculate the drying shrinkage in microstrain. The temperature of the drying chamber was maintained at 23 ± 1^0C and the relative humidity was kept at 50±5% at all times. A reference bar was used to check the zero setting of the comparator during measurement, as shown in Figure 5-15(a).

(a) Reference bar for measurement (b) Sample measurement

Figure 5-15: Drying shrinkage measurement

The calculation of drying shrinkage in micro strain is as follows:

Drying Shrinkage Strain = (Final Length-Initial length)/gauge length

$$= (L_t - L_0)/ L_g, \quad (5.4)$$

Where, L_0 =Initial Length of specimen in mm

L_t = Final length of specimen at time t (t in days) in mm

L_g = Guage length (250 mm).

From AS 3600 (AS, 2009), drying shrinkage can be calculated from the following equation:

$$\varepsilon_{csd} = k_1 k_4 \varepsilon_{csd.b} \quad (5.5)$$

Where, $k_1 = \frac{\propto_1 t^{0.8}}{t^{0.8}+0.15t_h}$

$\propto_1 = 0.8 + 1.2e^{-0.005t_h}$

t is in days and t_h is the theoretical thickness. k_4 is equal to 0.7for an arid environment, 0.65 for an interior environment, 0.6 for a temperate inland environment and 0.5 for a tropical or near coastal environment.

The basic drying shrinkage is given by $\varepsilon_{csd.b} = (1.0 - 0.008f_c') \times \varepsilon^*_{csd.b}$

Where, final drying basic shrinkage strain ($\varepsilon^*_{csd.b}$) shall be taken 800 x 10^{-6} for Sydney and Brisbane, 900 x 10^{-6} for Melbourne and 1000 x 10^{-6} elsewhere.

5.3.3 Durability measurement method

5.3.3.1 Water absorption test

Water absorption in HVFA concrete was determined according to standard Australia AS 1012.21 (AS, 1999). This standard procedure was used for determining immersed absorption, boiled absorption and apparent volume of permeable voids (AVPV).

Immersed absorption can be defined as the mass of water held in a concrete specimen, brought to the surface dry condition following soaking under water for not less than 48 hours, to the oven-dry mass of the concrete specimen.

Boiled absorption can be defined as the mass of water held in a concrete specimen, brought to the surface dry condition following boiling water under for a period of 5.5±0.5 hours to the oven-dry mass of the concrete specimen.

AVPV is the apparent volume of interconnected void space of a concrete specimen which is emptied during the specified oven drying and filled with water during the subsequent immersion and boiling.

(a) Sample weight measurement

(b) Oven drying

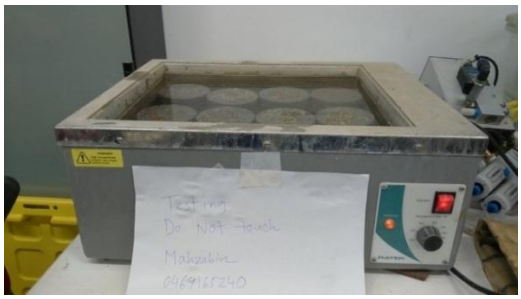

(c) Sample boiling

(d) Sample suspended to determine mass

Figure 5-16: Water absorption test

The procedure is explained as follows (Figure 5-16):

a) The specimens are oven dried at 100 to 110^{0}C for 24 hours.

b) After removing from oven, allowed it to cool to a temperature 23^0C and weighted (M_1).

c) Immersed the specimens in water at 23^0C for 48 hours.

d) Weight of the surface dry saturated specimens by removing the surface moisture is measured (M_{2i}).

e) For boiling absorption, surface dry specimens are placed in a water bath at room temperature, which is covered with water.

f) The specimens are boiled for a period of 5.5±0.5 hours. After that, the specimens are allowed to cool naturally still immersing in water to cool to a temperature 23^0C.

The boiled specimens are surface dried and the mass (M_{3b}) is determined.

After that, the specimens are suspended by a rack to determine the mass (M_{4ib}) of the specimens in water at 23^0C.

The calculations of water absorptions are as follows:

1) Immersed absorption, $Ai = \frac{(M_{2i}-M_1)}{M_1} x100\%$ (5.6)

2) Boiled absorption, $Ab = \frac{(M_{3b}-M_1)}{M_1} x100\%$ (5.7)

3) Apparent volume of permeable voids, $AVPV = \frac{(M_{3b}-M_1)}{(M_{3b}-M_{4ib})} x100\%$ (5.8)

5.3.3.2 Carbonation test

The carbonation test was conducted according to the RILEM recommendation CPC-18 (1988). This method consists of determining the depth of the carbonated layer on the surface of hardened concrete by means of an indicator. This carbonation process leads to a reduction of the pH-value of the pore solution to less than 9. The depth of the carbonated surface layer is called the depth of carbonation. The reduction of the pH-value can be made visible by the colour change of a suitable indicator. A solution of 1% phenolphthalein in 70% ethyl alcohol is suitable for determining the depth of carbonation. Phenolphthalein turns non-carbonated concrete purple, and remains colourless in carbonated concrete.

(b) Carbonation chamber

(a) Epoxy applied samples

(c) Cutting into two pieces

Figure 5-17: Carbonation test

This test is conducted for at least three specimens for each mix proportions. The specimens for this experiment have dimensions of 100 mm diameter and 60 mm height and are cut from cylinder of diameter 100 mm x 200 mm height. After curing period, the specimens are dried for 24 hours. The top and bottom surfaces of specimens were sealed using epoxy resins to allow the carbonation only occurs through curved surface (Figure 5-17(a)). Then it is allowed another 24 hrs to let the epoxy to dry.

The next step is to place the specimens in the carbonation chamber (Figure 5-17(b)). The carbonation chamber is set up at temperature of 20^{o}C, relative humidity of 70% and with CO_2

concentration of 2.0% according to RILEM recommendation for measurement of carbonation depth.

At the testing day of 28, the specimens were taken out from the testing chamber and then cut into two pieces (Figure 5-17(c)). For fiber concrete, saw is used to cut into two pieces. Shortly after cutting the specimens, phenolphthalein solution is sprayed to check the depth of carbonation. The phenolphthalein can change the colour of un-carbonated concrete into purple and remain colourless for carbonated concrete. Therefore, the depth of carbonation can be measured using calliper (Figure 5-18).

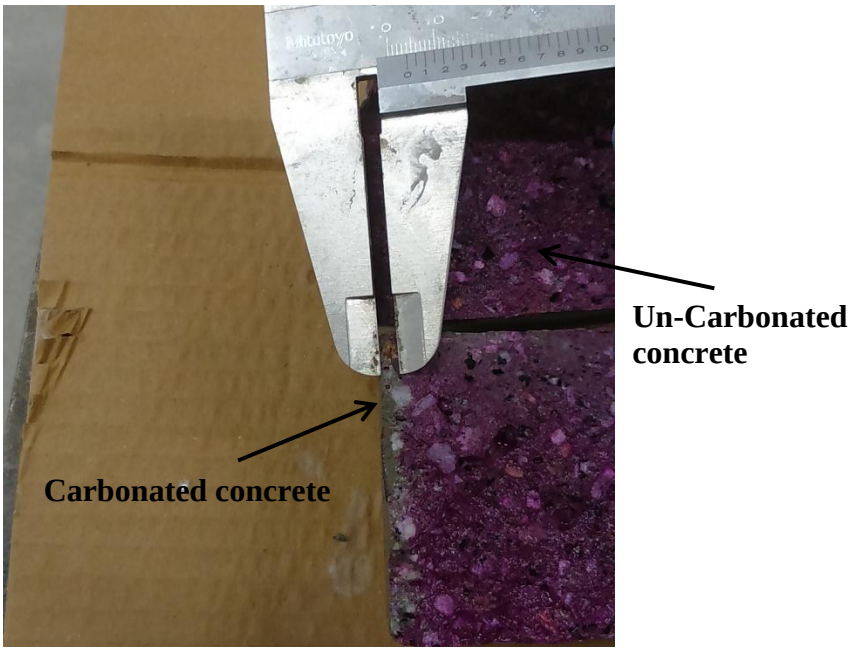

Figure 5-18: Measuring the depth of the carbonation

5.3.4 Porosity analysis

Dry hardened concrete was exposed to Computed Tomography (CT) x-ray scans by using Phoenix vtome xs scanner facility at RMIT University (Figure 5-19). Samples were cut into a 25mm cube shape for best scanning geometry. To get better spatial resolution in the pore microstructure, it is necessity to use reduced sample sizes (Landisa et al., 2003). In the studies, multiple samples (at least five) are considered randomly for control and fiber concrete porosity

analysis. All the scans were performed to record 1000 images for one 3600 rotation and kept image resolutions for 190 kV and 80µA. Per scan, total time required was approximately 20–25 min. System supplied VGStudio Max3 software was used for data analysis. Volume analysis tool was executed to calculate the average void percentage.

(a) Phoenix vtome xs scanner (b) Using VGStudio Max3 software

Figure 5-19: Porosity measurement by CT x-ray

By applying surface fit function in the histogram diagram, region of interest was produced for void percentage analysis. The smallest void volume was considered to be 64µm^3 and maximum void diameter was 1.0e^{13}mm. This volume analysis creates information on each defect including volume, diameter, sphericity, surface area etc.

5.4 Results and discussions

5.4.1 Mechanical properties of single fiber reinforced HVFA concrete

The results of some mechanical properties (compressive and flexural strength) of single fiber reinforced concrete are presented here and results are used to verify the numerical simulation model in Chapter 6. Furthermore, detailed investigations of the mechanical properties of optimum hybrid fibers are conducted.

In single fiber reinforced and control HVFA concrete, raw fly ash was used. Figure 5-20 shows that the compressive strength for fiber reinforced concrete is lower than the unreinforced concrete. The reduction of the compressive strength can be attributed to the increase of porosity due to the addition of fiber (Neves and Almeida, 2005). The compressive strength decreases with the increase of volume fraction of fibers. Furthermore, maximum reduction has happened for 0.5% basalt fiber concrete compared to control concrete, i.e., 13.2% which is also compatible with the preceding literature (Shaikh and Taweel, 2015). However, when hybrid combinations are used, the negative effect of basalt fiber in concrete can be overcome.

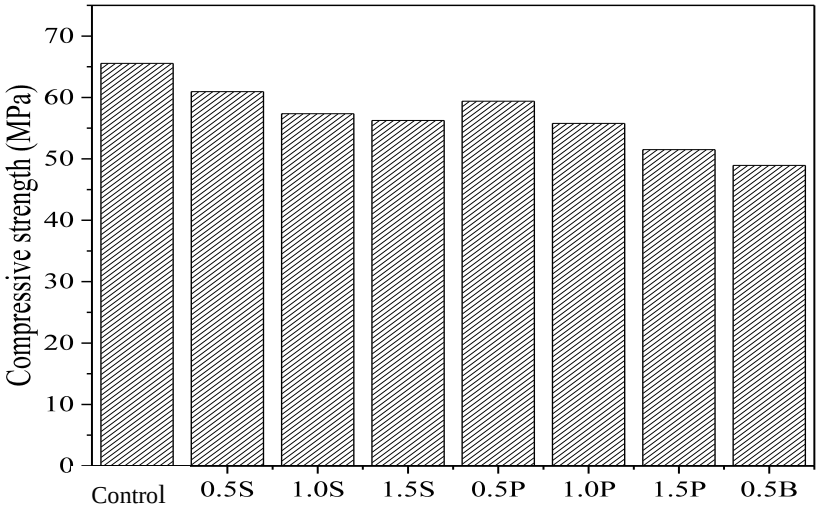

Figure 5-20: Compressive strength for single fiber reinforced HVFA concrete at 56 days

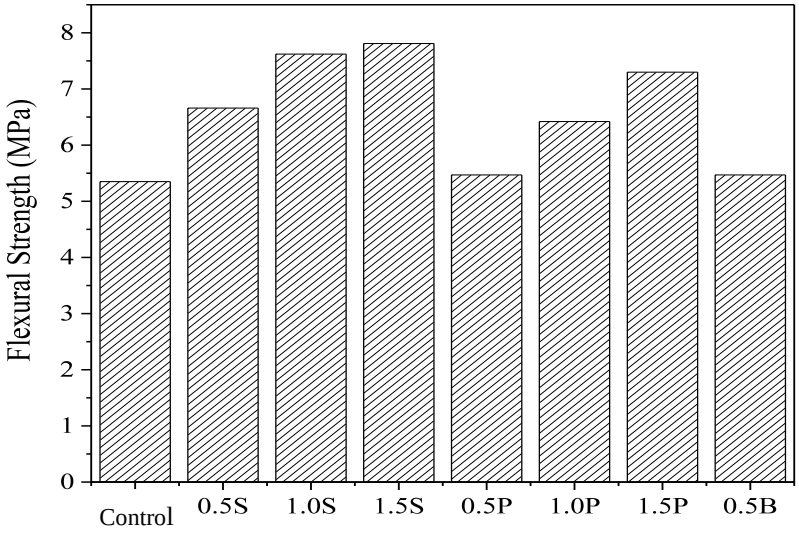

Figure 5-21: Flexural strength for single fiber reinforced HVFA concrete at 56 days

The measured average flexural strengths of control and single fibers high volume raw fly ash concrete are shown in Figure 5-21. It can be seen that higher volume fractions of fiber can produce elevated flexural strength. Within the test results, maximum 46% higher flexural strength can be measured for 1.5% steel fiber than the control samples. For 0.5P and 0.5B specimens, the flexural strength increases about 2 to 3%. The results can be ascribed due to the higher capacity of steel fiber and lower capacity of polypropylene and basalt fibers to bridging the macro crack. However, in hybrid combinations, polypropylene and basalt fibers can contribute to increase in strength delaying the initial micro crack.

5.4.2 Mechanical properties of optimum fiber reinforced HVFA concrete

5.4.2.1 Compressive strength

Figure 5-22 illustrates the influence of hybrid fiber on the compressive strength properties of concrete. It is observed that compressive strength of hybrid fiber HVFA cement concrete are decreased compared with the control sample. Generally, fiber causes certain perturbation of the matrix and it may cause higher voids in comparison to without fiber concrete. When the fiber

hybridization for 1.5% steel and 0.5% PP (1.5S0.5P), the 28days compressive strength decreased by 15.37% and 56days compressive strength decreased by 11.46%. Again, when the fiber hybridization for 1.0% steel, 0.5% PP and 0.5% BF (1.0S0.5P0.5B), the 28days compressive strength decreased by 9.22% and 56days compressive strength decreased by 6.02%. It can be seen that three fibers combinations can obtain more compatible compressive strength than two fibers combination. This may be attributed because of the similar chemical composition of the basalt fiber with the fly ash concrete, which results in a good chemical bonding with the matrix. However, because of good alkali resistance, modified basalt fiber can maintain good stability and adhesion with HVFA cement matrix. However, fiber usually reduces brittleness of concrete by providing post cracking ductility and increases toughness; basalt fiber can work as a micro aggregate (Punurai et al., 2018).

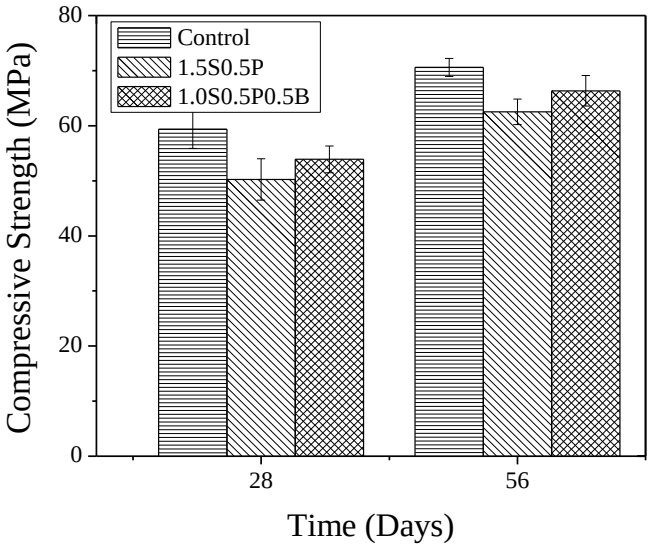

Figure 5-22: Compressive strength of HVFA concrete

5.4.2.2 Splitting tensile strength

Figure 5-23 shows the effect of hybridization on the splitting tensile strength. It can be seen that 28 and 56days indirect tensile strength of 1.5S0.5P concrete increased 81.83% and 76.16% respectively. For 1.0S0.5P0.5B specimens, the splitting tensile strength value improved by

90.40% and 82.93% for 28days and 56 days respectively. Generally, hybridization of a large diameter fiber with a smaller diameter fiber shows promising increase in performance because the number of fibers crossing a section becomes high when the fiber diameter is decreased (Banthia and Sappakittipakorn, 2007).

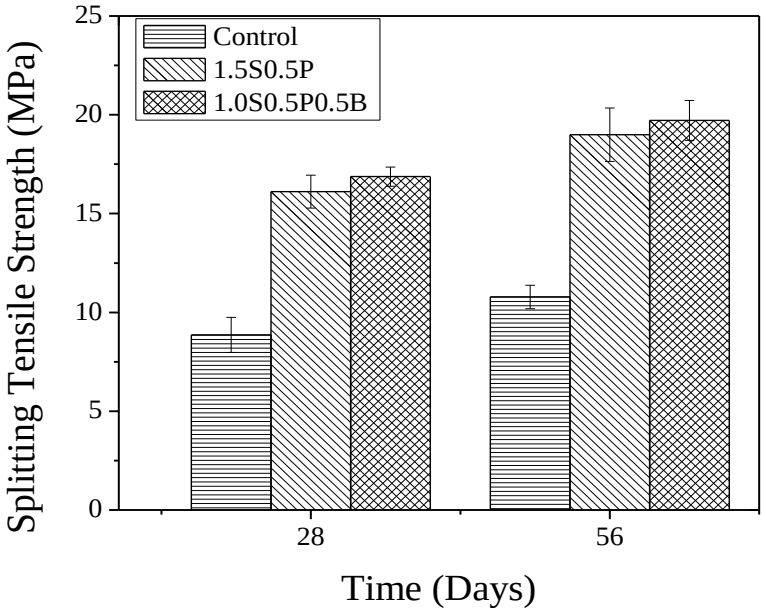

Figure 5-23: Splitting tensile strength of HVFA concrete

The improvement of the splitting tensile strength of 1.0S0.5P0.5B is owing to the excellent alkali resistance of basalt fiber and good bridging effect with steel and polypropylene on cracks, which inhibits the expansion of micro cracks in the initial stage.

5.4.2.3 Modulus of elasticity

The results of the modulus of elasticity and poisson's ratio are presented in Table 5.3.

Table 5.3: Average Modulus of elasticity and Poisson's ratio after 56 days

Sample	Modulus of elasticity (N/mm^2)	Poisson's ratio
RFA Control	43849.1	0.15
MFA Control	47479.85	0.1575
1.5S0.5P	50297.05	0.19
1.0S0.5P0.5B	49844.5	0.18

The experimental results of modulus of elasticity of high strength HVFA concrete can be compared with the following existing expressions for the prediction.

$E_c = (0.024\sqrt{f'_{cm}} + 0.12)w^{1.5}$ for f'_{cm}>40 MPa, f'_{cm}= 90%f'_c, AS 3600 (AS, 2009) (5.9)

$E_c = (3320\sqrt{f'_c} + 6900)(\frac{w}{2346})^{1.5}$ for 21≤f'_c≤83 MPa,(ACI 363) (ACI, 1998) (5.10)

$E_c = 9500{f'_c}^{0.3}(\frac{w}{2400})^{1.5}$ for f'_c≤85 MPa, (NS-3473) (NS-3473, 1992) (5.11)

$E_c = 9000{f'_c}^{0.33}$ for f'_c>27 MPa, Zhao (1990) (5.12)

$E_c = (3300\sqrt{f'_c} + 6900)(\frac{w}{2300})^{1.5}$ (CSA)(CSA, 1995) (5.13)

Where, f'_c (MPa) and E_c (MPa) are 28-day cylindrical compressive strength and modulus of elasticity of concrete, respectively; and w (kg/m^3) is the unit weight of concrete. Here, the equations are calculated and compared for 56 days compressive strength of control HVFA concrete.

Table 5.4: Comparison of MOE (MPa) with the existing equations

	Exp.	Eq. (5.9)	Eq. (5.10)	Eq. (5.11)	Eq. (5.12)	Eq. (5.13)
RFA Control	43849.10	50008.11	48847.87	46565.09	35785.86	50079.39
Variation (%)	--	14.05	11.40	6.19	18.39	14.21
MFA Control	47479.85	51019.38	50145.59	47491.74	36569.99	51408.19
Variation (%)	--	7.45	5.61	0.03	22.98	8.27

Based on the Table 5.4, the results of experimental and some existing equations can be varied up to 23% which is satisfactory. Moreover, the result for Eq. (5.11) is relatively similar to the experimental results.

5.4.2.4 Flexural properties

5.4.2.4.1 Un-notched beam

Figure 5-24 shows the effect of hybridization on the flexural strength of concrete. The 28 and 56 days average flexural strength of 1.5S0.5P concrete increased 48.6% and 53.4% respectively than that of control HVFA concrete. Therefore, the incorporation of the appropriate three types of fibers also significantly improves the flexural strength of concrete. At this time, the average flexural strength of specimens at 28 and 56days was 45.1% and 49.9% higher than that of control HVFA concrete. When fiber combination is appropriate, fibers which were perpendicular to the tensile axis could afford a part of stress because of its higher tensile and elastic modulus (Li and Xu, 2009). The discrepancy in between average flexural strength of 1.0S0.5P0.5B and 1.5S0.5P concrete is not significant.

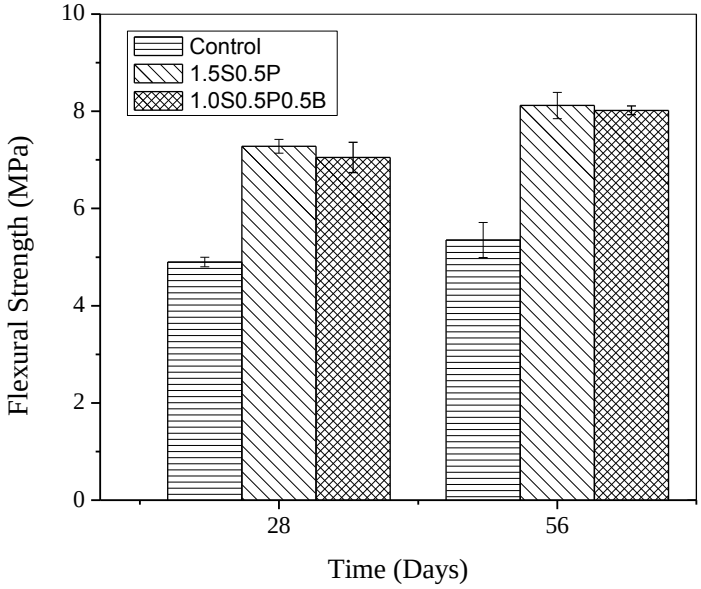

Figure 5-24: Flexural Strength of HVFA concrete

Figure 5-25 shows the load deflection for hybrid fiber HVFA concrete. Up to ultimate load, fibers mainly withstand the load and help to control the growth of the produced cracks (Yu et al., 2015). In this case, the trend is similar to that of the peak load. It is noticed that the ultimate

load after reaching the peak force sharply decreased for a while and then gradually decreased. Due to the good resistance of basalt fiber in alkaline and combined random distribution of all fibers alter the extension path of the crack. As a result, basalt fiber also plays a toughening role in 1.0S0.5P0.5B fibers HVFA concrete which shows the similar ductility failure of 1.5S0.5P fibers HVFA concrete.

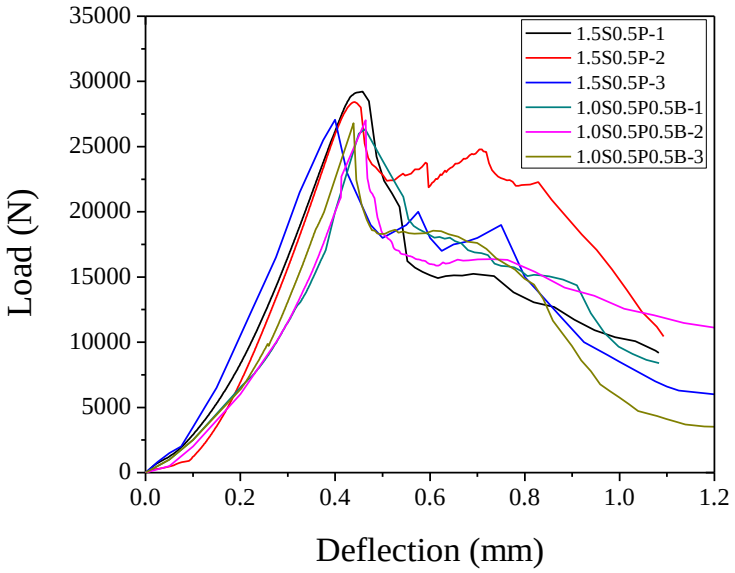

Figure 5-25: Load deflection curve of HVFA concrete

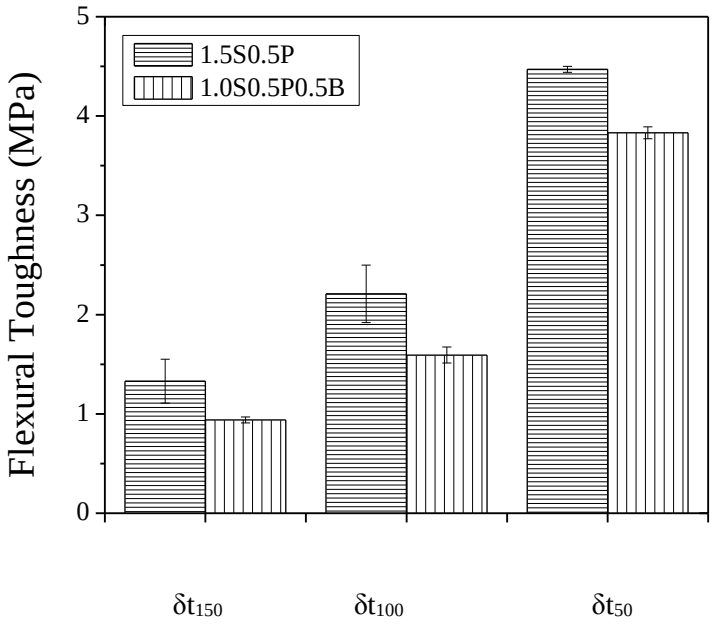

Figure 5-26: Flexural toughness of hybrid fiber HVFA

The load deflection curves were analysed by JSCE method and flexural toughness is presented in Figure 5-26. The addition of basalt fiber (0.5% steel fiber replacement in specimen 1.5S0.5P) in concrete specimen 1.0S0.5P0.5B may reduce the flexural toughness. In this study, due to the relatively micro diameter, many BFs can be slit after application of the load. On the other hand, extra steel fiber in 1.5S0.5P concrete may show better ability to restrain the propagation of macrocracks. However, in comparison with other researcher, 1.0S0.5P0.5B specimen attains virtuous flexural toughness (Soutsos et al., 2012, Yap et al., 2014).

5.4.2.4.2 Notched beam

Figure 5-27 illustrates the optimum triple hybrid fiber reinforced HVFA concrete tests results compared to unreinforced HVFA concrete.

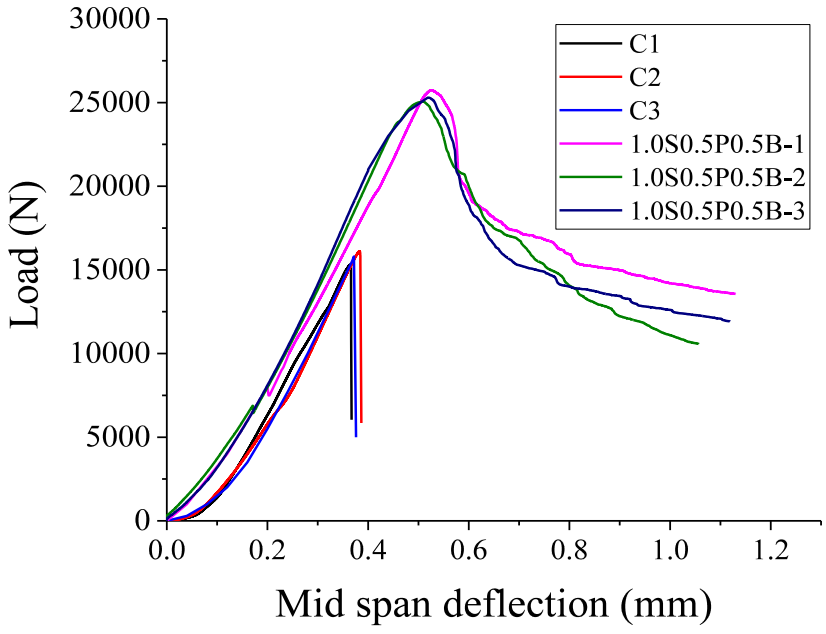

Figure 5-27: Load deflection curve of notched beam

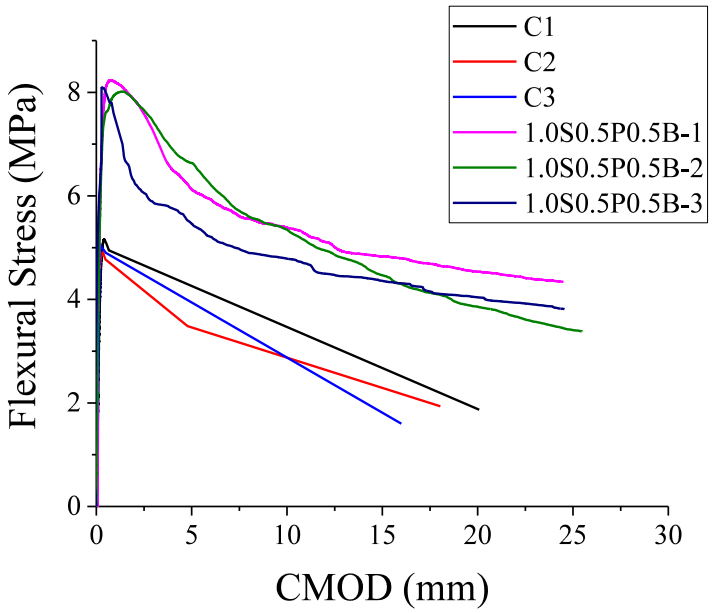

Figure 5-28: Flexural stress vs CMOD

The flexural properties of the optimum fiber HVFA concrete are presented with the statistical calculations from the experimental results in Table 5.5. Detailed calculations are shown in appendix A.

Table 5.5: Test results of optimum fiber reinforced notch beam.

Specimen	f_c (MPa)	K_I (MPa$\sqrt{m}$)	CTOD (mm)	G_f (N/mm)
1.0S0.5P0.5B-1	8.236	2.246	0.028	0.361
1.0S0.5P0.5B-2	8.016	2.006	0.021	0.336
1.0S0.5P0.5B-3	8.093	2.397	0.034	0.351
Average	8.115	2.216	0.027	0.349
Standard Deviation	0.112	0.197	0.006	0.012
COV (%)	1.375	8.896	23.517	3.602

From Figure 5-28, the optimum fiber concrete stress capacity is 60% (average) higher than control specimens. The critical stress intensity factor (K_I), crack tip opening displacement (CTOD) and fracture energy (G_f) for optimum three fiber notch beam is observed to be

sophisticated in comparison with the previous literature (Qian and Stroeven, 2000, Reis, 2006). The results display a notable increase and respectable coefficient of variance (COV).

5.4.2.5 Failure analysis of concrete

Figure 5-29 shows the failure image of control, 1.5S0.5P and 1.0S0.5P0.5B HVFA concrete of compressive, splitting tensile and flexural tests.

(i) Control (ii) 1.5S0.5P (iii) 1.0S0.5P0.5B

(a) Compressive strength test failure

(i) Control (ii) 1.5S0.5P (iii) 1.0S0.5P0.5B

(b) Splitting tensile strength test failure

(i) Control (ii)1.5S0.5P (iii) 1.0S0.5P0.5B

(c) Flexural strength test failure

Figure 5-29: Failure test specimens

For control sample (Figure 5-29 (a,b,c) (i)), brittle failure occurs accompanied by a strong, loud sound. Any crack cannot be identified before sudden failure at peak load. This is because of the localisation of maximum strain in a specific crack which is greater than the strain limit of the matrix (Hassan et al., 2012).

Besides, both type of hybrid fiber reinforced concrete show similar failure pattern for compressive and splitting tensile strength. Stress of fiber reinforced concrete is retained by the composite action of the fibers bridging across the cracks in the concrete. Figure 5.29 c (ii and iii) show that flexural crack is not expanding quickly. Microscopic diagonal cracks are observed first within the length of the middle third of the beam. After a crack appears, it slowly propagates and shows an excellent ductility after failure.

Figure 5-30 shows the failure image of notched beam. Similar to Figure 5-29 (i), the control beam breaks suddenly at the notch. The crack created in the notch area propagates very slowly for hybrid concrete and the length of the crack with in maximum load was about 45 to 48% of the total width of the beam.

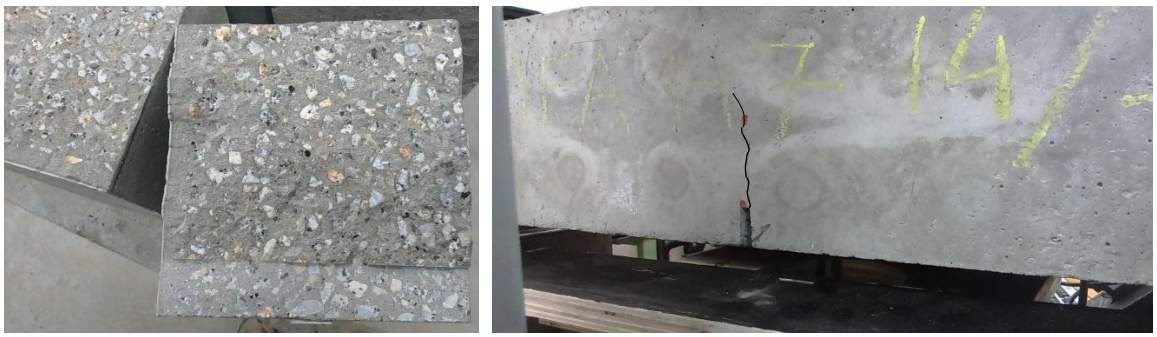

(a) Control (b) 1.0S0.5P0.5B

Figure 5-30: Failure of notched beam

5.4.3 Drying shrinkage

In the figure 5-31, time zero day means initial measurement day after seven days of curing. Here drying shrinkage value obtained from the experiments are compared with the calculated value

from Eq.(5.4) and previous work for 50% high volume fly ash concrete by Atiş (2003). It can be seen that drying shrinkage of control (UFFA) gives good agreement with the results given by Atis, 2003. However, UFFA concrete shows higher drying shrinkage according to the Australian standard AS 3600 (AS, 2009). This can be due to the use of superplasticizer as it may show shrinkage values of up to 50% when compared to the concrete made with no superplasticizer (Atiş, 2003).

The addition of triple hybrid fiber in ultrafine HVFA concrete will greatly reduce drying shrinkage in comparison to control and double fiber concrete sample. This can be attributed due to the presence of sufficient void filling materials in triple hybrid fiber reinforced concrete (Punurai et al., 2018).

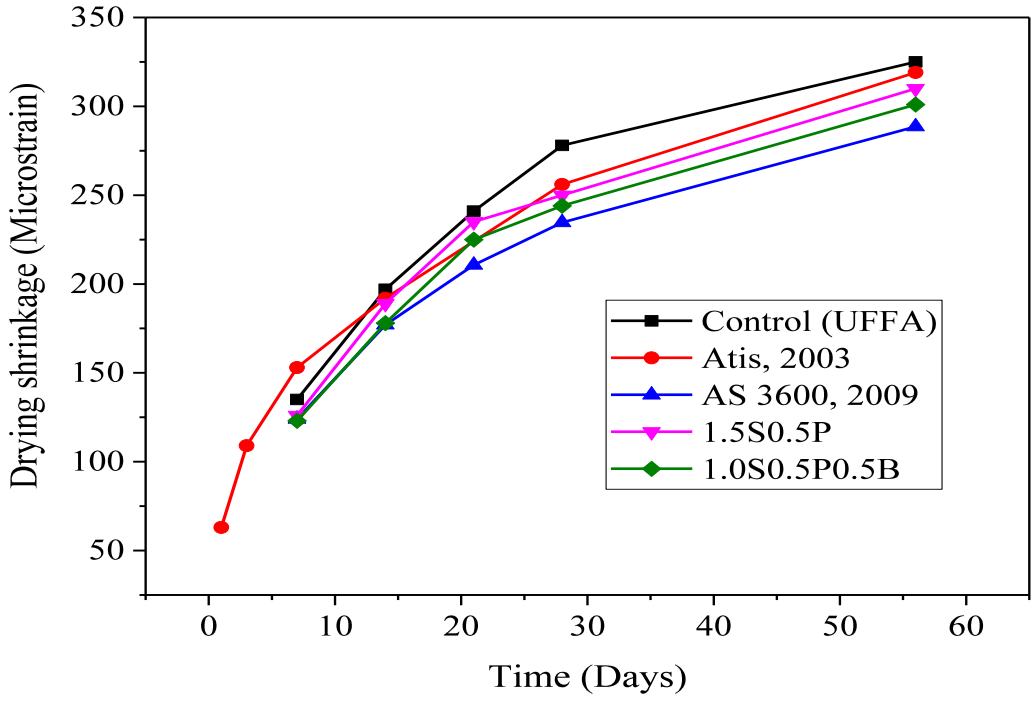

Figure 5-31: Comparison of drying shrinkage of hybrid fiber reinforced or unreinforced HVFA concrete

5.4.4 Durability properties

5.4.4.1 Water absorption

The water absorption of concrete gives an indirect indication of the pore structure of the concrete and durability performance in a corrosive environment. Figure 5-32 shows that the water absorption for hybrid fiber concrete is lower than control concrete samples. This can be accredited due to the lower porosity of fiber concrete than control sample. However, all the specimens show excellent durability of concrete according to VicRoads guidance of concrete durability classification which related to AVPV value (CCAA, 2009).

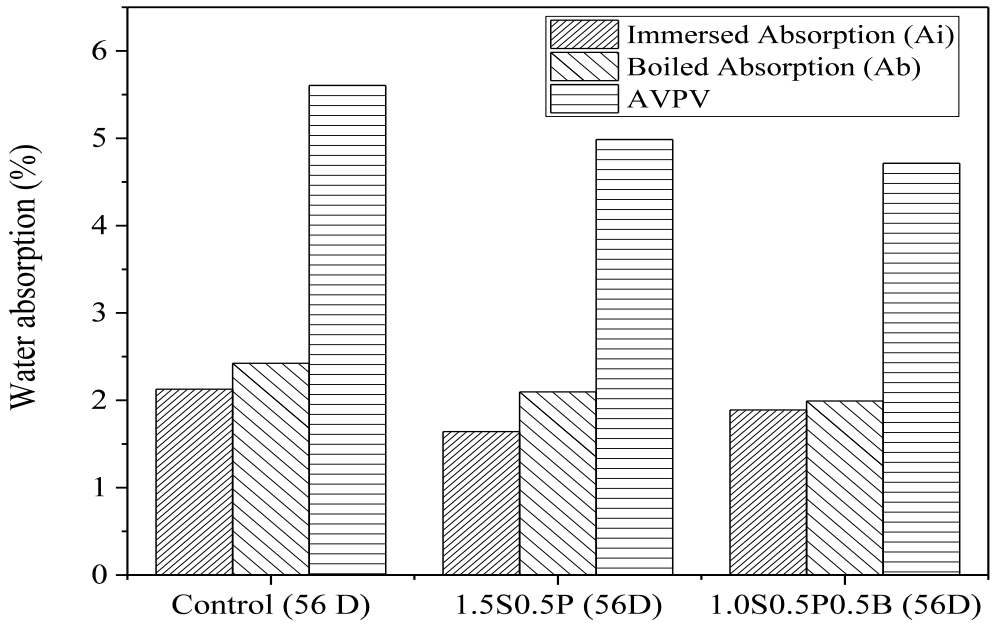

Figure 5-32: Comparison of water absorption

5.4.4.2 Carbonation

Figure 5-33 shows the depth of the carbonation of HVFA with or without hybrid fibers. The depths of the carbonation measurement of the concrete samples are presented in Table 5.6. It can be seen that the depth of carbonation decrease with the use of fibers and triple hybrid fiber gives very good carbonation resistance. This is because of the low permeability of concrete not

to allow carbon di oxide entrance into the concrete. However, the cutting procedures of fiber and without fiber concrete samples are different.

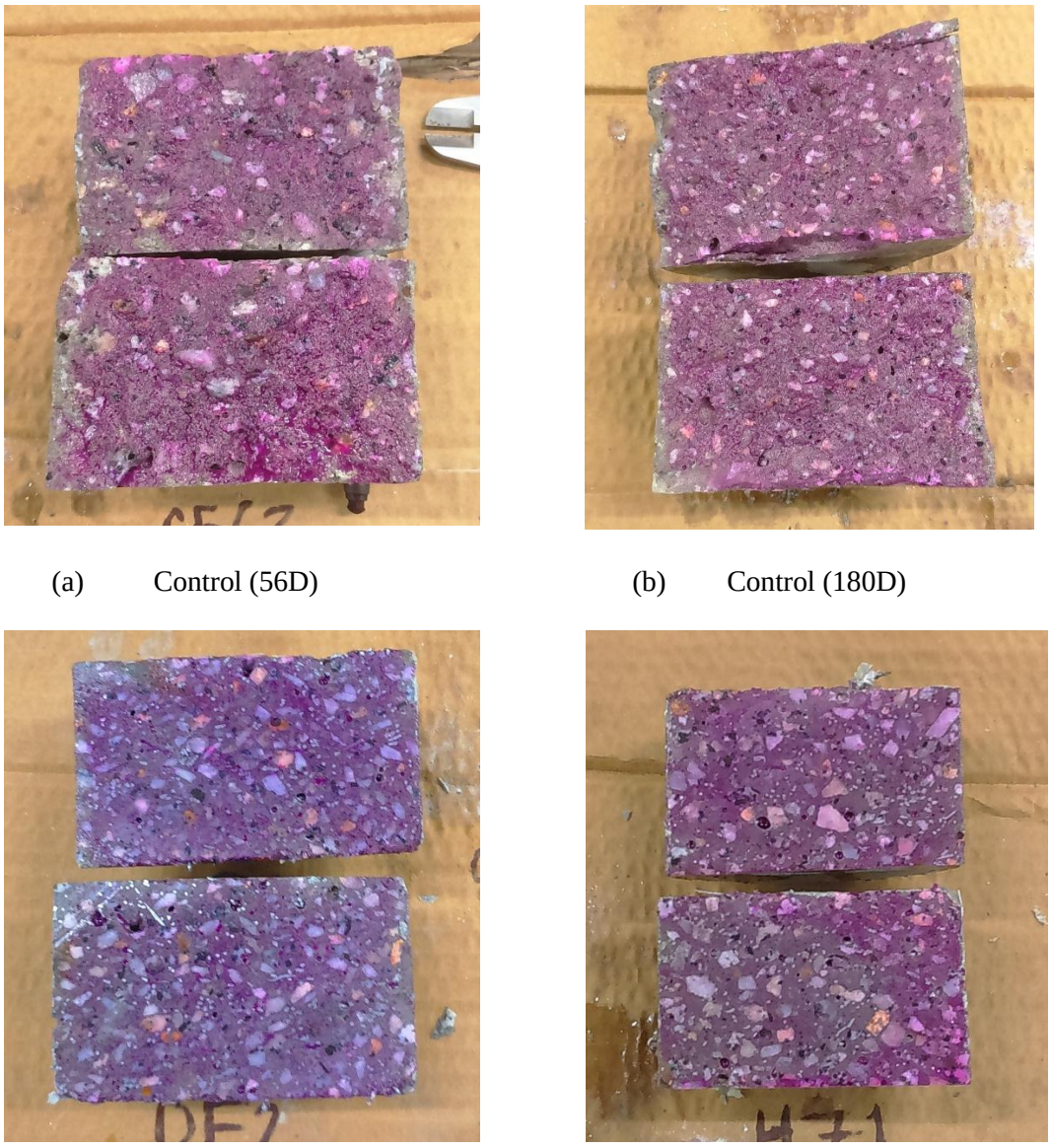

(a) Control (56D) (b) Control (180D)

(c) 1.5S0.5P (56D) (d) 1.0S0.5P0.5B (56D)

Figure 5-33: Depth of the carbonation of concrete samples.

Table 5.6: Average carbonation depth of concrete samples

Specimens	Control	Control	1.5S0.5P	1.0S0.5P0.5B
Time (Days)	(56)	(180)	(56)	(56)
Average carbonation depth (mm)	5.077	4.289	3.467	1.521

5.4.5 Porosity analysis

A scan of control and 1.0S0.5P0.5B concrete sample is shown in Figure 5-34 which is envisaged in 3D with different colour.

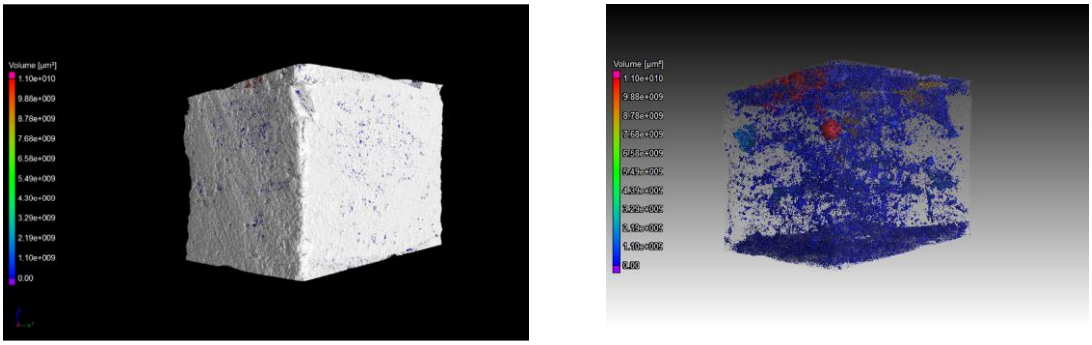

(a) Control sample

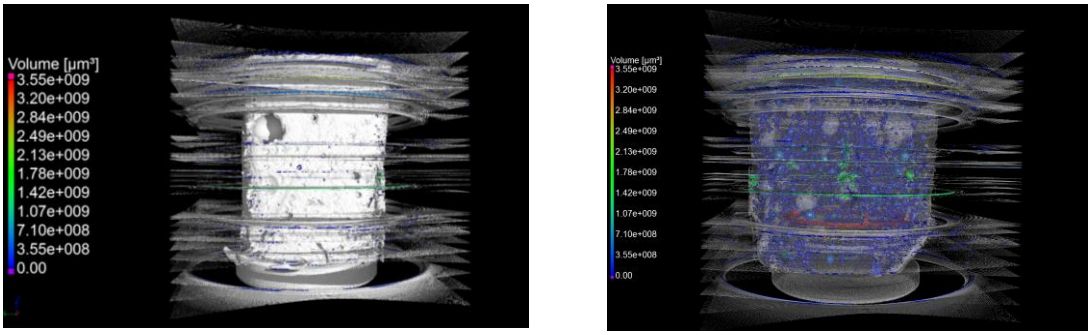

(b) 1.5S0.5P sample

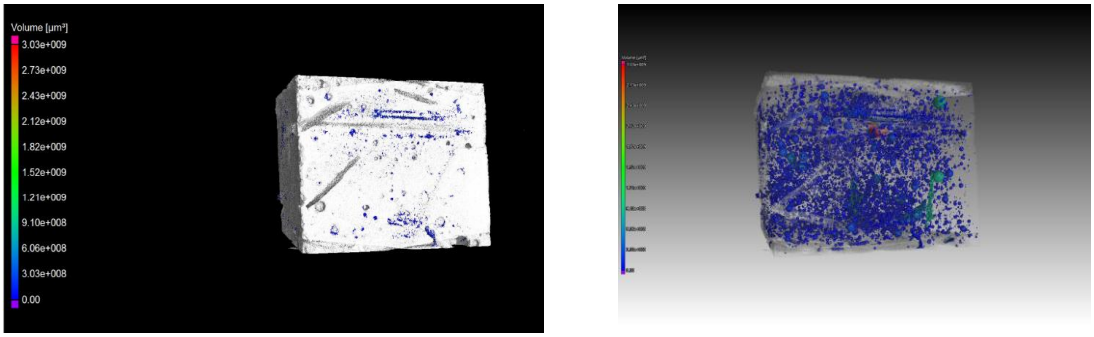

(c) 1.0S0.5P0.5B sample

Figure 5-34: 3D view of concrete sample with colour according to size

This investigation can be explained to yield 3D void size distribution data in histogram as in Figure 5-35. Total pore size distribution can be seen from the histogram. The largest detected void for control, 1.5S0.5P and 1.0S0.5P0.5B sample is 7.4 mm^3, 9.8 mm^3 and 11 mm^3

respectively. Average defect volume ratio for control, 1.5S0.5P and 1.0S0.5P0.5B concrete sample is 5.38%, 8.54% and 6.46 %. The difference of the average porosity of with and without fibers was found insignificant. Moreover, 1.0S0.5P0.5B sample shows better porosity resistance than 1.5S0.5P sample. This is because; basalt fiber may perform as the small aggregate to generate a homogeneous and dense microstructure (Landisa et al., 2003).

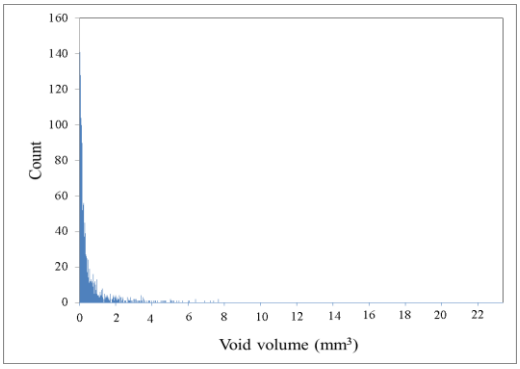

(a) Control sample

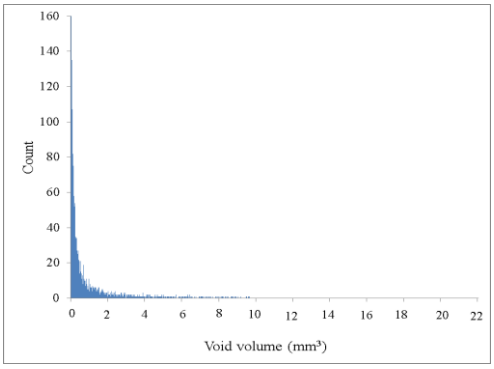

(b) 1.5S0.5P sample

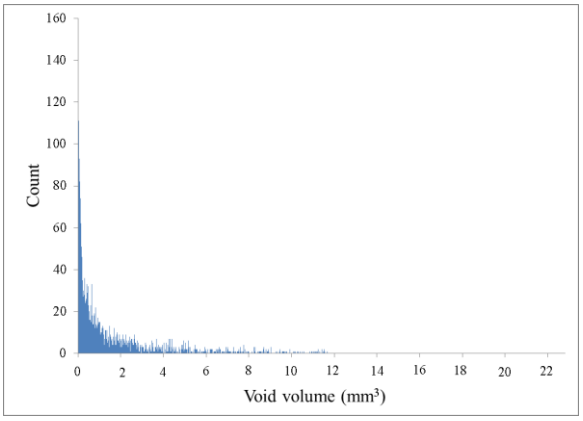

(c)1.0S0.5P0.5B sample

Figure 5-35: Histogram of void size distribution

Sphericity can be calculated by using the volume and 3D void surface area. Sphericity is plotted in Figure 5-36, which indicates that in both cases the biggest voids are not too spherical.

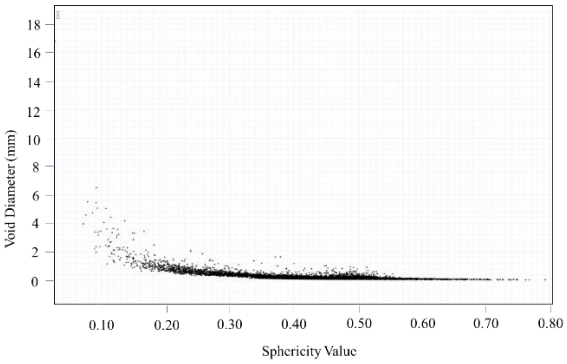

(a) Control sample

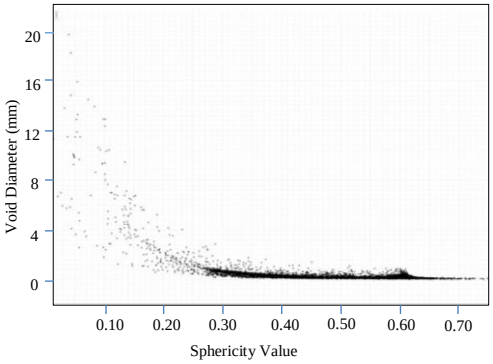

(b) 1.5S0.5P sample

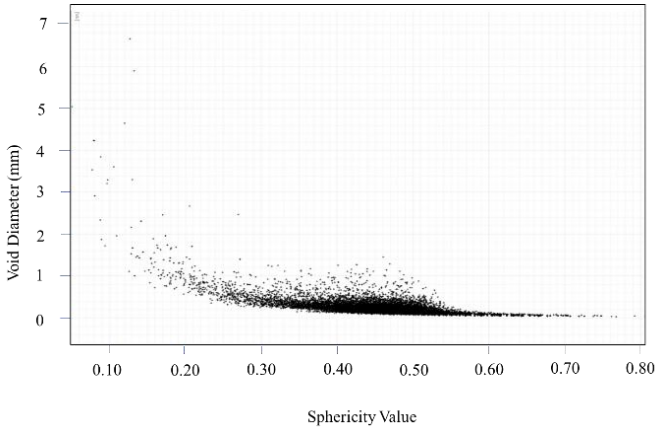

(c) 1.0S0.5P0.35B

Figure 5-36: Void diameter as a function of sphericity

5.5 CONCLUSION

In this chapter the benefits of two types of hybrid fiber (1.5S0.5P and 1.0S0.5P0.5B were compared) in high volume fly ash concrete based on mechanical and durability properties. An increase of about 5.0% to 7.0% is evident for compressive and splitting tensile strengths for 1.0S0.5P0.5B sample in comparison with 1.5S0.5P. Interestingly, a reduction in strength is also noted for three fiber combinations which suggest that the addition of any three fibers will not directly lead to increase in strength. Durability properties also confirm the suitability of three

fibers in hybrid in HVFA concrete in comparison control and two fiber hybrid concrete. Research ratifies that silane coated modified basalt fiber can be a good replacement albeit partially for the commonly used steel fiber. Contents of this chapter are also partially published in Journal of Building and Construction Materials, Vol. 215 (2019), pages 984–997

Chapter 6 Numerical simulation of fiber reinforced HVFA concrete by finite element analysis

6.1 Introduction

Finite element Method (FEM) is a well-established method for structural analysis. A numerical model of HVFA concrete along with the incorporation of hybrid fibers can rarely be found in the literature. Generally, attempts have been made on fiber reinforced concrete modelling, considering fibers as a component of the concrete similar to aggregates. This chapter documents the construction of a finite element model using experimental data of HVFA concrete with fibers using commercial software ANSYS Workbench 16.2. Initially, finite element analysis of control and single fiber reinforced high volume fly ash (HVFA) high strength concrete beam under static loadings were conducted to investigate their failure modes in terms of ultimate load. Starting with a three dimensional random distribution, the fiber orientation was simulated by spherical coordinate system. A high strength HVFA concrete beam was analysed with the appropriate modelling of element size and mesh by using nonlinear material properties implemented from experimental results to the ultimate failure by ANSYS. Post this analysis, it was reinforced with two hybrid fiber percentages (1.5S0.5P and 1.0S0.5P0.5B) by volume of HVFA concrete. All the necessary steps to create the model are explained in detail and the steps taken to validate the load-deformation response of the beam are discussed in this chapter. It is noted that the contents of this chapter are claimed as significant knowledge contribution arising from the thesis.

6.2 Finite element model

6.2.1 Element type

The high volume fly ash concrete was modelled using SOLID65 eight-node brick element, which is capable of simulating the cracking in tension and crushing in compression behaviour (Figure 6-1(a)). It is three-dimensional eight nodded element with three degrees of freedom at each node - translations in the x, y and z directions. Two nodded LINK8 bar is used in modelling the fibers throughout the concrete. This element is a 3D spar element – translations in the nodal x, y, and z directions. This element is also capable of plastic deformation. It works like a line element with two nodes at the ends (Figure 6-1(b)).

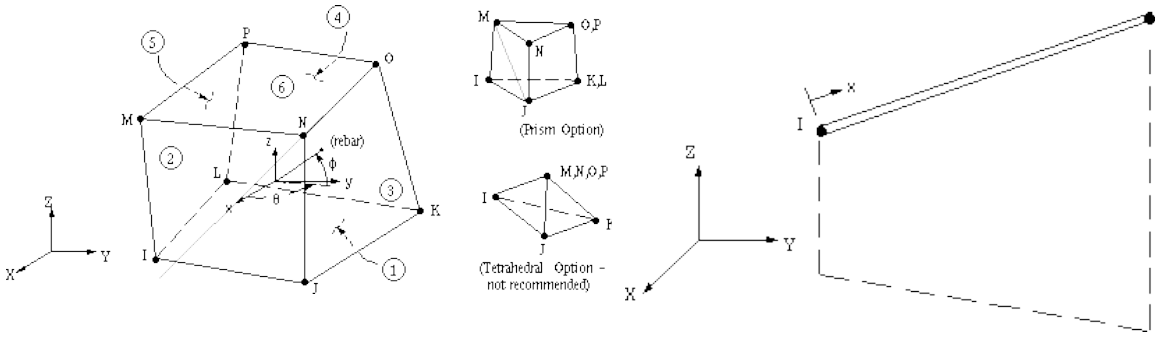

(a) Solid 65 3-D Reinforced Concrete Solid (b) LINK 8 3-D Spar

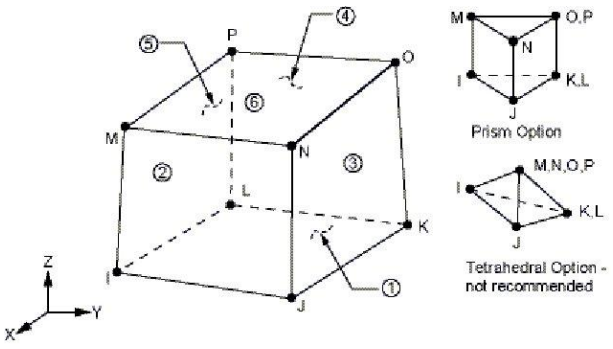

(c) Brick 8 node Solid 185

Figure 6-1: Elements used in calibration model

For steel plates and supports, element SOLID 185 is used. This element has eight nodes with three degrees of freedom at each node – translations in the nodal x, y, and z directions. The geometry and node locations for this element are shown in Figure 6-1(c).

Element CONTA175 and TARGE170 are used to simulate the bonding in between concrete and fibers. CONTA175 can be used to sliding between two surfaces (or between a node and a surface, or between a line and a surface) in 2-D or 3-D. This element is located on the surfaces of solid. TARGE170 can be used to represent target surfaces for the associated contact elements CONTA175. The contact elements themselves overlay the solid or line elements describing the boundary of a deformable body and are potentially in contact with the target surface (Figure 6-2).

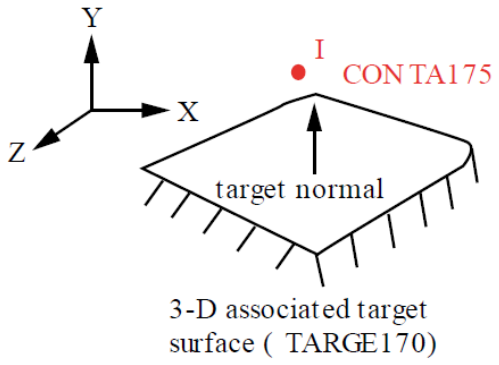

Figure 6-2: Geometry of CONTA175 and TARGE170

6.2.2 Material properties

To model the high strength high volume fly ash concrete, Solid65 element requires linear isotropic and multilinear isotropic material properties. The modulus of elasticity (E_c) and Poisson's ratio (υ) were considered 47480 MPa and 0.16 respectively from the experimental data of HVFA concrete. The compressive uniaxial stress-strain relationship for the HVFA concrete model was evaluated using the following equations (MacGregor, 1992).

$$f = \frac{E_c \varepsilon}{1+\left(\frac{\varepsilon}{\varepsilon_0}\right)^2} \qquad (6.1)$$

$$\varepsilon_0 = \frac{2f_c'}{E_c} \tag{6.2}$$

$$E_c = \frac{f}{\varepsilon} \tag{6.3}$$

Where,

f = stress at any strain ε, MPa

ε = strain at stress f

ε_0 = strain at the ultimate compressive strength f'_c

The first point of multilinear isotropic stress-strain curve must be satisfying Hooke's Law (Eq. 6.3). This curve will help for convergence of the nonlinear solution.

For example, if the compressive strength, modulus of elasticity and poisson's ratio becomes 80MPa, 42GPa and 0.18 respectively, the uniaxial stress strain curve can be illustrated by Figure 6-3. Point 1 is calculated for $0.30f'_c$ and the relationship is based on work done by Kachlakev et al. (2001). Points 2, 3, 4, 5 and 6 are calculated from Eq. 6.2 with ε_0 obtained from Eq. 6.1. Strains were selected and the stress was calculated. Point 7 is defined at ε_0 (0.00378 mm/mm) indicating traditional crushing strain for unconfined concrete.

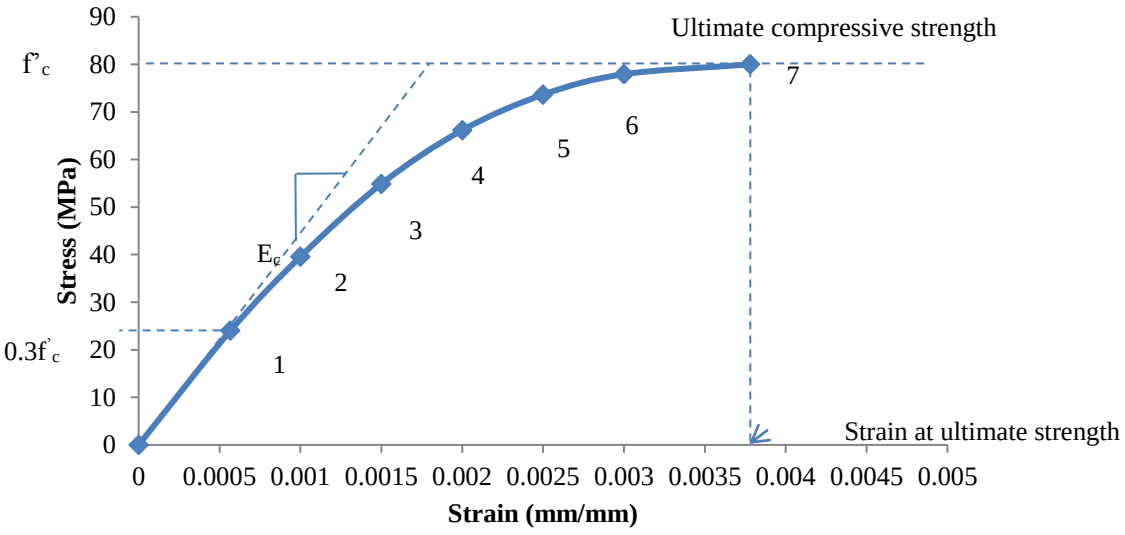

Figure 6-3: Uniaxial stress strain curve

To define the failure of the concrete, the multilinear isotropic material used the von Mises failure criterion along with the Willam and Warnke (1974) model. Typical shear transfer coefficients range from 0.0 to 1.0, with 0.0 representing a smooth crack (complete loss of shear transfer) and 1.0 representing a rough crack (no loss of shear transfer). The shear transfer coefficients for open and closed cracks were determined using the work of Kachlakev et al. (2001) as a basis. Convergence problems occurred when the shear transfer coefficient for the open crack dropped below 0.2. No deviation of the response occurs with the change of the coefficient. Therefore, the coefficient for the open crack was set to 0.3. So, the properties can be applied by using the following code in ANSYS workbench:

```
ET,MATID,SOLID65
R,MATID,0,0,0,0,0,0
RMORE,0,0,0,0,0

MP,EX,MATID,47480
MP,PRXY,MATID,0.16
MPTEMP,MATID,0

TB,CONCR,MATID,1,9
TBTEMP,22
TBDATA,1,0.3,0.8,4,66

TB,MISO,MATID,1,66,0
TBTEMP,22
TBPT,,0.000567,24.00
TBPT,,0.001,39.56
TBPT,,0.0015,54.86
TBPT,,0.002,66.00
```

Solid 45 element was used for the steel plates at loading points and supports on the beam. This element is modelled as a linear isotropic element with a modulus of elasticity (200GPa), and Poisson's ratio (0.3) for the steel.

Link 8 element is used for the fiber reinforcement in the beam. It is assumed to be bilinear isotropic. Bilinear isotropic material is based on the von Mises failure criteria. The bilinear model requires the yield stress and hardening modulus. Material properties are used as the same given in Chapter 4 Table 4.2.

6.2.3 Modelling

All the parts of the model were considered as volume. One quarter of each beam was three dimensionally modelled for numerical analysis with respect to the two symmetrical X-axis and Z-axis (Figure 6-4). So, the beam length is 175mm, with a cross-section of 50mm x 100mm. Here, 175mm for the X-coordinates is the mid-span of the beam. Because of symmetry, only one loading plate and one support plate are modelled. The support and loading plate is considered as 50mm x 25 mm x 5 mm steel plate.

To provide the geometry of fiber in concrete, a MATLAB code is programmed to generate the profile of the geometry of fiber. The assumption was that fibers were distributed randomly according to the spherical coordination system. Number of fibers was calculated with respect to the total volume of model beam and fibers and volume fraction of fibers.

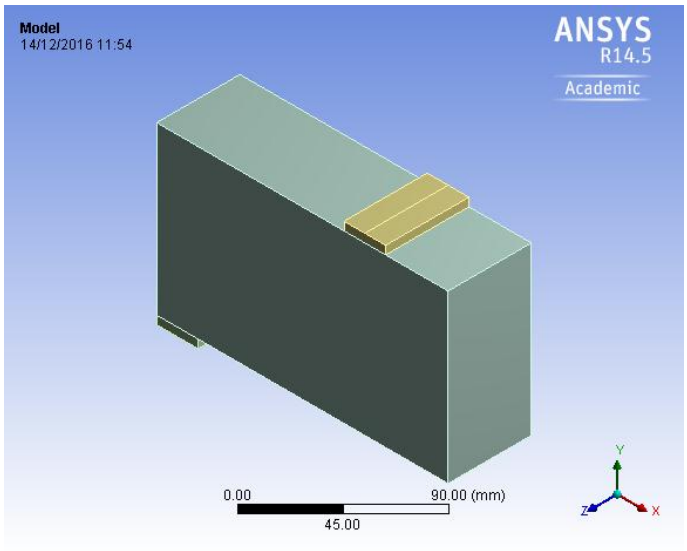

Figure 6-4: Volume created in ANSYS

In order to represent real condition, array function was used to select the first point of each fiber randomly within the geometry of model beam. Two angles α and β of spherical coordination system were also determined randomly in between 0 to 2π. MATLAB code for ramdom distribution of fibers can be illustrated as below:

% random distribution of x, y and z	% random distribution of α and β
N=floor(N)	α =pi*2
randomx=rand(1,N)	β =2*pi
x*randomx	randomα =rand(1,N)
randomy=rand(1,N)	α =360*randomα
y*randomy	cos(α)
randomz=rand(1,N)	sin(α)
z*randomz	randomβ =rand(1,N)
	β =360*randomβ
	cos(β)
	sin(β)

Finally the end point of each fibre was evaluated by using the following spherical coordination equations:

$$x_2 = x_1 + l_f . \cos\alpha . \cos\beta \quad (6.4)$$

$$y_2 = y_1 + l_f . \sin\alpha . \cos\beta \quad (6.5)$$

$$z_2 = z_1 + l_f . \sin\beta \quad (6.6)$$

Where, the length (l_f) of fiber. Before plotting the points, it should be confirmed that all the points are located inside the geometry of the beam. The combined volumes and dimensions of the plate, support, and beam are shown in Figure 6-5.

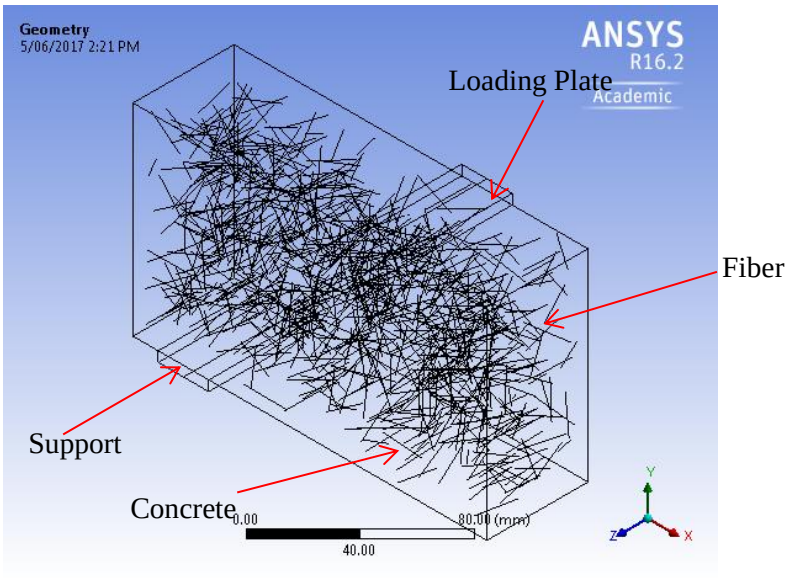

Figure 6-5: Volume of randomly distributed fibers

6.2.4 Connections

For the contact between fibers and matrix, contact pair was created by using element CONTA175 and TARGE170 (Table 6.1). High volume fly ash concrete is assumed to be a homogeneous solid which is considered as contact element. Contact element is also connected with the target support and loading plate face to face by using no separation contact. Multi point constraint (MPC) formulation was contrast for the connection.

Table 6.1: Detail of contact pair

Scope	
Scoping Method	Geometry Selection
Contact	1 Body
Target	1715 Edges
Contact Bodies	CONCRETE
Target Bodies	Multiple
Definition	
Type	Bonded
Scope Mode	Manual
Trim Contact	On
Trim Tolerance	0.5 mm
Suppressed	No
Advanced	
Formulation	Program Controlled
Detection Method	Program Controlled
Penetration Tolerance	Program Controlled
Elastic Slip Tolerance	Program Controlled
Normal Stiffness	Program Controlled
Update Stiffness	Program Controlled
Pinball Region	Program Controlled

6.2.5 Meshing

It is recommended that to get better results from the Solid65 element, rectangular mesh is good to use. Here, the mesh was considered as 5mm rectangular elements. Meshing of line (Link8) is done by dividing 15 to 35 numbers of elements for each fibers. The mesh of the concrete, loading plate, and support is presented in Figure 6-6 (a). Figure 6-6 (b) shows meshing of randomly distributed fibers.

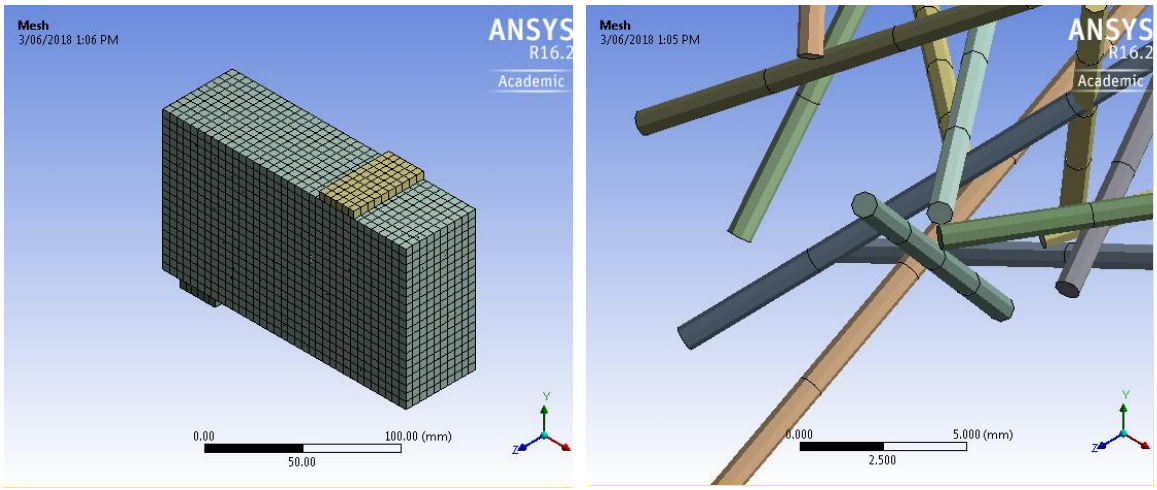

(a) Concrete model mesh (b) Fiber model mesh

Figure 6-6: Meshing of the model

6.2.6 Loads and boundary conditions

To confirm that the model acts in a similar way as the experimental beam, boundary conditions need to be applied at the points of supports and loadings. Firstly, the symmetry boundary conditions were fixed. The model being used is symmetric about X and Z axis. The boundary conditions for both planes of symmetry are shown in Figure 6-7.

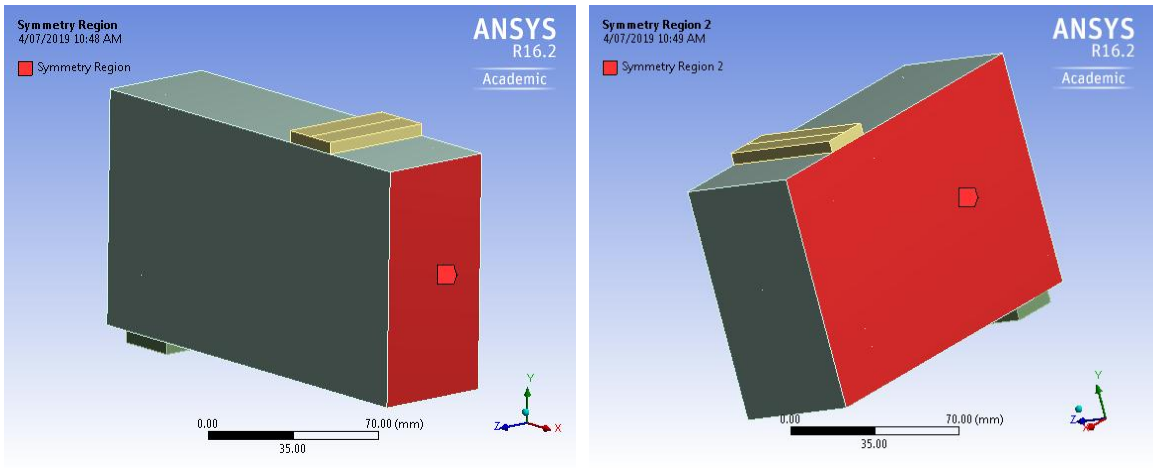

(a) Constraint at X direction (b) Constraints at Z direction

Figure 6-7: Boundary condition for Symmetry plane

A roller support was modelled where a single line of nodes on the plate were given constraint in the UY=0, and UZ=0. The boundary condition for support is shown in Figure 6-8.

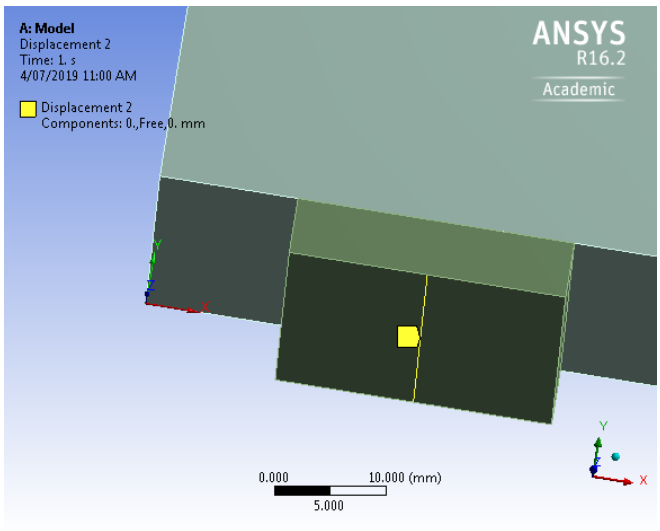

Figure 6-8: Support condition

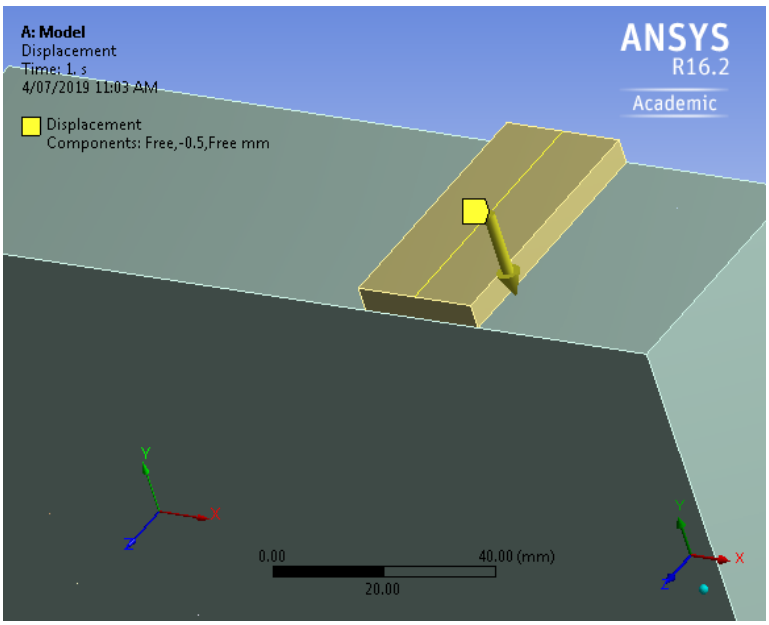

Figure 6-9: Boundary condition at loading plate

For four point symmetric loading beam, displacement at top is given only in negative Y direction (downward) at the steel plate across the entire centerline of the plate (Figure 6-9).

6.2.7 Analysis Settings

The details of the analysis settings are illustrated on Table 6.2. This model is prepared under static transverse loading. Various numbers of load steps, sub steps and loads were applied for different files. Solver type is selected under program controlled where weak spring is turned on (Table 6.2). For concrete, large deflection is not allowed. The restart command is utilized to restart an analysis after the initial run or load step has been completed. The Newton-Raphson procedure was applied up to the failure of the beam. Here, force convergence is kept to turn on with a tolerance 0.5%.

Table 6.2: Details of the analysis settings.

Step Controls	
Number Of Steps	1.
Current Step Number	1.
Step End Time	1. s
Auto Time Stepping	On
Define By	Substeps
Initial Substeps	50.
Minimum Substeps	20.
Maximum Substeps	50.
Solver Controls	
Solver Type	Program Controlled
Weak Springs	On
Spring Stiffness	Program Controlled
Solver Pivot Checking	Program Controlled
Large Deflection	Off
Inertia Relief	Off
Restart Controls	
Generate Restart Points	Program Controlled
Retain Files After Full Solve	No
Nonlinear Controls	
Newton-Raphson Option	Program Controlled
Force Convergence	On
--Value	Calculated by solver
--Tolerance	0.5%
--Minimum Reference	1.e-002 N
Moment Convergence	Program Controlled
Displacement Convergence	Program Controlled
Rotation Convergence	Program Controlled
Line Search	Program Controlled
Stabilization	Off
Output Controls	

Step Controls	
Solver Controls	
Restart Controls	
Nonlinear Controls	
Output Controls	
Stress	Yes
Strain	Yes
Nodal Forces	No
Contact Miscellaneous	No
General Miscellaneous	No
Store Results At	All Time Points
Analysis Data Management	
Solver Files Directory	C:\scratch\Final prograı
Future Analysis	None
Scratch Solver Files Direct...	
Save MAPDL db	No
Delete Unneeded Files	Yes
Nonlinear Solution	No
Solver Units	Active System
Solver Unit System	nmm
Visibility	
Remote Displacement (RX)	Suppressed
Displacement (Y)	Suppressed
[C] Displacement 2 (X)	Display
[D] Displacement 2 (Y)	Display
[E] Displacement 2 (Z)	Display
[F] Force	Display
Displacement 3 (X)	Suppressed
Displacement 3 (Y)	Suppressed
Displacement 3 (Z)	Suppressed
Force 2 (Force)	Suppressed

The rest of the commands were set to default. To illustrate the cracking pattern of concrete, additional command code (written below) need to be added to turn on the vector mode.

```
/SHOW,png
/ANG,1,
/VIEW,1,0,0,0
SET,1,1
/DEVICE,VECTOR,ON
!PLNSOL,s,eqv
!SET,Lstep,1
SET,Last
PLCRACK
```

6.3 Results and discussions

6.3.1 Control HVFA concrete

The aim of the comparison of the FE model for the control and single fiber reinforced concrete beam is to ensure that properties and convergence criteria are sufficient to model the response of the hybrid fiber reinforced beam.

(a) Failure load – 17066.7 N

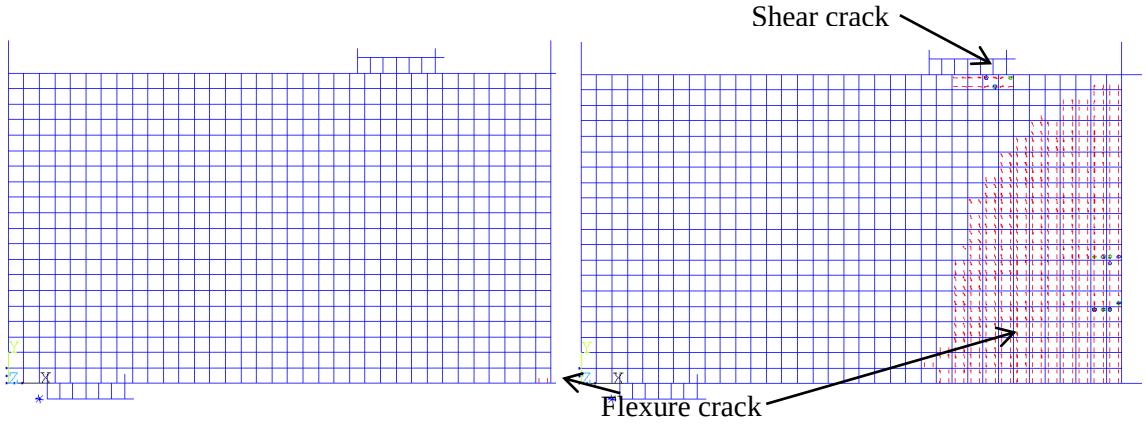

(b) First crack load - 13002 N (c) Failure load - 17641.2 N

Figure 6-10: Comparison of crack behaviour of control beam

First crack for the control beam model is a flexural crack and it occurs in constant moment region similar to experimental beam (Figure 6-10).

Shear cracks can be observed under the loading plate of the model beam. This crack mainly occurs due to the insufficient reinforcement. Comparison of full load deflection curves for control beam is illustrated in Figure 6-11. This load deflection of finite element analysis was

calibrated by setting the tolerances to 0.5% of default value. The load-deformation of the control beam model matches well with the response from the experiment. This gave confidence to model and analyse the fiber reinforced concrete beam.

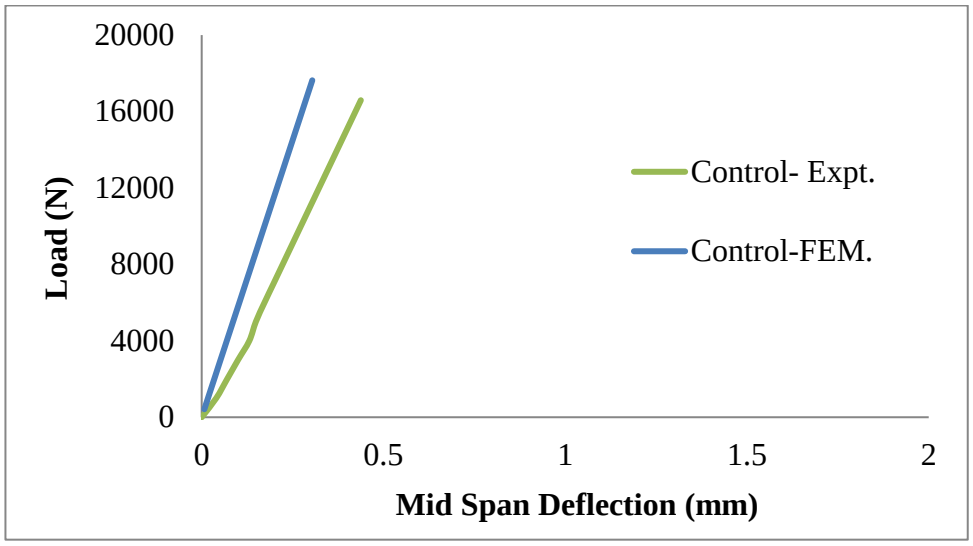

Figure 6-11: Comparison of load deflection curve of control beam

6.3.2 Single fiber reinforced HVFA concrete

Experimental and finite element model stress-deflection is given in Table 6.3. Generally, the results show a good agreement between the experimental data and FE model data. The variances between the experimental and FE data can be attributed due to the experimental errors in obtaining material properties, fiber orientation etc.

Table 6.3: Deflection at ultimate load for fiber reinforced beam

	Flexural stress (MPa)			Deflection (mm)		
	Expt.	FEA	SD	Expt.	FEA	SD
Control	5.12	5.29	0.085	0.416	0.212	0.102
0.5% St	6.66	6.81	0.075	0.492	0.291	0.1005
1.0% St	7.01	7.26	0.125	0.514	0.277	0.1185
1.5% St	7.22	7.57	0.175	0.475	0.181	0.147
0.5% PP	5.47	6.69	0.61	0.489	0.215	0.137
1.0% PP	6.42	7.03	0.305	0.429	0.213	0.108
1.5% PP	7.3	7.42	0.06	0.364	0.177	0.0935
0.5% BF	5.47	5.94	0.235	0.389	0.292	0.0485

*Expt. = Experimental value; SD= Standard deviation

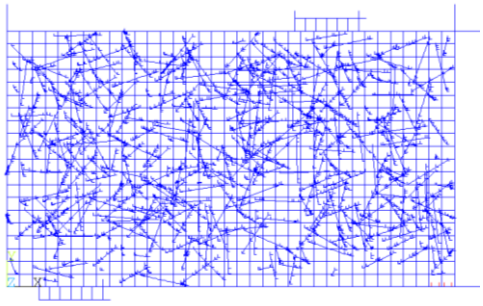

(i) First crack- 15825.5 N

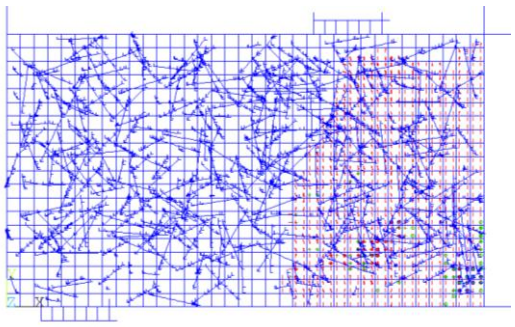

(ii) Failure load crack- 22725.3 N

(a) 0.5% steel fiber

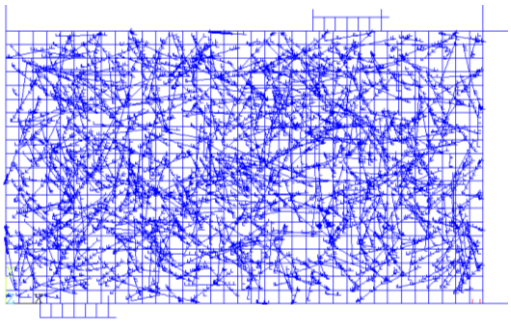

(i) First crack- 15875.2 N

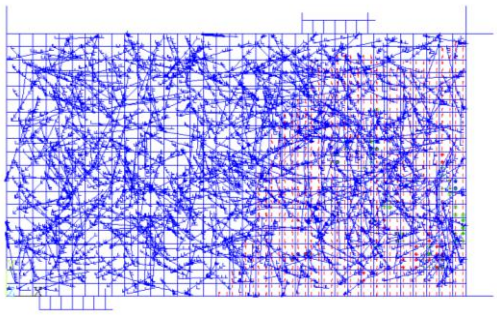

(ii) Failure load crack- 24202.4 N

(b) 1.0% steel fiber

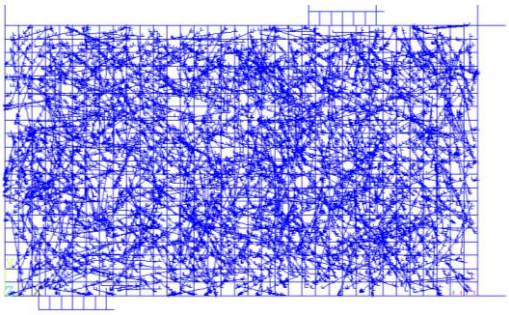

(i) First crack - 15948.4 N

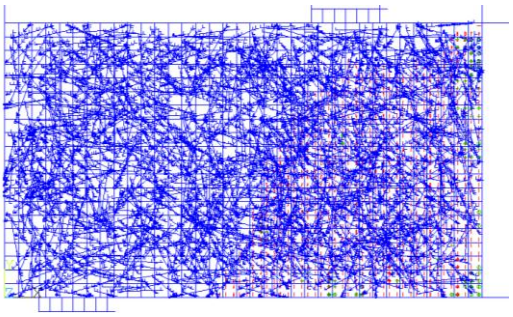

(ii) Failure load crack – 25258.0 N

(c) 1.5% steel fiber

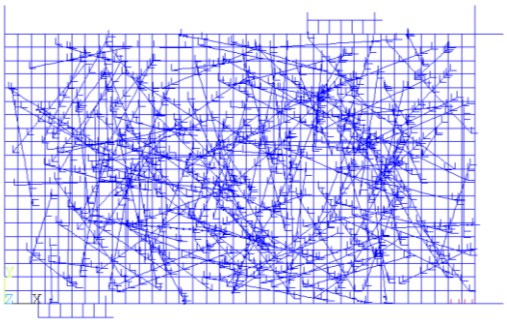

(i) First crack – 15800.0 N

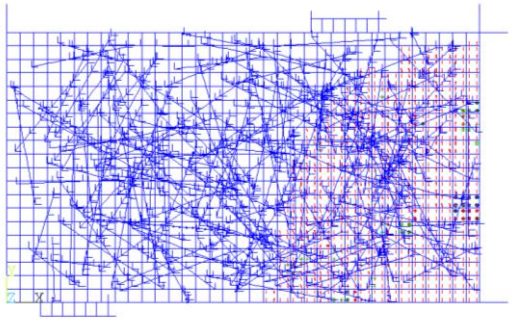

(ii) Failure load crack – 22320.0 N

(d) 0.5% polypropylene fiber

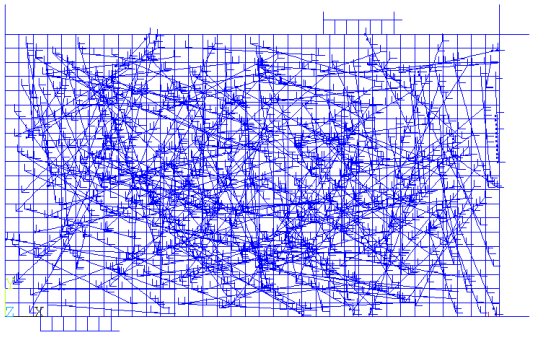

(i) First crack - 15805.6 N

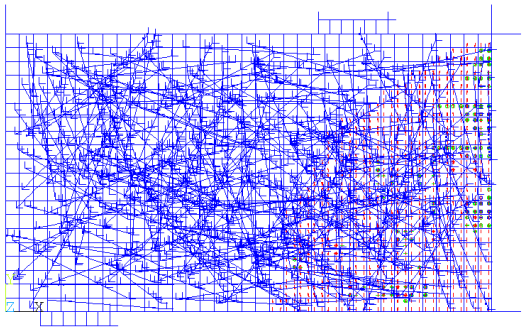

(ii) Failure load crack - 23455.6 N

(e) 1.0% polypropylene fiber

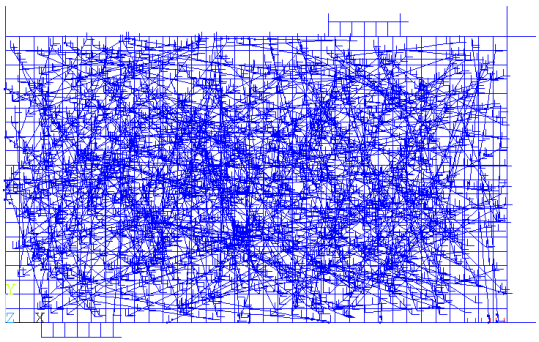

(i) First crack – 15948.0 N

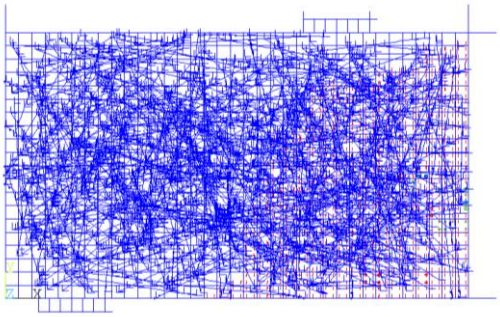

(ii) Failure load crack – 24764.0 N

(f) 1.5% polypropylene fiber

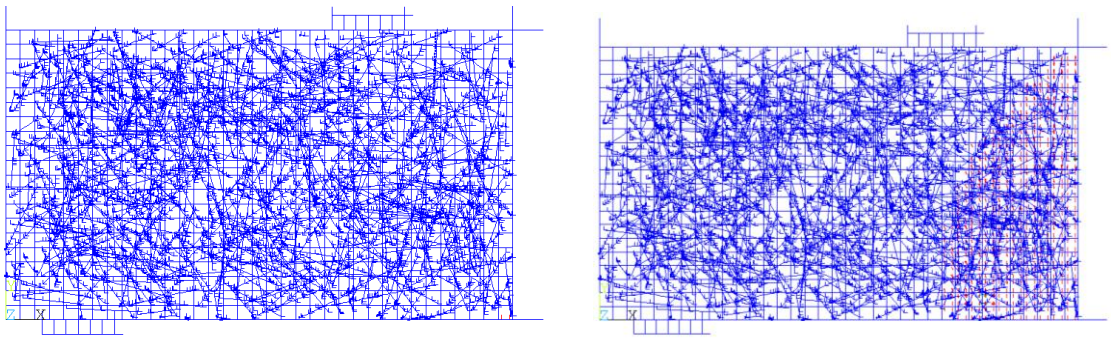

(i) First crack - 15861.2 N

(ii) Failure load crack - 19805.2 N

(g) 0.5% Basalt fiber

Figure 6-12: First crack and failure load of single fiber reinforced HVFA concrete beam model

First crack for fiber reinforced beam is a flexural crack and always occurs in the constant moment region similar to control beam. In the non-linear region, further cracking occurs as higher load is applied to the beam. With the increase of the load, cracking increases in the constant moment region and diagonal cracking starts. The load for crack of the single fiber reinforced concrete beam in the FE model is represented in Figure 6-12. From the figure, it is confirmed that fibers reduced the shear crack at support or loading zone and increased flexural strength in comparison to control sample. Furthermore, due to the addition of fibers, steel and polypropylene concrete crack propagates more towards the support than control or basalt fiber concrete. Among all three types of fibers, basalt fiber concrete shows relatively low flexural strength increment, however it is higher than control beam.

6.3.3 Hybrid fiber reinforced concrete

6.3.3.1 Behaviour of cracking

The first cracking of the 1.5S0.5P and 1.0S0.5P0.5B beam corresponds to the load 16100.2 N and 15800 N respectively. The first crack is shown in Figure 6-13 (i, ii). Similar to the control and single fiber reinforced concrete, the first crack occurs within the middle 1/3 region which is known as constant moment region. After first crack occurs, additional cracking occurs with the

increment of load. In nonlinear analysis, cracking increases in the middle third of the beam and the beam starts cracking towards the support. Substantial flexural cracking occurs in the beam 1.5S0.5P and 1.0S0.5P0.5B at 19900 N and 18400 N respectively and diagonal cracks begin to form in the model (Figure 6-13 (iii, iv)). Cacking reaches to the top of the beam and more cracks start to form including flexural, diagonal or multiple. The ultimate failure happens shortly. The ultimate failure stress for 1.5S0.5P and 1.0S0.5P0.5B specimens are 8.16 MPa and 8.10 MPa respectively and the beam can no longer support any additional load. Multiple cracking can be found throughout the constant moment region (Figure 6-13 (v, vi)). The cracking patterns for 1.5S0.5P and 1.0S0.5P0.5B samples are similar and compares well with the experimental beam.

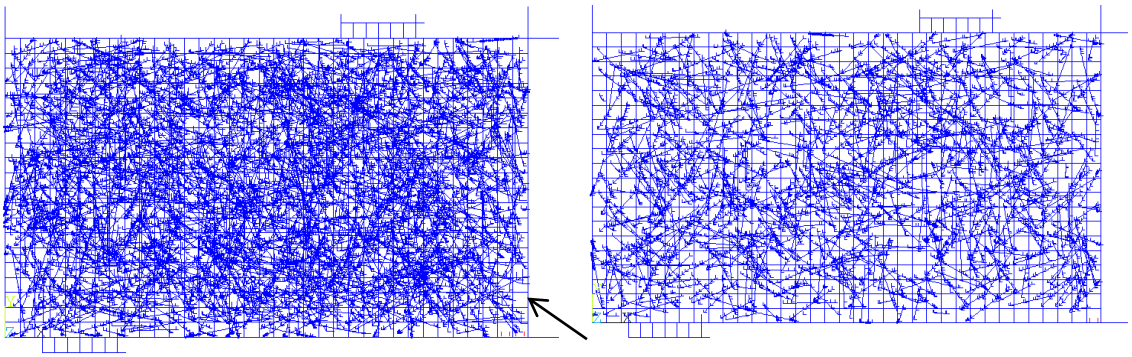

(i) First crack- 16100.2 N (ii) First crack- 15880 N

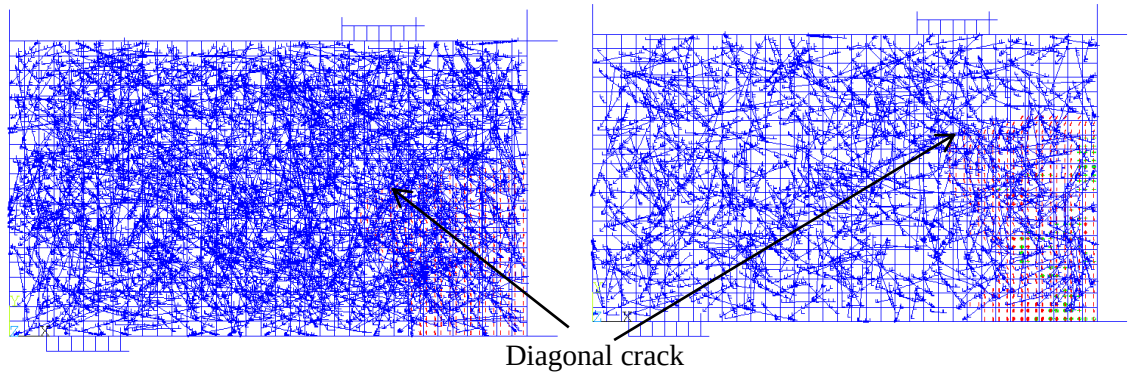

(iii) At 19900.0 N load (iv) At 18400 N load

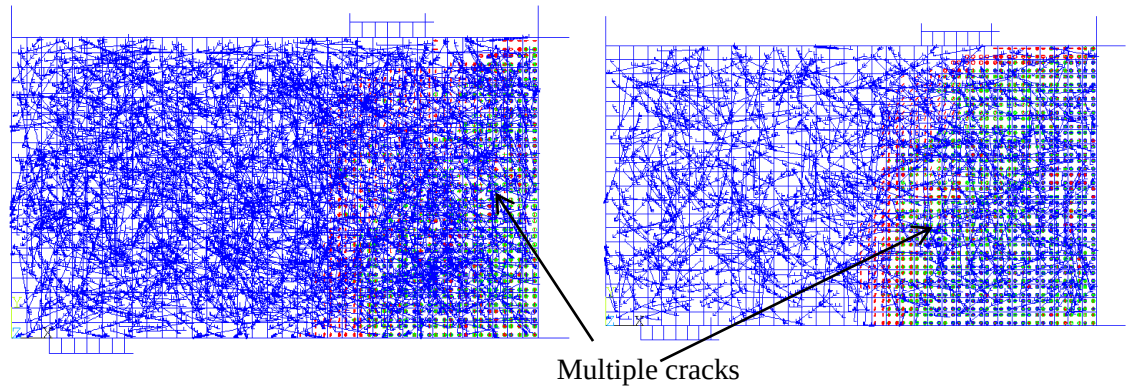

(v) Failure load- 27214.3 N (vi) Failure load- 27000 N

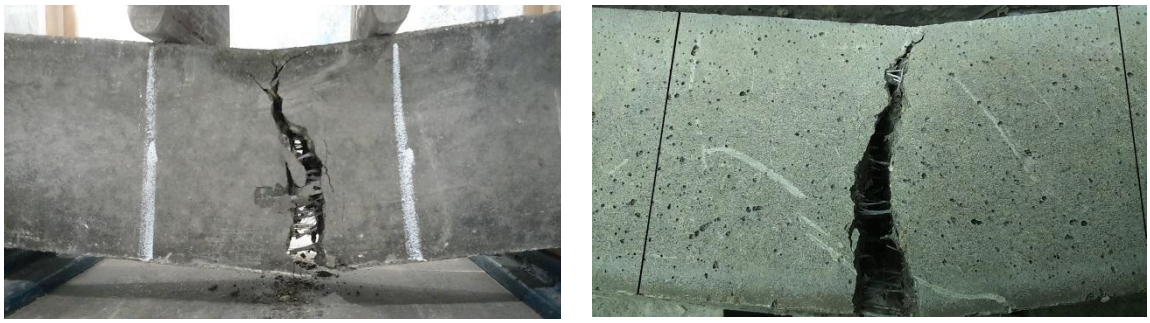

(vii) Expt. Failure crack – 26700 N (viii) Expt. Failure crack – 26400 N

(a) 1.5S0.5P beam (b) 1.0S0.5P0.5B beam

Figure 6-13: Comparison of crack pattern of 1.5S0.5P and 1.0S0.5P0.5B specimens

6.3.3.2 Behaviour of the fiber

Adding fiber helps to minimize shear crack at support or loading zone of the concrete beam. In nonlinear response, fibers increase the ability of the beam to distribute load throughout the cross section. The hybridizations of fibers are shown in Figure 6-14 and Figure 6-15. In fiber combination, it can be seen that basalt fiber have diminutive diameter in comparison to steel and polypropylene fiber (Figure 6-15).

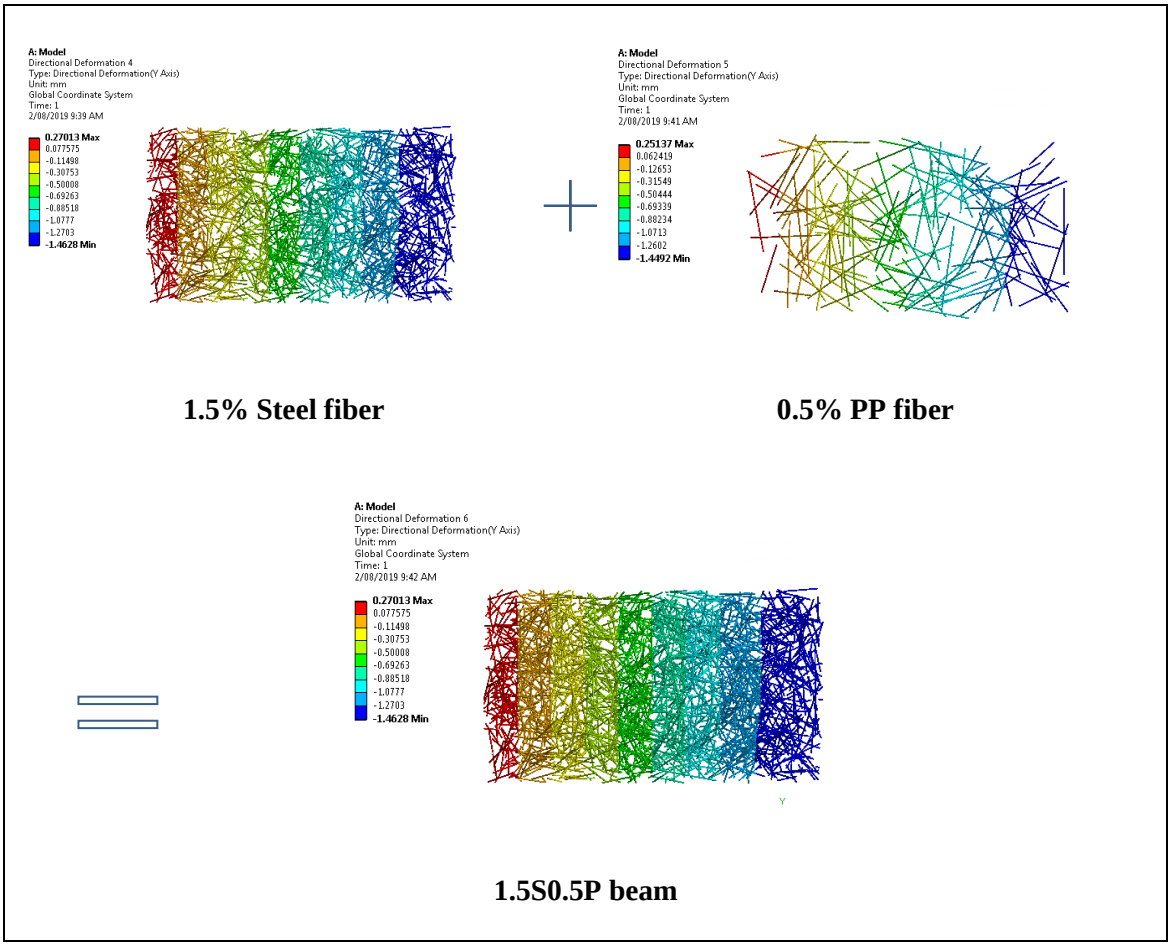

Figure 6-14: Incorporated hybrid fiber deformation pattern (1.5% ST + 0.5% PP =1.5S0.5P)

It can be observed that fibers deformation zone is divided throughout the length of the concrete beam. It confirms that fibers are well bonded with the concrete model and illustrates deflection for different loading actions with concrete.

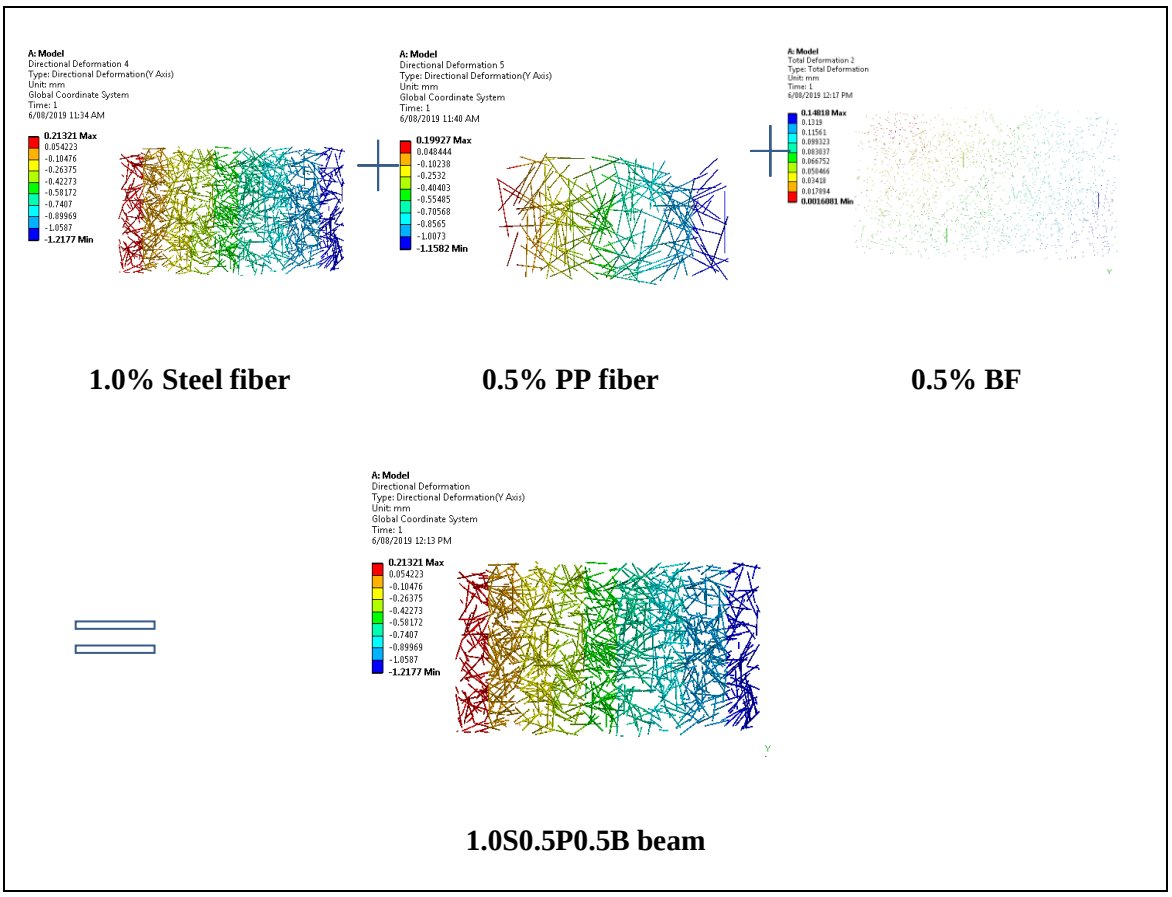

Figure 6-15: Incorporated hybrid fiber deformation pattern (1.0% ST + 0.5% PP+0.5% BF =1.0S0.5P0.5B)

6.3.3.3 Load Deflection Relationship

The full nonlinear load-deformation response can be seen in Figure 6-16. The curve determined using FEA is plotted upon the experimental response. From comparison of the beams shown in Figure 6-16, it is confirmed that after peak strength the downgrade curve does not decrease sharply due to hybrid effect of fibers. The load-deflection curves are almost linear up to the ultimate load. The deflection of experimental beam develops high because of the data acquisition system of experimental beam which allows deforming more in different cracking phases.

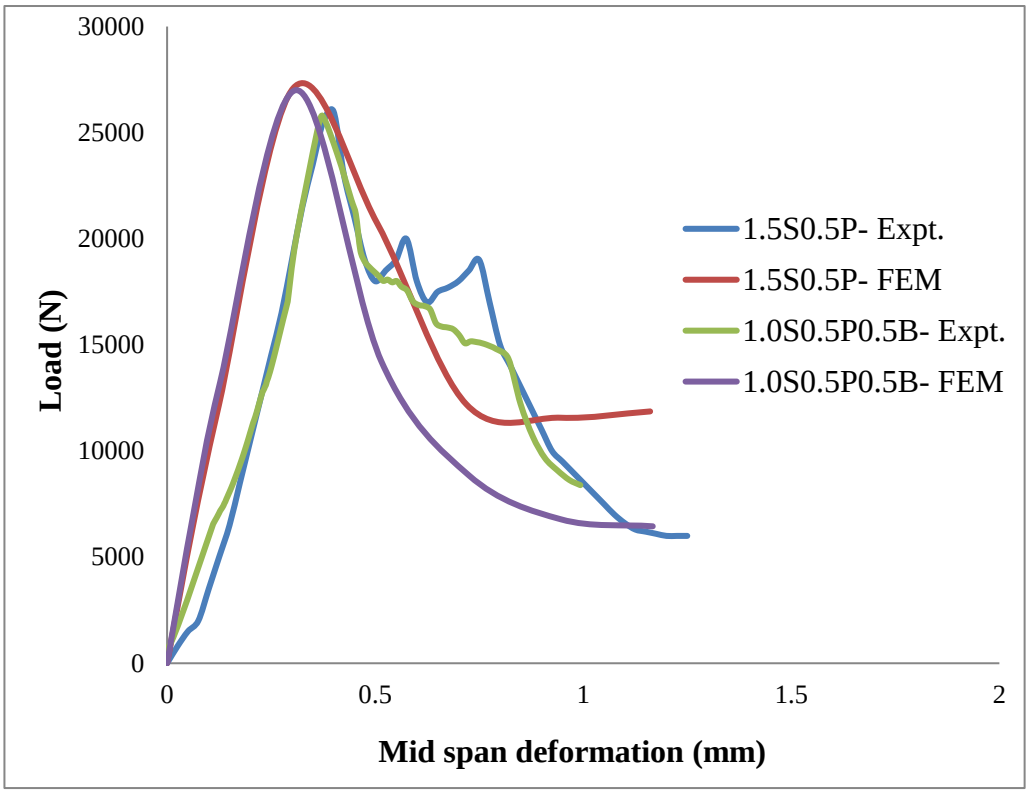

Figure 6-16: Load deflection curve comparison for FEA and experimental beam.

Table 6.4: Flexural stress and deflection results of experimental vs FEA beam

	Failure stress (MPa)				Deflection (mm)			
	Avg. Expt.	FEA	SD	COV (%)	Avg. Expt.	FEA	SD	COV (%)
1.5S0.5P	8.01	8.16	0.08	0.928	0.412	0.303	0.055	15.24
1.0S0.5P0.5B	7.82	8.10	0.09	1.124	0.373	0.309	0.032	9.38

However, the variations of the results are insignificant and the entire load-deformation curve of the model compares well with the experimental curve. From Table 6.4, it can be seen that the maximum flexural stress and deflections were well predicted from the FE models random fiber orientations. Though, the post-peak behaviors could vary due to the discrepancy between the real fiber orientation and the assumptions.

6.4 Conclusions

The numerical analyses for the beams were terminated after full cracking. The numerical analysis developed and presented in this chapter can predict the failure pattern and failure load of the beam consistent with experiment results. However, it can be seen that the strain for experimental results are higher in comparison to the numerical analysis which is insignificant. This model would be useful to predict the behaviour of different types and volume fractions of hybrid fiber reinforced HVFA concrete considering the random change of fiber orientation distribution.

Chapter 7 Conclusions and future recommendations

7.1 Introduction

This chapter presents the focal conclusions of this research work arising from the investigation of the effect of the hybrid fiber on high volume fly ash concrete and its numerical simulation and future recommendations. It concludes that the low cost natural basalt fibers has a positive effect on alkaline concrete medium and hybridization with steel and polypropylene fibers. Another innovative outcome of this investigation is the numerical simulation techniques treating the fiber presence as a separate entity; and its validation with experimental results by incorporating fibers as a separate geometry in HVFA concrete beam. This chapter also outlines the main recommendations of this work for future studies.

7.2 Low cost basalt fiber

Basalt fiber was one of the key target materials in this research work. Speciafically the deterioration of basalt fibers in alkaline medium was investigated. Two forms (modified or non-modified) of fibers were considered in the analyses purposes. The failure pattern and damage features of the fibers on the surface were rigorously analysed using scanning electron microscope (SEM) and further, compositions were identified using energy dispersive X-ray spectroscopy (EDX).

The silane coated modified basalt fiber exhibits superior properties compared to the non-modified fibers based on morphological and chemical analysis. All deterioration factors such as density of fibers, pH of the solutions (before and after immersion, concentration of solutions), and presence of coating materials were considered in the analysis.

Long term mass retention capacity was evaluated to determine the weights of modified and non-modified basalt fibers. In case of mass retention test, non-modified fibers immersed in Calcium

Hydroxide $Ca(OH)_2$ solutions created a ball-like formation and this ball was merely filled with dust. However, the modified basalt fibers did not form ball-like structures. Therefore, mass retention test alone is insufficient to evaluate fibers efficiency in alkaline concrete medium.

In chloride and sulphate medium, both sorts of basalt fibers were found to resist long term deterioration as Chloride (Ci^-) or sulphate (SO_4^{-2}) ion cannot attack the silica network of basalt fibers.

7.3 Hybrid fiber HVFA mortar

A further study of modified basalt fibers with the combination of well-known steel and polypropylene fiber in HVFA cement medium was carried out. Wide-ranging hybrid blends of fibers (both two types and three types) were tested on cement mortar specimens to identify the optimal fiber percentages. Two optimum hybrid combinations were found out from the overall analysis of compressive and flexural properties i.e., 1.5% steel, 0.5% polypropylene (1.5S0.5P) and 1.0% steel, 0.5% polypropylene, 0.5% basalt (1.S0.5P0.5B). However, a reduction in strength is also noted for three fiber combinations which suggest that the addition of any three fibers will not directly lead to increase in strength.

It is noted that optimal percentages were identified from the experimental data of cement mortar specimen later used to cast test specimens of concrete. Based on the experimental results, equations to predict the compressive and flexural strength were developed. The key variables of these equations are fiber percentages, raw or ultra-fine fly ash and testing time which is adequate for future investigations on different fiber blends. Artificial neural network was also further established to supplement the equations and verified by experimental data.

SEM analysis of modified basalt fibers in the cement mortar was carried out to confirm the long term stability in alkaline concrete medium. These discussions suggest the enhanced properties of the modified basalt fibers.

7.4 Hybrid fiber HVFA concrete

Mechanical and durability tests were conducted and analysed for both optimum hybrid fiber reinforced HVFA concrete. Furthermore, for finite element model verifications, particular single fibers reinforced HVFA concrete samples were cast and tested.

Attempts were taken to analyse the two optimum hybrid fiber percentages along with control specimens. An increase of about 5.0% to 7.0% was estimated for compressive and splitting tensile strengths for 1.0S0.5P0.5B sample in comparison with 1.5S0.5P. However, the incongruity for modulus of elasticity and flexural properties of these two samples are insignificant. This approves the application of silane coated modified basalt fibers as a good partial replacement for the commonly used steel fibers, albeit in hybrid combination.

The post cracking performance was determined and analysed by testing notched beam. Crack mouth opening displacement (CMOD) was measured along with the load deflection. The critical stress intensity factors (K_I), crack tip opening displacements (CTOD) and fracture energies (G_f) were determined and compared with the other established works. The results show a prominent increase and suitable coefficient of variance as shown in Chapter 5.

Along with the common test such as drying shrinkage, water absorption and carbonation, advanced computed tomography CT X-ray scan was used to examine the long-term durability issue of the hybrid fiber concrete. These techniques together confirmed the reduction in porosity and hence the durability of concrete directly suggesting the benefit of the added silane coated basalt fiber. Moreover, tests results of drying shrinkage, water absorption and/or carbonation were in conformance with the standards or specifications as per norms.

7.5 Numerical simulation

Numerical simulation technique of HVFA concrete incorporated with different fibers was developed by Finite Element Method. Commercial software package ANSYS Workbench 16.2 was used to construct the numerical model and validated with experimental data. The model

was prepared considering the geometry of concrete beam and fibers, material properties of HVFA concrete and fibers, boundary conditions similar to experimental methods. To prepare the fiber geometry and orientation throughout the concrete, spherical coordination equations were adopted. Nonlinear analysis was carried out under static load to investigate their failure modes in terms of ultimate load.

Firstly, control HVFA concrete model was validated with the experimental failure and ultimate loading capacity. Secondly, attempts were taken to validate single fibers (steel, polypropylene or basalt) reinforced HVFA concrete flexural strength. These results give a confidence to establish the model for hybrid fiber reinforced HVFA concrete.

Finally, two optimum hybrid fiber reinforced HVFA concrete beam models were developed and detail analysis of its failure pattern and load deflection curve was carried out in comparison with experimental beam. The results of the numerical simulation model compare very well with the experimental outcomes.

7.6 Recommendation for future studies

On the basis of current research, some recommendations are provided below:

1. Silane coated modified basalt fibers shows excellent mechanical and durability result as a hybrid fiber. Now, silane coated modified basalt fibers need to be compared with other modified basalt fibers.
2. The prediction equations of mortar from regression analysis and artificial neural network can be verified for other hybrid fibers reinforced experimental work which will enhance their acceptability.
3. Strain hardening under tensile loading can be evaluated.
4. Effect of the hybridization of these fibers can be evaluated for very high volume fly ash or geopolymer concrete.

5. Due to the addition of super plasticizer, it is required to measure the properties for self-consolidate concrete (SCC).
6. Long term mechanical properties such as creep need to be measured
7. A further study can be carried out to study the strain hardening mechanisms of such concrete.
8. Based on the numerical model and analysis, parametric analysis can be carried out for future hybridization of different types and percentages of fibers.

References

ABRISHAMBAF, A., BARROS, J. A. O. & CUNHA, V. M. C. F. 2015. Tensile stress–crack width law for steel fibre reinforced self-compacting concrete obtained from indirect (splitting) tensile tests. *Cement and Concrete Composites,* 57**,** 153-165.

ACI 1998. ACI Committee 363-92, State-of-the-art report on high-strength concrete. ACI Manual of Concrete Practice, Part 3.

AÇIKGENÇ, M., ULAŞ, M. & ALYAMAÇ, K. E. 2015. Using an Artificial Neural Network to Predict Mix Compositions of Steel Fiber-Reinforced Concrete. *Arabian Journal for Science and Engineering,* 40**,** 407-419.

AFROZ, M., PATNAIKUNI, I. & VENKATESAN, S. 2017. Chemical durability and performance of modified basalt fiber in concrete medium. *Construction and Building Materials,* 154**,** 191-203.

AGRAWAL, R., SAXENA, N. S., SHARMA, K. B., THOMAS, S. & SREEKALA, M. S. 2000. Activation energy and crystallization kinetics of untreated and treated oil palm fibre reinforced phenol formaldehyde composites. *Materials Science and Engineering: A,* 277**,** 77-82.

AHMED, S., MAALEJ, M. & PARAMASIVAM, P. 2006. Flexural responses of hybrid steel-polyethylene fiber reinforced cement composites containing high volume fly ash. *Constr. Build. Mater.,* 21**,** 1088-1097.

AHMED, S. F. U., MAALEJ, M. & PARAMASIVAM, P. 2007. Analytical model for tensile strain hardening and multiple cracking behavior of hybrid fiber-engineered cementitious composites. *Journal of Materials in Civil Engineering,* 19**,** 527.

AHMED SFU, M. M., PARAMASIVAM P. 2003. Strain-hardening behavior of hybrid fiber reinforced cement composites.

AÏTCIN, P. C. 1998. High-performance mix design methods. *High Performance Concrete.* 29 west 35th street, Routledge, New York.

ALBERTI, M. G., ENFEDAQUE, A., GÁLVEZ, J. C. & REYES, E. 2017. Numerical modelling of the fracture of polyolefin fibre reinforced concrete by using a cohesive fracture approach. *Composites Part B: Engineering,* 111**,** 200-210.

ALDAHDOOH, M. A. A., MUHAMAD BUNNORI, N. & MEGAT JOHARI, M. A. 2014. Influence of palm oil fuel ash on ultimate flexural and uniaxial tensile strength of green ultra-high performance fiber reinforced cementitious composites. *Materials & Design,* 54**,** 694-701.

ANADE, P. D., KATKAR, P. M. & RAYBAGI, A. A. *Basalt fiber Rock* [Online]. Available: http://www.fibre2fashion.com/industry-article/6728/basalt-rock-fibre [Accessed 22/08/2016.

AS 1985a. AS 1012.9-2014 Methods of testing concrete - Compressive strength tests - Concrete, mortar and grout specimens 476 Sydney NSW: SAI Global Limited under licence from Standards Australia Limited.

AS 1985b. AS 1012.10-1985: Method for the Determination of Indirect Tensile Strength of Concrete Cylinders 476 Sydney NSW: SAI Global Limited under licence from Standards Australia Limited.

AS 1985c. AS 1012.11-1985 Methods of testing concrete - Method for the determination of the flexural strength of concrete specimens. . 476 Sydney NSW: SAI Global Limited under licence from Standards Australia Limited.

AS 1997. AS 1012.17-1997 Methods of testing concrete-Determination of the static chord modulus of elasticity and Poisson's ratio of concrete specimens. 476 Sydney NSW: SAI Global Limited under licence from Standards Australia Limited.

AS 1998. AS 3582.1-1998 Supplementary cementitious materials for use with portland and blended cement - Fly ash. 476 Sydney NSW: SAI Global Limited under licence from Standards Australia Limited.

AS 1999. AS 1012.21-1999 Methods of testing concrete Determination of water absorption and apparent volume of permeable voids in hardened concrete. 476 Sydney NSW: SAI Global Limited under licence from Standards Australia Limited.

AS 2009. AS 3600- 2009. Concrete Structures. 476 Sydney NSW: SAI Global Limited under licence from Standards Australia Limited.

AS 2010. AS 3972-2010. General purpose and blended cements. 476 Sydney NSW: SAI Global Limited under licence from Standards Australia Limited.

AS 2014a. AS 1012.8.1-2014, Methods of testing concrete - Method for making and curing concrete - Compression and indirect tensile test specimens. 476 Sydney NSW: SAI Global Limited under licence from Standards Australia Limited.

AS 2014b. AS 1012.8.2-2014,Methods of testing concrete - Method for making and curing concrete - Flexure test specimens. 476 Sydney NSW: SAI Global Limited under licence from Standards Australia Limited.

AS 2015a. AS 1012.8.4:2015 Methods of testing concrete Method for making and curing concrete - Drying shrinkage specimens prepared in the field or in the laboratory. 476 Sydney NSW: SAI Global Limited under licence from Standards Australia Limited.

AS 2015b. AS 1012.13:2015 Methods of testing concrete-Determination of the drying shrinkage of concrete for samples prepared in the field or in the laboratory. 476 Sydney NSW: SAI Global Limited under licence from Standards Australia Limited.

ASTM 2002a. ASTM C109/ C109M - 02. (2002), Standard Test Method for Compressive Strength of Hydraulic Cement Mortars (Using 2-in. or [50-mm] Cube Specimens). *Annual Book of ASTM Standards.* Philadelphia, United States.

ASTM 2002b. ASTM C 348 – 02. (2002) Standard Test Method for Flexural Strength of Hydraulic-Cement Mortars. *Annual Book of ASTM Standards, Vol 04.01*. Philadelphia, United States.

ATICI, U. 2011. Prediction of the strength of mineral admixture concrete using multivariable regression analysis and an artificial neural network. *Expert Systems with Applications,* 38**,** 9609-9618.

ATIŞ, C. D. 2003. High-Volume Fly Ash Concrete with High Strength and Low Drying Shrinkage. *Journal of Materials in Civil Engineering,* 15**,** 153-156.

ATIŞ, C. D. & KARAHAN, O. 2009. Properties of steel fiber reinforced fly ash concrete. *Construction and Building Materials,* 23**,** 392-399.

BANTHIA, N. & NANDAKUMAR, N. 2003. Crack growth resistance of hybrid fiber reinforced cement composites. *Cement & Concrete Composites,* 25**,** 3-9.

BANTHIA, N. & SAPPAKITTIPAKORN, M. 2007. Toughness enhancement in steel fiber reinforced concrete through fiber hybridization. *Cement and Concrete Research,* 37**,** 1366-1372.

BANYHUSSAN, Q. S., YıLDıRıM, G., BAYRAKTAR, E., DEMIRHAN, S. & ŞAHMARAN, M. 2016. Deflection-hardening hybrid fiber reinforced concrete: The effect of aggregate content. *Construction and Building Materials,* 125**,** 41-52.

BENTZ, D. P., FERRARIS, C. F., AND SNYDER, K. A 2013a. "Best practices guide for high-volume fly ash concretes: Assuring properties and performance. *NIST Technical Note 1812, U.S. Dept. of Commerce, Washington, DC*.

BOUZIADI, F., BOULEKBACHE, B., HADDI, A. & DJELAL, C. 2018. Experimental and finite element analysis of creep behaviour of steel fibre reinforced high strength concrete beams. *Construction and Building Materials,* 173**,** 101-110.

BOUZOUBAÂ, N., ZHANG, M. H. & MALHOTRA, V. M. 2001. Mechanical properties and durability of concrete made with high-volume fly ash blended cements using a coarse fly ash. *Cement and Concrete Research,* 31**,** 1393-1402.

BRANDT, A. M. 2008. Fibre reinforced cement-based (FRC) composites after over 40 years of development in building and civil engineering. *Composite Structures,* 86**,** 3-9.

CCAA 2009. Chloride Resistance of Concrete. NSW, Australia, Cement Concrete & Aggregates Australia.

CHEN, B. & LIU, J. 2003. Effect of fibers on expansion of concrete with a large amount of high f-CaO fly ash. *Cement and Concrete Research,* 33**,** 1549-1552.

CHI, Y., XU, L. & YU, H.-S. 2014. Constitutive modeling of steel-polypropylene hybrid fiber reinforced concrete using a non-associated plasticity and its numerical implementation. *Composite Structures,* 111**,** 497-509.

CHOI, Y.-S., KIM, J.-G. & LEE, K.-M. 2006. Corrosion behavior of steel bar embedded in fly ash concrete. *Corrosion Science,* 48**,** 1733-1745.

CPC-18 1988. CPC-18 Measurement of hardened concrete carbonation depth, RILEM Recommendations for the Testing and Use of Constructions Materials. 56-58.

CROUCH, L. K., HEWITT, R. & BYARD, B. 2007. High Volume Fly Ash Concrete. *World of Coal Ash (WOCA)* Northern Kentucky.

CSA 1995. CSA A23.3-94. Design of concrete structures. Canadian Standard Association, Rexdale, Ontario, Canada.

DAWOOD, E. T. & RAMLI, M. 2010. Development of high strength flowable mortar with hybrid fiber. *Construction and Building Materials,* 24**,** 1043-1050.

DAWOOD, E. T. & RAMLI, M. 2011. High strength characteristics of cement mortar reinforced with hybrid fibre. *Construction and Building Materials,* 24**,** 2240-2247.

DE LA VARGA, I., SPRAGG, R. P., DI BELLA, C., CASTRO, J., BENTZ, D. P. & WEISS, J. 2014. Fluid transport in high volume fly ash mixtures with and without internal curing. *Cement and Concrete Composites,* 45**,** 102-110.

DEAK, T. & CZIGANY, T. 2009 Chemical Composition and Mechanical Properties of Basalt and Glass Fibers: A Comparison. *Textile Research Journal,* 79**,** 645-651.

DHAND, V., MITTAL, G., RHEE, K. Y., PARK, S.-J. & HUI, D. 2014. A short review on basalt fiber reinforced polymer composites. *Composites Part B,* 73**,** 166-180.

DIAS, D. P. & THAUMATURGO, C. 2005. Fracture toughness of geopolymeric concretes reinforced with basalt fibers. *Cement and Concrete Composites,* 27**,** 49-54.

DURÁN-HERRERA, A., JUÁREZ, C. A., VALDEZ, P. & BENTZ, D. P. 2011. Evaluation of sustainable high-volume fly ash concretes. *Cement and Concrete Composites,* 33**,** 39-45.

ELSHAFIE, S. & WHITTLESTON, G. 2016. Evaluating the Efficiency of Basalt and Glass Fibres on Resisting the Alkaline, Acid, and Thermal Environments. *American Journal of Materials Science,* 6**,** 19-34.

FIORE, V., SCALICI, T., DI BELLA, G. & VALENZA, A. 2015. A review on basalt fibre and its composites. *Composites Part B,* 74**,** 74-94.

GHAZY, A., BASSUONI, M. T., MAGUIRE, E. & O'LOAN, M. 2016. Properties of Fiber-Reinforced Mortars Incorporating Nano-Silica. *Fibers,* 4**,** 1-16.

GU, P., BEAUDOIN, J. J., ZHANG, M. H. & MALHOTRA, V. M. 1999. Performance of Steel Reinforcement in Portland Cement and High-Volume Fly Ash Concretes. *ACI Materials Journal,* 96**,** 551-559.

GUTIERREZ, R. M., DıAZ, L. N. & DELVASTO, S. 2005. Effect of pozzolans on the performance of fiber-reinforced mortars. *Cement & Concrete Composites,* 27**,** 593-598.

HASSAN, A. M. T., JONES, S. W. & MAHMUD, G. H. 2012. Experimental test methods to determine the uniaxial tensile and compressive behaviour of ultra high performance fibre reinforced concrete (UHPFRC). *Construction and Building Materials,* 37**,** 874-882.

HOSSAIN, K. M. A., GLADSON, L. R. & ANWAR, M. S. 2016. Modeling shear strength of medium- to ultra-high-strength steel fiber-reinforced concrete beams using artificial neural network. *Neural Computing and Applications*.

HUANG, K. & DENG, M. 2009. Stability of basalt fibers in alkaline solution and its effect on the mechanical property of concrete. *Fuhe Cailiao Xuebao (Acta Materiae Compositae Sinica),* 27**,** 150-154.

HUANG, K., DENG, M., MO, L. & WANG, Y. 2013. Early age stability of concrete pavement by using hybrid fiber together with MgO expansion agent in high altitude locality. *Construction and Building Materials,* 48**,** 685-690.

JIANG, C., FAN, K., WU, F. & CHEN, D. 2014. Experimental study on the mechanical properties and microstructure of chopped basalt fibre reinforced concrete. *Materials & Design,* 58**,** 187-193.

JIANG, C., T.J., M., D. CHEN & DONG, Q. Q. 2010. Influence of Basalt Fiber on Performance of Cement Mortar *Key Engineering Materials,* 426-427**,** 93-96.

KABAY, N. 2014. Abrasion resistance and fracture energy of concretes with basalt fiber. *Construction and Building Materials,* 50**,** 95-101.

KACHLAKEV, D., MILLER, T., YIM, S., CHANSAWAT, K. & POTISUK, T. 2001. Finite Element Modelling of Reinforced Concrete Structures Strengthening with FRP Laminates,. *Special Report SP316,Oregon Department Of Transportation, USA, May*.

KARAHAN, O. & ATIS, C. D. 2011. The durability properties of polypropylene fiber reinforced fly ash concrete. *Materials and Design,* 32**,** 1044-1049.

KAYALI, O. 2004. Effect of high volume fly ash on mechanical properties of fiber reinforced concrete. *Mater. Struct.,* 37**,** 318-327.

KAYALI, O. 2008. Fly ash lightweight aggregates in high performance concrete. *Construction and Building Materials,* 22**,** 2393-2399.

KHALIQ, W. & KODUR, V. 2011. Effect of High Temperature on Tensile Strength of Different Types of High-Strength Concrete. *ACI Materials Journal,* 108**,** 394-402.

KHUNTHONGKEAW, J., TANGTERMSIRIKUL, S. & LEELAWAT, T. 2006. A study on carbonation depth prediction for fly ash concrete. *Construction and Building Materials,* 20**,** 744-753.

KIM, M. T., RHEE, K. Y., PARK, S. J. & HUI, D. 2012. Effects of silane-modified carbon nanotubes on flexural and fracture behaviors of carbon nanotube-modified epoxy/basalt composites. *Composites Part B: Engineering,* 43**,** 2298-2302.

LANDISA, E. N., NAGYA, E. N. & KEANEB, D. T. 2003. Microstructure and fracture in three dimensions. *Eng. Fracture Mech. ,* 70**,** 911-925.

LANGLEY, W. S., CARETTE, G. G. & MALHOTRA, V. M. 1989. Structural concrete incorporating high volumes of ASTM class F fly ash. *ACI Mater. J.***,** 507-514.

LAWLER, J. S., WILHELM, T., ZAMPINI, D. & SHAH, S. P. 2003. Fracture processes of hybrid fiber-reinforced mortar. *Materials and Structures,* 36**,** 197-208.

LEE, D. H., HWANG, J.-H., JU, H., KIM, K. S. & KUCHMA, D. A. 2012. Nonlinear finite element analysis of steel fiber-reinforced concrete members using direct tension force transfer model.(Report). *Finite Elements in Analysis & Design,* 50**,** 266.

LEE, J. J., SONG, J. & KIM, H. 2014. Chemical stability of basalt fiber in alkaline solution. *Fibers and Polymers,* 15**,** 2329-2334.

LEHNE, J. & PRESTON, F. 2018. Making Concrete Change: Innovation in Low-carbon Cement and Concrete. Great Britain: Chatham House, The Royal Institute of International Affairs.

LI, G. 2004. Properties of high-volume fly ash concrete incorporating nano-SiO2. *Cement and Concrete Research,* 34**,** 1043-1049.

LI, Q., ZHAO, X., XU, S. & GAO, X. 2016. Influence of steel fiber on dynamic compressive behavior of hybrid fiber ultra high toughness cementitious composites at different strain rates. *Construction and Building Materials,* 125**,** 490-500.

LI, W. & XU, J. 2009. Mechanical properties of basalt fiber reinforced geopolymeric concrete under impact loading. *Materials Science and Engineering: A,* 505**,** 178-186.

LIPATOV, Y. V., GUTNIKOV, S. I., MANYLOV, M. S., ZHUKOVSKAYA, E. S. & LAZORYAK, B. I. 2015. High alkali-resistant basalt fiber for reinforcing concrete. *Materials & Design,* 73**,** 60-66.

LIU, K. W., DENG, M. & MO, L. W. 2013. Effect of Fly Ash on Resistance to Sulfate Attack of Cement-Based Materials. *Key Engineering Materials,* 539**,** 124-129.

LIU, S. B. & XU, L. H. 2013. Finite Element Analysis of Hybrid Fiber Reinforced HPC Deep Beams under Shear Load. *Applied Mechanics and Materials,* 419**,** 889-894.

MACGREGOR, J. G. 1992. *Reinforced Concrete: Mechanics and Design*, Prentice Hall.

MAHJOUB, R., YATIM, J. M., MOHD SAM, A. R. & HASHEMI, S. H. 2014. Tensile properties of kenaf fiber due to various conditions of chemical fiber surface modifications. *Construction and Building Materials,* 55**,** 103-113.

MAHMUD, G. H., YANG, Z. & HASSAN, A. M. T. 2013. Experimental and numerical studies of size effects of Ultra High Performance Steel Fibre Reinforced Concrete (UHPFRC) beams. *Construction and Building Materials,* 48**,** 1027-1034.

MALHOTRA, V. M., CARETTE, A., G. G. & BILODEAU, A. 1994. Mechanical properties and durability of polypropylene fiber reinforced high volume fly ash concrete for shortcrete applications. *ACI Materials Journal,* 91**,** 478-486.

MALHOTRA, V. M., ZHANG, M. H., READ, P. H. & RYELL, J. 2000. Long-Term Mechanical Properties and Durability Characteristics of High-Strength/High-Performance Concrete Incorporating Supplementary Cementing Materials under Outdoor Exposure Conditions. *Materials Journal*, 97.

MALHOTRA, V. M. A. M., P.K. 2005. High-Performance, High-Volume Fly Ash Concrete. *Supplementary Cementing Materials for Sustainable Development, Inc., Ottawa, Canada.*, 2nd ed.

MASTALI, M., ABDOLLAHNEJAD, Z. & PACHECO-TORGAL, F. 2018. 15 - Carbon dioxide sequestration of fly ash alkaline-based mortars containing recycled aggregates and reinforced by hemp fibers: Mechanical properties and numerical simulation with a finite element method. *In:* PACHECO-TORGAL, F., SHI, C. & SANCHEZ, A. P. (eds.) *Carbon Dioxide Sequestration in Cementitious Construction Materials.* Woodhead Publishing.

MEHTA, P. K. High performance, high volume fly ash concrete for sustainable development. *In:* WANG, K., ed. International Workshop on SUSTAINABLE DEVELOPMENT & CONCRETE TECHNOLOGY, 2004 Beijing, China. 3-14.

MILITKÝ, J., KOVAČIČ, V. R. & RUBNEROVÁ, J. 2002. Influence of thermal treatment on tensile failure of basalt fibers. *Engineering Fracture Mechanics,* 69**,** 1025-1033.

MOHAPATRA, M. & ANAND, S. 2010. Synthesis and applications of nano-structured iron oxides/hydroxides – a review. *International Journal of Engineering, Science and Technology,* 2.

MOROZOV, N. N., BAKUNOV, V. S., MOROZOV, E. N., ASLANOVA, L. G., GRANOVSKII, P. A., PROKSHIN, V. V. & ZEMLYANITSYN, A. A. 2001. Materials Based on Basalts from the European North of Russia. *Glass and Ceramics,* 58**,** 100-104.

NAIK, T. R., SINGH, S. S. & HOSSAIN, M. M. 1994. Permeability of concrete containing large amounts of fly ash. *Cement and Concrete Research,* 24**,** 913-922.

NAZARI, A. & RIAHI, S. 2011. Prediction split tensile strength and water permeability of high strength concrete containing TiO2 nanoparticles by artificial neural network and genetic programming. *Composites Part B: Engineering,* 42**,** 473-488.

NEVES, R. D. & ALMEIDA, J. C. O. F. 2005. Compressive behaviour of steel fibre reinforced concrete. *Structural concrete,* 6.1**,** 1-8.

NEVES, R. D. & GONLLALVES, A. 2000. Steel Fibre Reinforced Conerete-Durability Related Properties, LNEC, Lisbon, Portuguese.

NOVÁK, J. & KOHOUTKOVÁ, A. 2017. Fire response of Hybrid Fiber Reinforced Concrete to High Temperature. *Procedia Engineering,* 172**,** 784-790.

NOVITSKII, A. G. 2004. High-Temperature Heat-Insulating Materials Based on Fibers from Basalt-Type Rock Materials. *Refractories and Industrial Ceramics,* 45**,** 144-146.

NS-3473 1992. Concrete structures-design rules, in Norges Standardiserings Forbund. Norwegian Council for Strandardization, Oslo, Norway.

NYSTRÖM, U. & GYLLTOFT, K. 2011. Comparative numerical studies of projectile impacts on plain and steel-fibre reinforced concrete. *International Journal of Impact Engineering,* 38**,** 95-105.

OWEN, P. L. 1979. Fly Ash and Its Usage in Concrete. *Journal of Concrete Society,* 13**,** 21-26.

OZCAN, D. M., BAYRAKTAR, A., SAHIN, A., HAKTANIR, T. & TURKER, T. 2009. Experimental and finite element analysis on the steel fiber-reinforced concrete (SFRC) beams ultimate behavior. *Constr. Build. Mater.,* 23**,** 1064-1077.

PADMARAJAIAH, S. K. & RAMASWAMY, A. 2002. A finite element assessment of flexural strength of prestressed concrete beams with fiber reinforcement. *Cement and Concrete Composites,* 24**,** 229-241.

PAKRAVAN, H. R., JAMSHIDI, M. & LATIFI, M. 2016. Study on fiber hybridization effect of engineered cementitious composites with low- and high-modulus polymeric fibers. *Construction and Building Materials,* 112**,** 739-746.

PAPIRER, E. 2000. *Adsorption on Silica Surfaces*, New York- 10016, Marcel Dekker Inc.

PATNAIKUNI, I., MYADARABOINA, H. & ATMAJA, E. S. Stability of Basalt Fibers in Concrete Medium. 2nd R. N. Raikar Memorial International Conference, 18-19 December 2015 Mumbai, India 29-35.

PELED, A., MICHELE F. CYR & SHAH, S. P. 2000. High Content of Fly Ash (Class F) in Extruded Cementitious Composites. *ACI Materials Journal,* 97.

PRASAD, B. K. R., ESKANDARI, H. & REDDY, B. V. V. 2009. Prediction of compressive strength of SCC and HPC with high volume fly ash using ANN. *Construction and Building Materials,* 23**,** 117-128.

PUNURAI, W., KROEHONG, W., SAPTAMONGKOL, A. & CHINDAPRASIRT, P. 2018. Mechanical properties, microstructure and drying shrinkage of hybrid fly ash-basalt fiber geopolymer paste. *Construction and Building Materials,* 186**,** 62-70.

QIAN, C. & STROEVEN, P. 2000. Fracture properties of concrete reinforced with steel–polypropylene hybrid fibres. *Cement and Concrete Composites,* 22**,** 343-351.

QUAGLIARINI, E., MONNI, F., LENCI, S. & BONDIOLI, F. 2012. Tensile characterization of basalt fiber rods and ropes: A first contribution. *Construction and Building Materials,* 34**,** 372-380.

RABINOVICH, F. N., ZUEVA, V. N. & MAKEEVA, L. V. 2001. STABILITY OF BASALT FIBERS IN A MEDIUM OF HYDRATING CEMENT. *Glass and Ceramics,* 12**,** 29 – 32.

RAMACHANDRAN, B. E., VELPARI, V. & BALASUBRAMANIAN, N. 1981. Chemical durability studies on basalt fibres. *Journal of Materials Science,* 16**,** 3393-3397.

RAMANALINGAM, N., PARAMASIVAM, P., MANSUR, M. A. & MAALEJ, M. 2001. Flexural Behavior of Hybrid Fiber-Reinforced Cement Composites Containing High-Volume Fly Ash. 199**,** 147-162.

RAO.P, R. M. & A, R. C. 2012. Effect of hybrid fibres on the properties of class C fly ash based concrete. *International Journal of structural and Civil Engineering,* 1.

REIS, J. M. L. 2006. Fracture and flexural characterization of natural fiber-reinforced polymer concrete. *Construction and Building Materials,* 20**,** 673-678.

ROMUALDI, J. P. & BATSON, G. B. 1963. Mechanics of crack arrest in concrete. *J Eng Mech Div ASCE Proc,* 89 (EM3)**,** 147-168.

RONG, Z., SUN, W. & ZHANG, Y. 2010. Dynamic compression behavior of ultra-high performance cement based composites. *International Journal of Impact Engineering,* 37**,** 515-520.

RYBIN, V. A., UTKIN, A. V. & BAKLANOVA, N. I. 2013. Alkali resistance, microstructural and mechanical performance of zirconia-coated basalt fibers. *Cement and Concrete Research,* 53**,** 1-8.

ŞAHMARAN, M. & LI, V. C. 2009. Durability properties of micro-cracked ECC containing high volumes fly ash. *Cement and Concrete Research,* 39**,** 1033-1043.

ŞAHMARAN, M., ÖZBAY, E., YÜCEL, H. E., LACHEMI, M. & LI, V. C. 2011. Effect of Fly Ash and PVA Fiber on Microstructural Damage and Residual Properties of Engineered Cementitious Composites Exposed to High Temperatures. *JOURNAL OF MATERIALS IN CIVIL ENGINEERING,* 23**,** 1735-1745.

SAHMARAN, M. & YAMAN, I. 2005. Hybrid fiber reinforced self-compacting concrete with a high-volume coarse fly ash. *Constr. Build. Mater.,* 21**,** 150-156.

SANJAYAN, J. G., NAZARI, A. & POURALIAKBAR, H. 2015. FEA modelling of fracture toughness of steel fibre-reinforced geopolymer composites. *Materials & Design,* 76**,** 215-222.

SARıDEMIR, M. 2009. Predicting the compressive strength of mortars containing metakaolin by artificial neural networks and fuzzy logic. *Advances in Engineering Software,* 40**,** 920-927.

SCHEFFLER, C., FÖRSTER, T., MÄDER, E., HEINRICH, G., HEMPEL, S. & MECHTCHERINE, V. 2009. Aging of alkali-resistant glass and basalt fibers in alkaline solutions: Evaluation of the failure stress by Weibull distribution function. *Journal of Non-Crystalline Solids,* 355**,** 2588-2595.

SEVIL, T., BARAN, M., BILIR, T. & CANBAYA, E. 2011. Use of steel fiber reinforced mortar for seismic strengthening. *Construction and Building Materials,* 25**,** 892–899.

SF-4, J. 1984. Method of Test for Flexural Strength and Flexural Toughness of Fiber Reinforced Concrete (SF-4), Japan Society of Civil Engineers, Tokyo.

SHAH, S. P. & CARPINTERI, A. 1991. *Fracture mechanics test for concrete*, 2 Park Square, Milton Park, Abingdon, Oxon, OX 14 4RN, Taylor & Francis.

SHAIKH, F. U. A. & TAWEEL, M. 2015. Compressive strength and failure behaviour of fibre reinforced concrete at elevated temperatures. *Advances in Concrete Construction,* 3**,** 283-293.

SHEHATA, M. H. & THOMAS, M. D. A. 2000. The effect of fly ash composition on the expansion of concrete due to alkali–silica reaction. *Cement and Concrete Research,* 30**,** 1063-1072.

SHING, P. B. & TANABE, T. A. 2001. *Modelling of inelastic behavior of RC structures under seismic loads,* American Society of Civil Engineers, Dearborn, MI.

SIDDIQUE, R. 2004. Properties of concrete incorporating high volumes of class F fly ash and san fibers. *Cement and Concrete Research,* 34**,** 37-42.

SIM, J., PARK, C. & MOON, D. Y. 2005. Characteristics of basalt fiber as a strengthening material for concrete structures. *Composites Part B: Engineering,* 36**,** 504-512.

SINGH, M., SHEIKH, A. H., MOHAMED ALI, M. S., VISINTIN, P. & GRIFFITH, M. C. 2017. Experimental and numerical study of the flexural behaviour of ultra-high performance fibre reinforced concrete beams. *Construction and Building Materials,* 138**,** 12-25.

SIVASUNDARAM, V., CARETTE, G. G. & MALHOTRA, V. M. 1989. Properties of concrete incorporating low quantity of cement and high volumes of low-calcium fly ash. *ACI Special Publication SP-114,* 1**,** 45-71.

SLISERIS, J. 2018a. Numerical analysis of reinforced concrete structures with oriented steel fibers and re-bars. *Engineering Fracture Mechanics,* 194**,** 337-349.

SLISERIS, J. 2018b. Numerical Estimation of the Mechanical Properties of a Steel-Fiber-Reinforced Geopolymer Composite. *Mechanics of Composite Materials,* 54**,** 621-634.

SOLIKIN, M. 2012. *High Performance Concrete with High Volume Ultra Fine Fly Ash Reinforced with Basalt Fibre.* Doctor of Philosophy, RMIT University, Mrlbourne, Australia.

SOLIKIN, M., SETUNGE, S. & PATNAIKUNI, I. 2011. The influence of lime water as mixing water on the compressive strength development of high volume ultra fine fly ash mortar. *ISEC-6.* Zurich.

SOLIKIN, M., SETUNGE, S. & PATNAIKUNI, I. 2013. Experimental design analysis of ultra fine fly ash, lime water, and basalt fibre in mix proportion of high volume fly ash concrete.

SOLIS, A. V., DURHAM, S. A., RENS, K. L. & RAMASWAMI, A. Sustainable Concrete for the Urban Environment: A Proposal to increase Fly ash Use in Concrete *In:* WEINSTEIN, N. E., ed. Green Streets and Highways 2010 Conference, 2010 Denvern Colorado . American Society of Civil Engineers.

SONG, P. S. & HWANG, S. 2004. Mechanical properties of high-strength steel fiber-reinforced concrete. *Construction and Building Materials,* 18**,** 669-673.

SOUTSOS, M. N., LE, T. T. & LAMPROPOULOS, A. P. 2012. Flexural performance of fibre reinforced concrete made with steel and synthetic fibres. *Construction and Building Materials,* 36**,** 704-710.

STURTEVANT. 2000. *Micronizer jet mill* [Online]. Massachusettes, USA, Sturtevant, Inc. Available: https://sturtevantinc.com/products/micronizer-jet-mill/ [Accessed 05/01/2019.

SUPIT, S. W. M., SHAIKH, F. U. A. & SARKER, P. K. 2014. Effect of ultrafine fly ash on mechanical properties of high volume fly ash mortar. *Construction and Building Materials,* 51**,** 278-286.

TABATABAEIAN, M., KHALOO, A., JOSHAGHANI, A. & HAJIBANDEH, E. 2017. Experimental investigation on effects of hybrid fibers on rheological, mechanical, and durability properties of high-strength SCC. *Construction and Building Materials,* 147**,** 497-509.

TC89-FMT, R. 1989. Determination of fracture parameters (KsIc and CTODc) of plain concrete using three-point bend tests. *Mater Struct***,** 457-460.

TOPCU, I. & CANBAZ, M. 2007. Effect of different fibers on the mechanical properties of concrete containing fly ash. *Constr. Build. Mater.*, 21**,** 1486-1491.

TOSUN-FELEKOGLU, K. & FELEKOGLU, B. 2013. Effects of fibre hybridization on multiple cracking potential of cement-based composites under flexural loading. *Construction and Building Materials,* 41**,** 15-20.

TYSMANS, T., WOZNIAK, M., REMY, O. & VANTOMME, J. 2015. Finite element modelling of the biaxial behaviour of high-performance fibre-reinforced cement composites (HPFRCC) using Concrete Damaged Plasticity. *Finite Elements in Analysis and Design,* 100**,** 47-53.

UYSAL, M. & TANYILDIZI, H. 2012. Estimation of compressive strength of self compacting concrete containing polypropylene fiber and mineral additives exposed to high temperature using artificial neural network. *Construction and Building Materials,* 27**,** 404-414.

WANG, K., SHAH, S. P. & PHUAKSUK, P. 2001. Plastic shrinkage cracking in concrete materials - Influence of fly ash and fibers. *Aci Materials Journal* 98**,** 458-464.

WANG, M., ZHANG, Z., LI, Y., LI, M. & SUN, Z. 2008. Chemical Durability and Mechanical Properties of Alkali-proof Basalt Fiber and its Reinforced Epoxy Composites. *Journal of Reinforced Plastics and Composites*.

WANG, S. & LI, V. C. 2007. Engineered Cementitious Composites with High-Volume Fly Ash. *ACI Materials Journal,* 104**,** 233-241.

WANG, Y. 1990. Tensile Properties of Synthetic Fiber Reinforced Mortar. *Cement & Concrete Composites,* 12**,** 29-40.

WEI, B., CAO, H. & SONG, S. 2010. Environmental resistance and mechanical performance of basalt and glass fibers. *Materials Science and Engineering: A,* 527**,** 4708-4715.

WEI, B., SONG, S. & CAO, H. 2011. Strengthening of basalt fibers with nano-SiO2–epoxy composite coating. *Materials & Design,* 32**,** 4180-4186.

WILLAM, K. J. & TANABE, T. 2001. *Finite Element Analysis of Reinforced Concrete Structures*, ACI International.

WILLAM, K. J. & WARNKE, E. P. Constitutive model for triaxial behaviour of concrete. In: Seminar on concrete structures subjected to triaxial stresses. International association of bridge and structural engineering conference, 1974 Bergamo, Italy. 174.

WU, G., WANG, X., WU, Z., DONG, Z. & ZHANG, G. 2015. Durability of basalt fibers and composites in corrosive environments. *Journal of Composite Materials* 49**,** 873-887. .

WU, Y., SUN, Q., GUO, Y., LI, W., XU, C. & SUN, C. 2013. The improvement of setting time and early strength of fiber-reinforced concrete with high-volume fly ash. *Composite Interfaces,* 20**,** 201-209.

XIE, Y., LIU, B., YIN, J. & ZHOU, S. 2002. Optimum mix parameters of high-strength self-compacting concrete with ultrapulverized fly ash. *Cement and Concrete Research,* 32**,** 477-480.

XU, L., CHI, Y., SU, J. & XIA, D. 2008. Nonlinear finite element analysis of steel fiber reinforced concrete deep beams. *Wuhan University Journal of Natural Sciences,* 13**,** 201-206.

YANG, E. H., YANG, Y. & LI, V. 2007. Use of High Volumes of Fly Ash to Improve ECC Mechanical Properties and Material Greenness. *ACI Materials Journal,* 104**,** 620-628.

YAP, S. P., BU, C. H., ALENGARAM, U. J., MO, K. H. & JUMAAT, M. Z. 2014. Flexural toughness characteristics of steel–polypropylene hybrid fibre-reinforced oil palm shell concrete. *Materials & Design,* 57**,** 652-659.

YING, S. & ZHOU, X. 2013. Chemical and thermal resistance of basalt fiber in inclement environments. *Journal of Wuhan University of Technology-Mater. Sci. Ed.,* 28**,** 560-565.

YOO, D.-Y. & BANTHIA, N. 2015. Numerical simulation on structural behavior of UHPFRC beams with steel and GFRP bars. *Computers and Concrete . Techno Press,* 16**,** 759-774.

YOO, D.-Y., KANG, S.-T., BANTHIA, N. & YOON, Y.-S. 2017. Nonlinear finite element analysis of ultra-high-performance fiber-reinforced concrete beams. *International Journal of Damage Mechanics,* 26**,** 735-757.

YU, R., SPIESZ, P. & BROUWERS, H. J. H. 2015. Development of Ultra-High Performance Fibre Reinforced Concrete (UHPFRC): Towards an efficient utilization of binders and fibres. *Construction and Building Materials,* 79**,** 273-282.

YUSOF, M. A., NOR, N. M., ISMAIL, A., PENG, N. C., SOHAIMI, R. M. & YAHYA, M. A. 2013. Performance of Hybrid Steel Fibers Reinforced Concrete Subjected to Air Blast Loading. *Advances in Materials Science and Engineering*.

ZHANG, P. & LI, Q.-F. 2013. Effect of polypropylene fiber on durability of concrete composite containing fly ash and silica fume. *Composites Part B: Engineering,* 45**,** 1587-1594.

ZHAO, J. 1990. *Mechanical Properties of Concrete at Early-ages.Master thesis, University of Ottawa, Canada.*

ZOMORODIAN, A., BRUSCIOTTI, F., FERNANDES, A., CARMEZIM, M. J., MOURA E SILVA, T., FERNANDES, J. C. S. & MONTEMOR, M. F. 2012. Anti-corrosion performance of a new silane coating for corrosion protection of AZ31 magnesium alloy in Hank's solution. *Surface and Coatings Technology,* 206**,** 4368-4375.

Annex: List of Abbreviations

AS	Australian Standard
ASTM	American Society for Testing and Materials
ASR	Alkali silica reaction
ANN	Artificial neural network
AVPV	Absorption and apparent volume of permeable voids
BF	Basalt fiber
CDP	Concrete damage plasticity
CT	Computed tomography
CS	Compressive strength
COV	Coefficient of variance
CA	Coarse aggregate
CMOD	Crack mouth opening displacement
CTOD	Crack tip opening displacement
DTFTM	Direct tension force transfer model
EDX	Energy-dispersive X-ray spectroscopy
FE	Finite element
FEM	Finite element method
FA	Fly ash
FRC	Fiber reinforced concrete
FS	Flexural strength
HVFA	High volume fly ash
HRFC	Hybrid fiber reinforced concrete
JSCE	Japan Society of Civil Engineers
LVDT	Linear variable displacement transducer
MTS	Material test specification
MOE	Modulus of elasticity

MPC	Multi point constraint
NLFEA	Nonlinear finite element analysis
OPC	Ordinary Portland Cement
PVA	Polyvinyl alcohol
PFRC	Polymer fiber reinforced concrete
PP	Polypropylene fiber
RFA	Raw fly ash
RMSE	Root mean square error
SP	Super plasticizer
ST	Steel fiber
SFRC	Steel fiber reinforced concrete
SEM	Scanning electron microscope
SSD	Saturated surface dry
SD	Standard deviation
UFFA	Ultra-fine fly ash
UMAT	User defined material
Vf	Volume fraction
WR	Water reducer

Appendix A: Mix design of mortar

Control UFFA mortar mix design

w/b ratio: 0.30

Specific gravity of material used

Materials	Specific gravity	%
Cement	3.16	50
UFFA	2.20	50
RFA	2.35	
Sand	2.65	
Super.P	1.0	

Water correction of fine aggregate

Aggregate	GssD	Wabs	Wtot	Wh
Sand	2.65	1.12	0.42	-0.7

Super plasticizer

Super P S.G.	Solid Dosage (%)	Msol= (C*d/100)	Vliq= (Msol*100)/(s*Gsup)	Vw= (Vliq*Gsup*(100-s)/100	Vsol= Vliq-Vw
1	40	5	12.5	7.5	5

Mix design for UFFA mortar

Materials	**Content** (kg/m3)	**Volume** (l/m3)	**Dosage SSD** (kg/m3)	**Water Correction** (l/m3)	**Composition** 1m3
Water	160	160	160		164
Cement	275	87	235		235
UFFA	275	126	235		235
Sand		612	1621	11	1610
Air	1.2	12	0		
Super.P	1.0		5	-7.5	10.33
Total		1000	2336	4	

Sample hybrid fiber reinforced UFFA mortar mix design

w/b ratio: 0.30

Specific gravity of material used

Materials	Specific gravity	%
Cement	3.16	50
UFFA	2.20	50
RFA	2.35	
Sand	2.65	
Super.P	1.0	
Steel	7.8	
PP	0.97	
BF	2.67	

Water correction of fine aggregate

Aggregate	GssD	Wabs	Wtot	Wh
Sand	2.65	1.12	0.42	-0.7

Fiber percentage (%)

Steel fiber	0.5
Polypropylene fiber	0.5
Basalt fiber	0.5

Super plasticizer

Super P S.G.	Solid Dosage (%)	Msol= (C*d/100)	Vliq= (Msol*100)/(s*Gsup)	Vw= (Vliq*Gsup*(100-s)/100	Vsol= Vliq-Vw
1	40	5	12.5	7.5	5

Mix design for hybrid fiber reinforced (0.5% st +0.5% PP+ 0.5% BF) UFFA mortar

Materials	**Content** (kg/m3)	**Volume** (l/m3)	**Dosage SSD** (kg/m3)	**Water Correction** (l/m3)	**Composition** 1m3
Water	160	160	160		164
Cement	275	87	235		235
UFFA	275	126	235		235
Sand		597	1581	11	1570
Steel	39	5	39		39
PP	4.85	5	4.85		4.85
Basalt	13.13	5	13.35		13.35
Air	1.2	12	0		
Super.P	1.0		5	-7.5	10.33
Total		1000	2354	4	

Appendix B: Mix design of concrete

Control UFFA concrete mix design

w/b ratio: 0.30

Specific gravity of material used

Materials	Specific gravity	%
Cement	3.16	50
UFFA	2.20	50
RFA	2.35	
Sand	2.65	
Super.P	1.0	

Water correction of fine aggregate

Aggregate	GssD	Wabs	Wtot	Wh
Coarse	2.80	0.8	0.3	-0.5
Sand	2.65	1.12	0.12	-1

Super plasticizer

Super P S.G.	Solid Dosage (%)	Msol= (C*d/100)	Vliq= (Msol*100)/(s*Gsup)	Vw= (Vliq*Gsup*(100-s)/100	Vsol= Vliq-Vw
1	40	5	12.5	7.5	5

Mix design for UFFA concrete

Materials	**Content** (kg/m3)	**Volume** (l/m3)	**Dosage SSD** (kg/m3)	**Water Correction** (l/m3)	**Composition** 1m3
Water	140	140	140		152
Cement	235	75	235		235
UFFA	235	103	235		235
Coarse	1080	386	1080	8	1075
Sand		284	751	7	744
Air	1.2	12			
Super.P		1.06	1.88	-2.8	3.88
Total		1000	2443	12	

Sample hybrid fiber reinforced UFFA mortar mix design

w/b ratio: 0.30

Specific gravity of material used

Materials	Specific gravity	%
Cement	3.16	50
UFFA	2.20	50
RFA	2.35	
Sand	2.65	
Super.P	1.0	
Steel	7.8	
PP	0.97	
BF	2.67	

Water correction of fine aggregate

Aggregate	GssD	Wabs	Wtot	Wh
Coarse	2.80	0.8	0.3	-0.5
Sand	2.65	1.12	0.12	-1

Fiber percentage (%)	
Steel fiber	1.5
Polypropylene fiber	0.5
Basalt fiber	0.0

Super plasticizer

Super P S.G.	Solid Dosage (%)	Msol= (C*d/100)	Vliq= (Msol*100)/(s*Gsup)	Vw= (Vliq*Gsup*(100-s)/100	Vsol= Vliq-Vw
1	40	5	12.5	7.5	5

Mix design for hybrid fiber reinforced (1.5% st +0.5% PP) UFFA concrete

Materials	**Content** (kg/m3)	**Volume** (l/m3)	**Dosage SSD** (kg/m3)	**Water Correction** (l/m3)	**Composition** 1m3
Water	140	140	140		152
Cement	235	75	235		235
UFFA	235	103	235		235
Coarse	1080	386	1080	8	1075
Sand		264	698	7	691
Steel	117	15	117		117
PP	4.85	5	4.85		4.85
Air	1.2	12			
Super.P		1.064	1.88	-2.8	3.88
Total			2512	12	

Appendix C: Water absorption of concrete

	Oven dry M1	After 48hrs curing M2i	After boiling M3b	Wt. in water M4ib
Micro Fly Ash (56 Days)	1167.9	1178.7	1178.8	681.7
	1201.4	1230.4	1234.8	713
	1146.4	1167.5	1170.1	677.4
1.5S0.5P (56D)	1258.4	1279.4	1285.7	756.1
	1125.7	1143.9	1148.5	675.3
	1200.9	1213.5	1218.1	715.8
1.0S0.5P0.5B (56D)	1164.2	1185.5	1184.4	692.9
	1244.8	1268.2	1267.2	734.2
	1182.9	1206.1	1204.7	701.2

	Immersed Absorption (Ai) (%)	Boiled Absorption (Ab) (%)	AVPV (%)
Micro Fly	0.924736707	0.933299084	2.192718
Ash (56	2.413850508	2.780089895	6.40092
Days)	1.840544313	2.067341242	4.810229
Average	2.12719741	2.423715569	5.605575
1.5S0.5P	1.66878576	2.169421488	5.154834
(56D)	1.616771786	2.025406414	4.818259
	1.04921309	1.432259139	3.424248
Average	1.642778773	2.097413951	4.986546
1.0S0.5P0.5B	1.829582546	1.735097062	4.109868
(56D)	1.879820051	1.799485861	4.202627
	1.961281596	1.842928396	4.329692
Average	1.890228064	1.792503773	4.214062

Appendix D: Fracture model parameter

Critical stress intensity factor (K_I) sample calculation:

Specimen 1:

a_c = (a_0 + crack at peak) = (25 + 20) = 45

$\alpha = a_c/D$ = 45/150 = 0.3

$$F(\alpha) = \frac{1.99 - \alpha(1-\alpha)(2.15 - 3.93\alpha + 2.7\alpha^2)}{\sqrt{\pi}\ (1+2\alpha)(1-\alpha)^{3/2}}$$

$$= \frac{1.99-0.3(1-0.3)(2.15-3.93*0.3+2.7*0.3^2)}{\sqrt{\pi}\ (1+2*0.3)(1-0.3)^{3/2}} = 1.0446$$

$$K_I = 3P_{max}\frac{S(\pi a_c)^{1/2}\,F(\alpha)}{2d^2b}$$

$$= 3 * 26601 * \frac{500 * (\pi * 45)^{1/2} * 1.0446}{2 * 150^2 * 150}$$

= 2.246 MPa√m

CTOD calculation:

β=a_0/a_c = 25/45 = 0.556

$$V_1(\alpha) = 0.76 - 2.28\alpha + 3.87\alpha^2 - 2.04\alpha^3 + 0.66/(1-\alpha)^2$$

$$= 0.76 - 2.28 * 0.3 + 3.87 * 0.3^2 - 2.04 * 0.3^3 + 0.66/(1-0.3)^2$$

$$= 1.716$$

$$CTOD = \frac{6P_{max}Sa_c}{d^2bE}V_1(\alpha)\{(1-\beta)^2 + (-1.149\alpha + 1.081)(\beta - \beta^2)\}^{1/2}$$

$$= \frac{6 * 26601 * 500 * 45}{150^2 * 150 * 39000} * 1.716$$

$$* \{(1-0.556)^2 + (-1.149 * 0.3 + 1.081)(0.556 - 0.556^2)\}^{1/2}$$

= 0.0276

Fracture energy calculation:

$G_f = \frac{T_b + mg\delta_{max}}{A_{lig}}$ mg = 0.003055*150*150*500 =34368.75 gm

= 34.4 kg

$$= \frac{6753.1264 + 34.4 * 0.5248}{150 * (150 - 25)}$$

= 0.361 N/mm